Site-selective Probing of Surfactant Assemblies using Excited State Proton Transfer of Pyranine

A dissertation

as partial fulfilment of requirement

for the degree of Doctor of Philosophy in Chemistry

by

Aparajita Phukon

136122027

Department of Chemistry

Indian Institute of Technology Guwahati

Guwahati, Assam-781039

Dedicated to my

Family

Declaration

I do hereby declare that the work contained in this thesis entitled **"Site-selective Probing of Surfactant Assemblies using Excited State Proton Transfer of Pyranine"** is the outcome of the research work carried out by me under the supervision of Dr. Kalyanasis Sahu, Associate Professor, Department of Chemistry, Indian Institute of Technology Guwahati, India.

In keeping with the general practice of reporting scientific observations, due acknowledgements have been made whenever work described here has been based on the findings of other investigators. This work has not been submitted elsewhere for the award of any degree.

Dated:

Aparajita Phukon
Department of Chemistry
Indian Institute of Technology Guwahati,
Guwahati-781039, India

INDIAN INSTITUTE OF TECHNOLOGY GUWAHATI

Department of Chemistry

CERTIFICATE

This is to certify that **Aparajita Phukon** (Roll No. 136122027) has been working under my supervision since July, 2013 as a regular registered Ph. D. student. Her thesis entitled **"Site-selective Probing of Surfactant Assemblies using Excited State Proton Transfer of Pyranine"** is an authentic record of the results obtained from the research work carried out under my supervision in the Department of Chemistry, Indian Institute of Technology Guwahati, Assam, India. I am forwarding her thesis to submit for the award of degree of Doctor of Philosophy, from this institute. I hereby certify that she has fulfilled all the requirements, according to the rules of this institute regarding the investigations embodied in her thesis and this work has not been submitted elsewhere for a degree.

Dr. Kalyanasis Sahu
(Thesis Supervisor)
Associate Professor
Department of Chemistry
IIT Guwahati
Assam - 781039, India

Acknowledgement

This opportunity to extend my gratitude should commence with my parents, dearest sister and brother, whose love and inspiration have always been strength for me. Besides, no words would suffice to express my feelings for my beloved Romen, whose love and care have so luxuriously continued to enrich my life.

At this stage of ending my PhD programme, I take the opportunity to convey my earnest gratitude and respect to my supervisor, Dr. Kalyanasis Sahu for his help and guidance. His enthusiasm, inspiration and efforts have helped me in making this thesis a reality.

I would like to acknowledge my doctoral committee members Prof. Gopal Das (Chairman), Prof. Anumita Paul, and Dr. Debasis Manna who have been constantly guiding me with their valuable suggestions, encouragements and constructive criticism which helped to improve my thesis. I take this opportunity to thank Prof. T. Punniyamurthy (HOD) and Prof. B. K. Patel (former HOD) and other technical and non-technical staff members of the Department of Chemistry, IIT Guwahati for providing me with the necessary facilities whenever required.

I also like to thank my Lab members and friends Naba da, Debu, Dilip, Sudipta, Rabiul, Tapash and Nilanjona for their help and co-operation in my research work, without which it would not been easy to complete this journey. It was great to work and spend times with these interesting human beings and I will always cherish the memories of their jokes, laughter and humour throughout my life I wish them success in every aspects of their life.

Finally, I would like to pay my sincere thanks to Chumi, Madhu, Niva, Swastika, Yashmin, Dhriti and Gaurangi for enriching my life with their eternal friendship.

Sincerely

Aparajita Phukon

Table of Contents

SYNOPSIS OF THE THESIS

ABSTRACT

The thesis includes our investigations on the nature and behavior of water entrapped in the nano-confined surfactant assemblies, in particular, reverse micelles and micelles. The hydration behavior depends critically on the type of polar headgroup of surfactants and also on the presence of co-surfactants. We mainly employed the hydration sensitive excited state proton transfer (ESPT) property of a site selective anionic probe 8-hydroxypyrene-1, 3, 6-trisulfonate (HPTS or pyranine) to study these systems.

In *chapter 1*, we briefly discuss the recent trends of various ESPT studies in different confined media and summarize how these dynamics differ from that in bulk water. *Chapter 2* includes the summary of measurement techniques and experimental methods that we adopted in our studies. In the *chapter 3*, we investigated the effect of confinement on the solubility behaviour of the water pool of water/AOT/n-heptane reverse micelle towards a so called insoluble alcohol *n*-octanol. In *Chapter 4*, we confirmed the presence of finite level of hydration at the interface of a cationic surfactant reverse micelle (water/ BHDC/ benzene) by detecting non-negligible ESPT. The effect of co-surfactant on the hydration at the interfacial region of a quaternary water/CTAB/octanol/cyclohexane reverse micelle is discussed in the *chapter 5*. The modification of the interfacial hydration associated with the structural transition of water/DDAB/cyclohexane reverse micelle from rod to sphere is discussed in the *chapter 6*. In the *chapter 7*, we compared the interfacial properties between micelles formed by two different surfactants- zwitterionic sulfobetaine (SB12 and SB16) and cationic n-alkyl tertiary ammonium (DTAB and CTAB).

CHAPTER 1: INTRODUCTION:

Proton transfer is a ubiquitous process occurring frequently both in the biological and chemical environments. In a typical spectroscopic investigation, the proton transfer event is usually initiated upon irradiating of a fluorophore with light. Acidity of such a fluorophore enhances dramatically in the electronic excite state and ejects a proton to the neighbouring acceptor or solvent and the phenomena is termed as

excited state proton transfer (ESPT). 8-hydroxypyrene-1, 3, 6-trisulfonic acid (HPTS or pyranine) is one such photoacids with ground state pK_a of 7.2-7.7[1,2] and excited state pK_a^* of 0.5-1.5.[2,3] Thus, in neutral or slightly acidic water, HPTS mainly remains in the protonated form and shows an absorption maximum at 403nm. It displays a strong emission centered at ~512 nm and a very feeble emission band at ~440 nm characteristics of the deprotonated and the protonated forms, respectively (**Figure 1.1**). The ratio of the emission intensity of the two forms is very sensitive to the nature of the proton acceptor (usually water) around the fluorophore. This makes HPTS a suitable probe to study nature and properties of water encaged inside confined media like membrane,[4,5] cyclodextrin,[6,7] protein,[8,9] micelle,[10] reverse micelle[11] etc. Moreover, the photoacid is highly anionic in nature due to the presence of three sulfonate and one hydroxyl group (this group also becomes negative after deprotonation). This charge criterion is extremely important in dictating the location of the probe inside different self-assemblies having net charges. This allows us to site-specific probing of ESPT in these assemblies and these aspects are particularly exploited in this thesis.

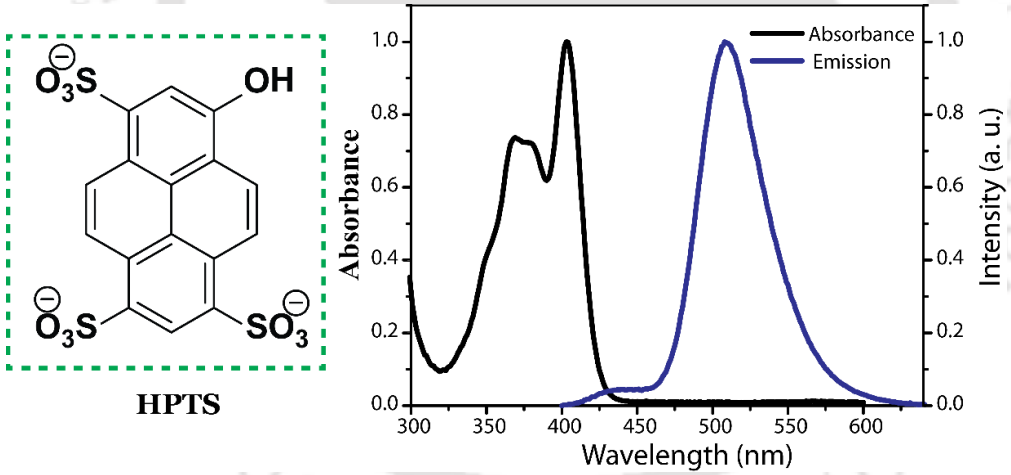

Figure 1.1. Chemical structure and absorbance and emission spectra of HPTS in water at pH=5.5.

CHAPTER 2: EXPERIMENTAL METHODS:

In this chapter, we have mentioned specifications of all the spectrometers used in our works including UV-Vis, steady-state and time-resolved fluorescence, nuclear magnetic resonance (NMR) and dynamic light scattering (DLS). We also added sources of all chemicals used and all sample preparation procedures including various data analysis methods, models and so on.

Chapter 3: Confinement Induced variable solubility of n-octanol inside the aqueous core of water/AOT/n-heptane reverse micelle.[12]

In this chapter, we reported a remarkably different partitioning of a normally water-immiscible alcohol, *n*-octanol, inside the aqueous core of water/AOT/n-heptane reverse micelle at two different levels of confinement – highly confined (at $w_0 = 5$) and quasi-confined (at $w_0 = 10$). We cleverly used the ratio-metric alcohol sensing ESPT property of HPTS located at the center of the water pool of the anionic reverse micelle. At low w_0, we observed significant modulation of ESPT signifying partitioning of *n*-octanol into the highly-confined water. However, no ESPT modulation was found at $w_0 = 10$, supporting the absence of *n*-octanol in the quasi-confined water. The observation was further corroborated by very different modulation of reverse micelle size, depending on the initial state of water in the water pool of the reverse micelle.

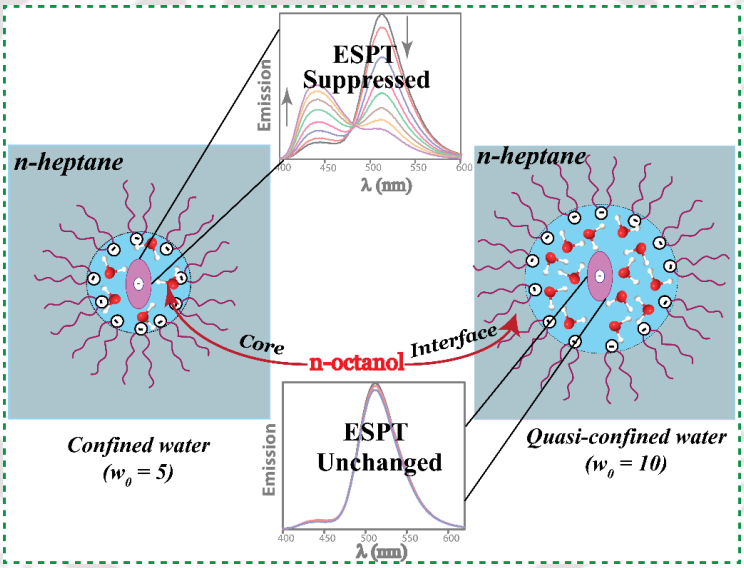

Figure 3.1: Schematic representation of ESPT modulation in confined and quasi-confined water with incorporation of *n*-octanol in the water/AOT/n-heptane reverse micelle.

Thus, the study demonstrated a strikingly unusual variation of solubilization properties of water with degree of confinement. The results revealed that confined water behaves like more hydrophobic solvent compared to quasi-confined or bulk water. The overall concept of this chapter has been schematically presented in **Figure 3.1**.

Chapter 4: Is the interface of the reverse micelle dry or wet? Insights from ESPT of HPTS in the case of cationic water/BHDC/benzene reverse micelle.[13]

This chapter includes our ESPT study to trace penetration of any water molecule to the interface of a cationic surfactant reverse micelle BHDC/water/benzene. In a pioneering work of Levinger and co-workers reported the absence of ESPT of HPTS at the interface of a quaternary reverse micelle cyclohexane/water/CTAB/*n*-octanol using ultrafast pump-probe spectroscopy.[14] However, the presence of co-surfactant (*n*-octanol) and the limited time window of their ultrafast study, may lead complicated conclusion. Thus we used the BHDC reverse micelle which does not require any co-surfactant to form reverse micelle. We also confirmed the presence of HPTS at the interface of the reverse micelle by 2D NOESY NMR and fluorescence anisotropy. Interestingly, we observed significant ESPT at the interface and the ESPT modulates moderately with variation of $w_0 (= \frac{[water]}{[surfactant]})$ value (**Figure 4.1**). Our results signify penetration of the water molecules into the interface of cationic tertiary reverse micelle with increase of hydration level.

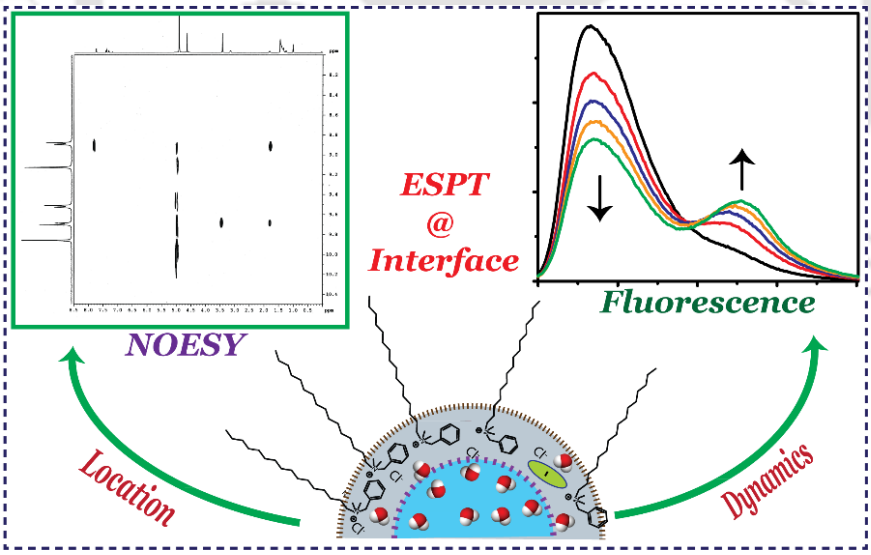

Figure 4.1: Schematic representation of the water/ BHDC/Benzene reverse micelle interface. The presence of HPTS was confirmed by NOESY cross peaks. Significant ESPT modulation indicates wet nature of the interface.

Chapter 5: The Impact of co-surfactant on the interfacial hydration of cationic quaternary water/CTAB/octanol/ cyclohexane reverse micelle.[15]

In this chapter, we have included our ESPT study to elucidate effect of co-surfactant, *n*-octanol on the hydration properties of the water/CTAB/*n*-octanol/ cyclohexane reverse micelle interface. In this reverse micelle, *n*-octanol assists CTAB to satisfy the necessary geometric condition $^{v}/_{al} > 1$, where *v*, *l* and *a* refer to volume, chain length of the hydrocarbon tail and area of polar head group of the surfactant molecule, respectively and help to form a stable reverse micelle.[16,17] The co-surfactant is usually assumed to be inserted in-between the CTAB surfactants at the interface and introduced a new adjustable parameter p_0 $(=^{[cosurfactant]}/_{[surfactant]})$ in addition to the prevalent parameter,$w_0 (= \frac{[water]}{[surfactant]})$. This new parameter can control size and properties of the RM, like flexibility and applicability of the RM.[18] In this study, we observed distinct ESPT modulation at nanosecond time domain which can be tuned by varying p_0 and w_0 values (**Figure 5.1**). Our study signifies that the presence of co-surfactant at the interface modulates the penetration of water into the interfacial region of quaternary reverse micelle.

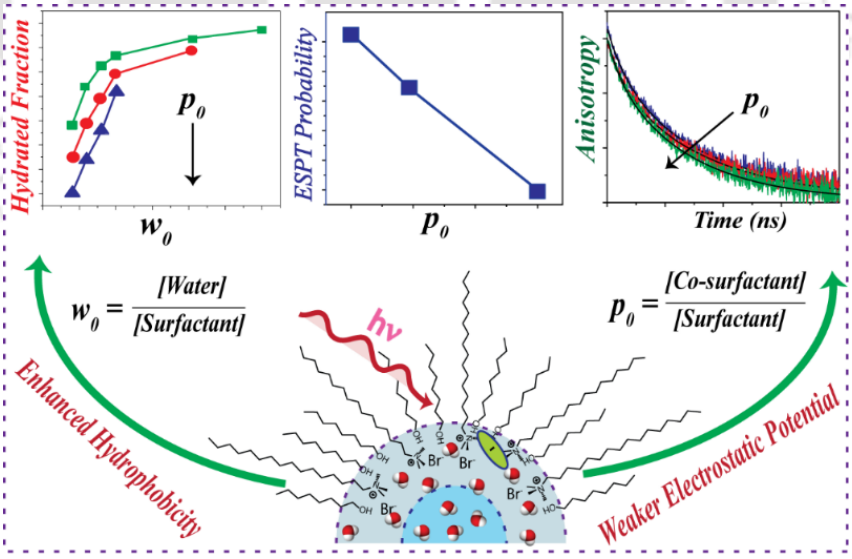

Figure 5.1: Schematic representation of the interface of water/CTAB/*n*-octanol /cyclohexane quaternary RM and the ESPT and fluorescence anisotropy results. The *n*-octanol modulates the extent of penetration of water molecules into the interface and makes the interface more flexible.

Chapter 6: How does interfacial hydration alter during rod to sphere transition in DDAB/water/Cyclohexane reverse micelles?[19]

In this chapter, we extended our ESPT study in correlating the interfacial packing and hydration of didodecyldimethylammonium bromide (DDAB/water/cyclohexane) reverse micelle. This is an interesting assembly that undergoes a structural transition from rod to spherical shape above a particular value (w_0 ~ 8). The ESPT process is markedly inhibited within the interface at low w_0 and gradually favoured with the increase of w_0. The time-resolved fluorescence decays could be best analysed by assuming distribution of HPTS over two distinct interfacial regions- partly hydrated and mostly dehydrated. The relative population of the two regions varies distinctly at low w_0 (< 6) and high w_0 (> 6) regimes. Moreover, fluorescence anisotropy (steady-state and time-resolved) varies differently with respect to w_0, before and after the transition point (w_0 ~ 8), (**Figure 6.1**).

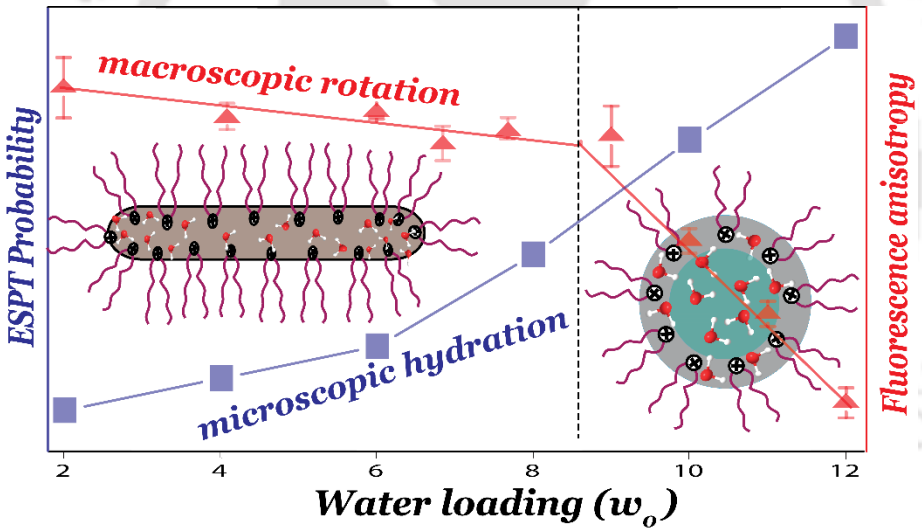

Figure 6.1: Schematic representation of change in ESPT probability and interface packing of DDAB/water/cyclohexane reverse micelle with shape transition from rod-like to spherical reverse micelle.

Chapter 7: How do the interfacial properties of zwitterionic sulfobetaine micelles differ from those of cationic alkyl quaternary ammonium micelles?[20]

We compared the interfacial properties; specially, nature of interfacial hydration and rigidity of zwitterionic sulfobetaine (e.g. SB-12, SB-16) and cationic alkyl-ammonium (e.g. CTAB, DTAB) surfactant micelles. Zwitterionic surfactants (e.g.

sulfobetaine), comprising both positive and negative groups in their headgroups, are essentially electro-neutral as monomer, but their micelles preferentially uptake anions like that of a cationic surfactant micelle. Two sulfobetaine surfactants (SB-12 and SB-16) and two cationic surfactants (DTAB and CTAB) with matching alkyl tails were selected for an effective comparison. The ESPT dynamics was observed to be significantly suppressed inside the zwitterionic micelle interface compared to that of the cationic micelle. This was attributed to a less hydrated interface of the zwitterionic micelles compared to that of the cationic one. Fluorescence anisotropy decay inside the zwitterionic micellar interface was also slower compared to that of the cationic one indicating a better packing of the zwitterionic surfactants at the interface (**Figure 7.1**).

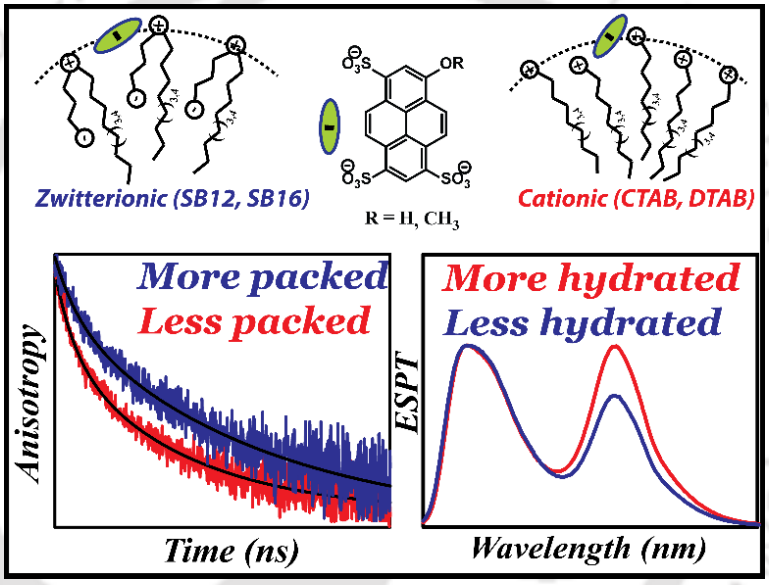

Figure 7.1: Schematic comparison of the interfacial properties between zwitterionic (SB12 and SB16) and cationic (DTAB and CTAB) micelles. The interface of zwitterionic sulfobetaine micelle is found to be more hydrophobic and rigid than that of the cationic micelle.

REFERENCES:

(1) Pines, E.; Huppert, D.: Observation of geminate recombination in excited state proton transfer. *J. Chem. Phys.* **1986**, *84*, 3576-3577.

(2) Bardez, E.; Goguillon, B. T.; Keh, E.; Valeur, B.: Dynamics of excited-state reactions in reversed micelles. 1. Proton transfer involving a hydrophilic fluorescent probe. *J. Phys. Chem.* **1984**, *88*, 1909-1913.

(3) Smith, K. K.; Kaufmann, K. J.; Huppert, D.; Gutman, M.: Picosecond proton ejection: an ultrafast pH jump. *Chem. Phys. Lett.* **1979**, *64*, 522-527.

(4) Dishari, S. K.; Hickner, M. A.: Confinement and Proton Transfer in NAFION Thin Films. *Macromolecules* **2013**, *46*, 413-421.

(5) Moilanen, D. E.; Levinger, N. E.; Spry, D. B.; Fayer, M. D.: Confinement or the Nature of the Interface? Dynamics of Nanoscopic Water. *J. Am. Chem. Soc.* **2007**, *129*, 14311-14318.

(6) Mondal, S. K.; Sahu, K.; Ghosh, S.; Sen, P.; Bhattacharyya, K.: Excited-State Proton Transfer from Pyranine to Acetate in γ-Cyclodextrin and Hydroxypropyl γ-Cyclodextrin. *J. Phys. Chem. A* **2006**, *110*, 13646-13652.

(7) Mondal, S. K.; Sahu, K.; Sen, P.; Roy, D.; Ghosh, S.; Bhattacharyya, K.: Excited state proton transfer of pyranine in a γ-cyclodextrin cavity. *Chem. Phys. Lett.* **2005**, *412*, 228-234.

(8) Chowdhury, R.; Saha, A.; Mandal, A. K.; Jana, B.; Ghosh, S.; Bhattacharyya, K.: Excited State Proton Transfer in the Lysosome of Live Lung Cells: Normal and Cancer Cells. *J. Phys. Chem. B* **2015**, *119*, 2149-2156.

(9) Sahu, K.; Roy, D.; Mondal, S. K.; Karmakar, R.; Bhattacharyya, K.: Study of protein–surfactant interaction using excited state proton transfer. *Chem. Phys. Lett.* **2005**, *404*, 341-345.

(10) Roy, D.; Karmakar, R.; Mondal, S. K.; Sahu, K.; Bhattacharyya, K.: Excited state proton transfer from pyranine to acetate in a CTAB micelle. *Chem. Phys. Lett.* **2004**, *399*, 147-151.

(11) Cohen, B.; Huppert, D.; Solntsev, K. M.; Tsfadia, Y.; Nachliel, E.; Gutman, M.: Excited State Proton Transfer in Reverse Micelles. *J. Am. Chem. Soc.* **2002**, *124*, 7539-7547.

(12) Phukon, A.; Sahu, K.: The strikingly different miscibility of n-octanol in highly-confined and quasi-confined water. *Chem. Commun.* **2015**, *51*, 14103-14106.

(13) Phukon, A.; Barman, N.; Sahu, K.: Wet Interface of Benzylhexadecyldimethylammonium Chloride Reverse Micelle Revealed by Excited State Proton Transfer of a Localized Probe. *Langmuir* **2015**, *31*, 12587-12596.

(14) Sedgwick, M.; Cole, R. L.; Rithner, C. D.; Crans, D. C.; Levinger, N. E.: Correlating Proton Transfer Dynamics To Probe Location in Confined Environments. *J. Am. Chem. Soc.* **2012**, *134*, 11904-11907.

(15) Phukon, A.; Ray, S.; Sahu, K.: Effect of Cosurfactants on the Interfacial Hydration of CTAB Quaternary Reverse Micelle Probed Using Excited State Proton Transfer. *Langmuir* **2016**, *32*, 10659-10667.

(16) Lang, J.; Mascolo, G.; Zana, R.; Luisi, P. L.: Structure and dynamics of cetyltrimethylammonium bromide water-in-oil microemulsions. *J. Phys. Chem.* **1990**, *94*, 3069-3074.

(17) Mills, A. J.; Wilkie, J.; Britton, M. M.: NMR and Molecular Dynamics Study of the Size, Shape, and Composition of Reverse Micelles in a Cetyltrimethylammonium Bromide (CTAB)/n-Hexane/Pentanol/Water Microemulsion. *J. Phys. Chem. B* **2014**, *118*, 10767-10775.

(18) Khan, M. F.; Singh, M. K.; Sen, S.: Measuring Size, Size Distribution, and Polydispersity of Water-in-Oil Microemulsion Droplets using Fluorescence Correlation Spectroscopy: Comparison to Dynamic Light Scattering. *J. Phys. Chem. B* **2016**, *120*, 1008-1020.

(19) Phukon, A.; Ray, S.; Sahu, K.: How Does Interfacial Hydration Alter during Rod to Sphere Transition in DDAB/Water/Cyclohexane Reverse Micelles? Insights from Excited State Proton Transfer and Fluorescence Anisotropy. *Langmuir* **2016**, *32*, 6656-6665.

(20) Phukon, A.; Sahu, K.: How do the interfacial properties of zwitterionic sulfobetaine micelles differ from those of cationic alkyl quaternary ammonium micelles? An excited state proton transfer study. *Phys. Chem. Chem. Phys.* **2017**, *19*, 31461-31468.

LIST OF PUBLICATIONS

PAPER INCLUDED IN THIS THESIS:

1) **Phukon, A**.; Sahu, K.: The strikingly different miscibility of *n*-octanol in highly-confined and quasi-confined water. *Chem. Commun.* **2015**, *51*, 14103-14106.

2) **Phukon,A**., Barman, N.; Sahu, K.: Wet Interface of Benzylhexadecyldimethylammonium Chloride Reverse Micelle Revealed by Excited State Proton Transfer of a Localized Probe. *Langmuir* **2015**, *31*, 12587-12596.

3) **Phukon, A**.; Ray, S.; Sahu, K.: How Does Interfacial Hydration Alter during Rod to Sphere Transition in DDAB/Water/Cyclohexane Reverse Micelles? Insights from Excited State Proton Transfer and Fluorescence Anisotropy. *Langmuir* **2016**, *32*, 6656-6665.

4) **Phukon, A**.; Ray, S.; Sahu, K.: Effect of Cosurfactants on the Interfacial Hydration of CTAB Quaternary Reverse Micelle Probed Using Excited State Proton Transfer. *Langmuir* **2016**, *32*, 10659-10667.

5) **Phukon, A**.; Sahu, K.: How do the interfacial properties of zwitterionic sulfobetaine micelles differ from those of cationic alkyl quaternary ammonium micelles? An excited state proton transfer study. *Phys. Chem. Chem. Phys.* **2017**, *19*, 31461-31468.

PAPER NOT INCLUDED IN THIS THESIS:

1. Singha, D.; Barman, N.; **Phukon, A**.; Sahu, K.: Selective Probing of Reverse Micelle Interfacial Layer upon Silver Nanoparticle Formation using Dynamic Stokes Shift Measurements. *J. Phys. Chem. C* **2014**, *118*, 10366-10374.

2. **Phukon, A.**; Nandi, N.; Sahu, K.: Pre-micellar interaction or direct monomer to micelle transition for zwitterionic sulfobetaine surfactant in water? a comparative fluorescence study with cationic surfactant. *J. Photochem. Photobiol.* **2018 (**doi.org/10.1016/j.jphotochem.2018.02.033).

Conference Presentations:

1. Poster presented in ***Chemconvene 2015,*** Indian Institute of Technology Guwahati, Guwahati.

2. Poster presented in ***ICANN 2015,*** Indian Institute of Technology Guwahati, Guwahati.

3. Oral Presentation at ***Frontiers in Chemical Sciences (FICS) -2016,*** IIT Guwahati and achieved **best Oral Presentation Award**.

4. Poster Presentation at ***20th CRSI National Symposium in Chemistry, 2017***.
5. Poster Presentation at ***Research Conclave, 2017, IIT Guwahati.***
6. Poster Presentation at ***National Workshop on FLUORESCENCE and RAMAN spectroscopy (FCS), 2017,*** IIT Guwahati***.***
7. Poster Presentation at ***International Conference on Emerging Trends in Chemical Sciences (ETCS), 2018,*** Dibrugarh University.

LIST OF SCHEMES

LIST OF TABLES

Chapter 6

LIST OF FIGURES

Chapter 1

LIST OF ABBREVIATIONS

AOT	Sodium bis(2-ethylhexyl) sulfosuccinate
BHDC	Benzylhexadecyl dimethylammonium chloride
BSA	Bovine serum albumin
CAC	Critical aggregation concentration
CB	Cucurbit-urils
CD	Cyclodextrin
CMC	Critical micellar concentration
CTAB	Cetyltrimethylammonium bromide
CTAC	Cetyltrimethylammonium chloride
DCM	Dichloromethane
DDAB	Didodecyldimethylammonium bromide
DLS	Dynamic light scattering
DTAB	Dodecyltrimethylammonium bromide
ESPT	Excited state proton transfer
HSA	Human serum albumin
HP-γ-CD	2-hydroxypropyl-γ-cyclodextrin
HPTS	8-hydroxypyrene-1, 3, 6-trisulfonate
KIE	Kinetic isotope effect
LLC	Lyotropic liquid crystalline
MCM-41	Mobil Composition of Matter No. 41
MPTS	8-methoxypyrene-1,3,6-trisulfonate
PT	Proton transfer
QCy9	Qinone-cyanine 9 dye
RM	Reverse micelle
SB-3-16 or SB16	3-(hexadecyldimethylammonio)-propane sulfonate
SB-3-12 or SB12	3-(dodecyldimethylammonio)-propanesulfonate
TCSPC	Time Correlated Single Photon Counting
TRES	Time Resolved Emission Spectra
Trp	Tryptophan
TRANES	Time Resolved Area Normalised Emission Spectra
WIC	Wobbling in Cone Model

Chapter-1

Introduction

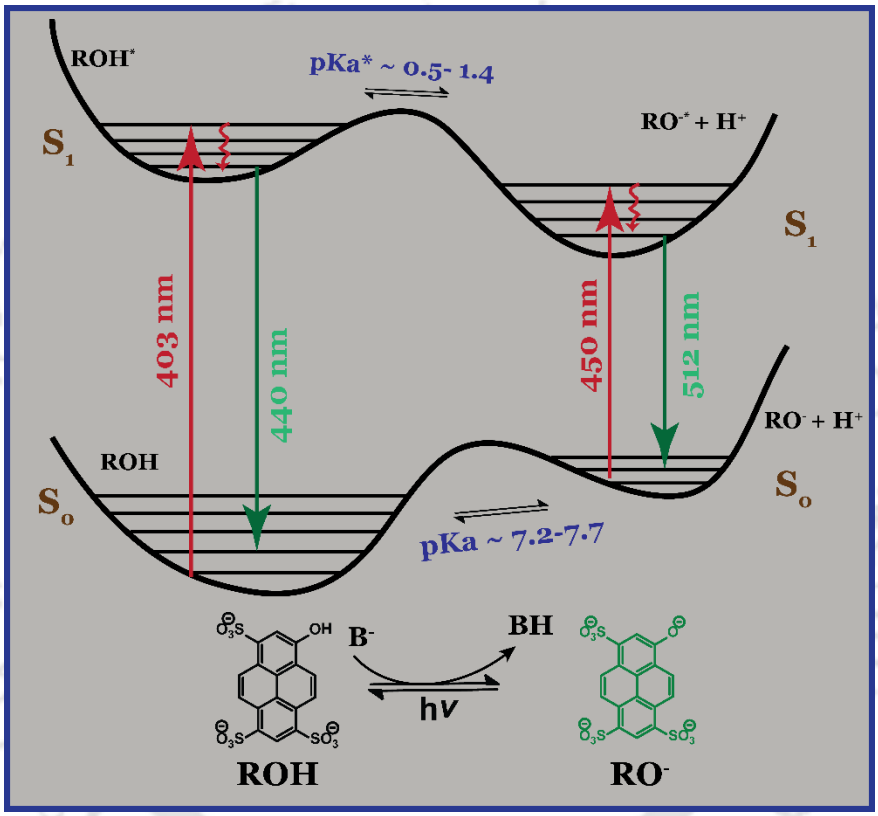

CHAPTER 1: INTRODUCTION

1.1. EXCITED STATE PROTON TRANSFER

Among many ultrafast fundamental chemical processes, proton transfer (PT) plays a key role in numerous chemical reactions, biological processes, and material properties.[1-3] Excited state proton transfer (ESPT), a variant of PT that occurs in the electronic excited state of a molecule, has been a subject of intensive research, both theoretically[4-6] and experimentally.[3] An ESPT process is commonly initiated by photo-excitation of a suitable molecule, known as photoacid. In the electronically excited state, the molecule can eject a proton to surrounding solvent or a base. Since an ESPT process usually occurs in sub-ps or ps times, the process can be probed by ultrafast laser spectroscopy.[7,8].

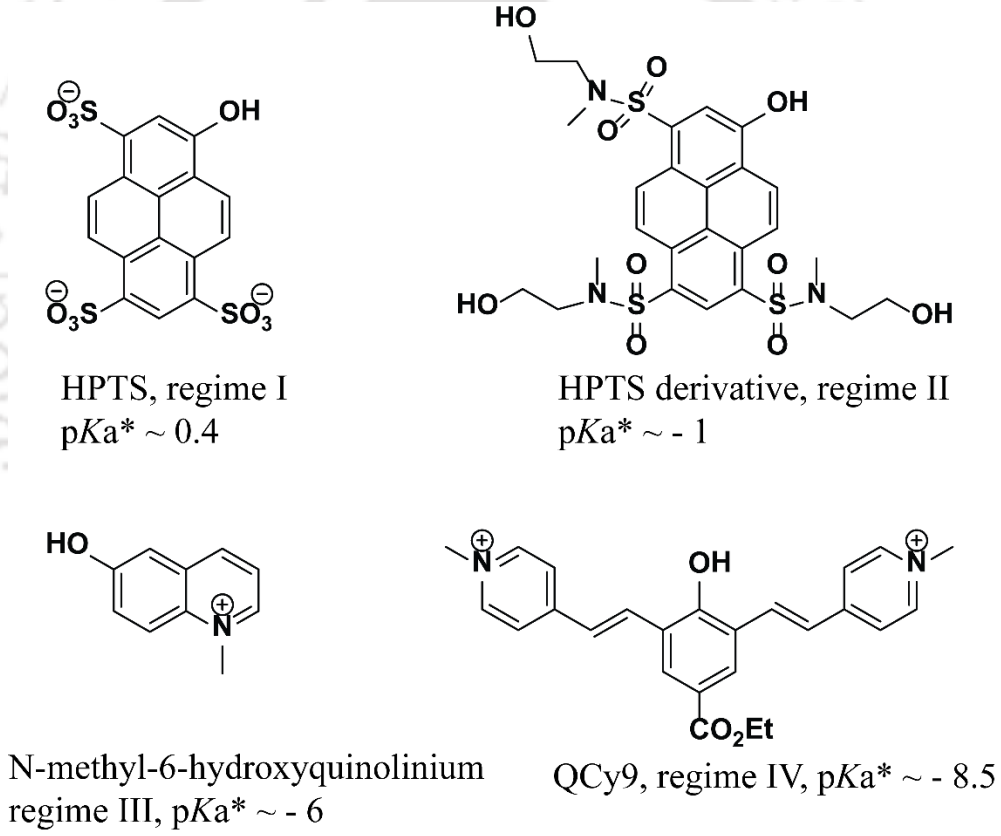

Scheme1.1: Different photo-acids representing the classified four regime.[9]

Photoacids are aromatic organic molecule that are generally weak acids in the ground state but become much stronger acids in the excited electronic state. The enhancement of photoacidity is usually governed by the ΔpK_a which denotes the difference between the p*K*a and p*K*a* values. There are numerous examples of photo-acids e.g. hydroxyl-aryls, aromatic amines etc. Huppert and co-worker have grouped photoacids into four categories according to their strength.[9] For each

group, the ESPT rate is limited by a certain physical parameter or by a fundamental stage in the proton transfer mechanism. In **Scheme1.1**, a list representing an example for each class is represented. The photoacids belonging to *regime I* are weak to intermediate strength with $pK_a^* > 0$ in water. These photoacids can effectively transfer a proton to water but not to other protic solvents like methanol, ethanol, etc.[10] Photoacids belonging to *regime II* can transfer a proton to many protic solvents. They have pK_a^* values in the range $-4 < pK_a^* < 0$. The larger the pK_a^* value, the faster is the ESPT rate. Photoacids that belong to *regime III* are even stronger photoacids with pK_a^* values of about −6 and their ESPT rate is of the same order of the dynamics of solvent orientation motion. The photoacids that belong to *regime IV* are the strongest photo-acids with $pK_a^* < -7$ and are only recently explored: e.g. Qinone-cyanine 9 dye (QCy9) and its derivatives[11] show an exceptionally rapid ESPT rate, $\tau_{PT} \sim 100$ fs was measured in water, methanol, and ethanol. These photo-acids can undergo ESPT faster than solvation dynamics.

1.2. HPTS AS MULTIFUNCTIONAL PROBE:

We employed 8-hydroxypyrene-1, 3, 6-trisulfonate (HPTS or pyranine, **Scheme 1.1**) as an ESPT probe in our studies. The probe HPTS belongs to *regime I* category of photo-acids that can undergoes ESPT only in the presence of water. This photoacid is tri-anionic and tetra-anionic, respectively, in the protonated (ROH) and deprotonated (RO^-) forms. The strong anionic nature of the RO^- strongly favours reversible geminate recombination with the detached proton over singly charged photo acids, like 2-naphthol.[12,13] The pK_a and pK_a^* of HPTS are 7.2 and 0.5, respectively.[14]

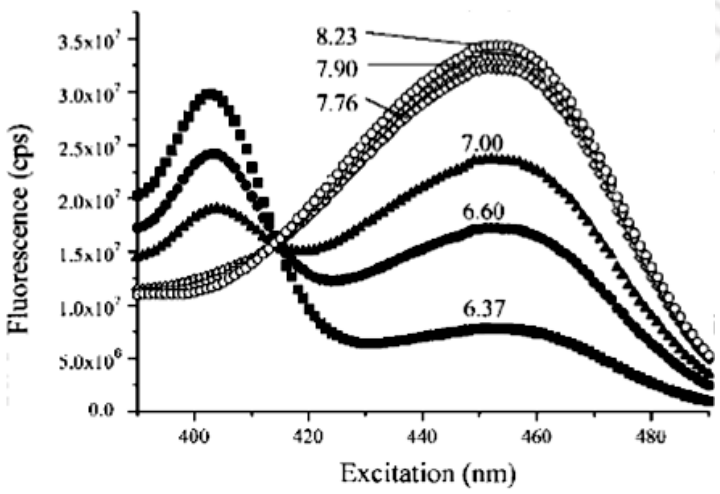

Figure1.1: Excitation spectra of HPTS dissolved in seawater (salinity of 32) at different pH values. HPTS is a dual excitation (405/450 nm) single emission (520 nm) fluorophore with pH dependent excitation and emission maxima in bulk water.[19]

For a long time HPTS has been used as a probe across different fields. The pH sensitivity of HPTS (**Figure 1.1**) is employed as an indicator in time-lapse pH imaging to explore transport of calcium and other ions from seawater within corals.[15] The high water-solubility, low toxicity and most importantly it's disability to cross the cell membrane,[16] made HPTS an appropriate choice to study intracellular pH variation.[17,18]

Interestingly, HPTS can selectively detect the greenhouse gas CO_2 when adsorbed on Ni-Fe-Layered double hydroxide (LDH) nanocomposite (**Figure 1.2**)[20] and can selectively detect amino acid arginine and lysine even with naked eye in aqueous solution and from amino acid mixture.[21]

Figure 1.2: The anionic probe loss fluorescence on intercalation within cationic interlayer of Ni-Fe-LDH nanocomposite. On exposing to CO_2 gas to the composite, CO_2 undergo intercalation as CO_3^{2-} ions replacing HPTS and thereby leading to the fluorescence recovery of HPTS.[20]

However, since we are interested in the ESPT dynamics, here we have discussed the recent trends of ESPT studies in bulk water and in different confined media and also account the various factors that control ESPT dynamics.

1.2.1. ESPT of HPTS in Water:

Water is a ubiquitous solvent of the nature. It accepts proton in aqueous acid-base neutralization reactions, where a proton is exchanged between an acid and a base, forming the conjugate base and conjugate acid, respectively; even in the excited state. Moreover, a numerous theoretical study remarked water as a facilitating agent in efficient charge separation when the proton leaves the acid[22-24].

HPTS is a weak photo-acid and transfer its acidic proton to water in the excited state at the rate of $10^{10} s^{-1}$.[25] Due to its anionic nature, HPTS can strongly attract the diffusing hydrated proton and further increases the probability of geminate recombination process.[25] The ESPT process with geminate recombination can be schematically represented in the **Scheme 1.2**.

$$ROH^* + H_2O \leftrightharpoons RO^{-*} + H_3O^+$$

Scheme 1.2 Schematic representation of geminate recombination process.[25]

The dynamics of HPTS in water was investigated initially by Pines and Huppert[26] and later by Tran-Thi et al. and Leiderman et al.[27] in the ultrafast domain.[28] Using femtosecond fluorescence and absorption spectroscopy, Pines and Huppert showed that the ESPT process occurs in ~ 70ps timescale followed by an extended tail representative of a reversible geminate recombination of the HPTS anion with the ejected proton.[26] Tran-Thi and co-workers observed three times constants of 0.3ps, 2.5ps and 87ps.[26] The first two ultrafast components were attributed to solvation dynamics and locally excited charge transfer (LE-CT) transition, respectively, while the 87ps component was assigned to proton transfer.[28] Later, Mohammed et al. reassigned these ultrafast components (0.3ps and 3ps) to H-bond rearrangement of water around HPTS prior to proton transfer.[29]

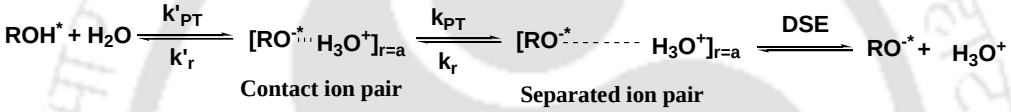

Scheme 1.3: The *Extended Reversible Diffusion-Influenced Two-Step Model*.[27]

To explain the ESPT process, in bulk water, Huppert group proposed "*Extended Reversible Diffusion-Influenced Two-Step Model"* (**Scheme 1.3**).[27] This *Extended Reversible Diffusion-Influenced Two-Step Model* suggests dissociation of excited protonated acid ROH* to a contact ion pair, consisting of an anion and a hydrogen bonded hydrated proton complex, designated as H_3O^+. The contact ion pair $RO^- \cdots H_3O^+$exhibits almost similar spectroscopic signature as the RO^-emission band in the separated and solvated ion pair. Similar models for acid dissociation were also suggested by Eigen[30] and Hynes[22,31]. To explain the bridging role of water in the proton exchange between an acid and a base in aqueous solution, two hydration structures have been proposed for the hydrated proton: the Eigen cation,[30] $H_9O_4^+$ and Zundel cation, $H_5O_2^+$.[32] The Eigen cation is composed of H_3O^+ ion strongly H-bonded to three water molecules(**Figure 1.3a**).

On the other hand, the proton resides in between two water molecules for Zundel cation. Interestingly, molecular dynamics simulations[34,35] and femtosecond mid-infrared spectroscopy[36] reveal rapid interconversion between these two types of hydrated proton species. Proton transfer rate in aqueous solution depends on the number of water molecules that separate the acid and base units and the proton proceeds between the donor-acceptor pair following Grotthuss-like mechanism in a similar way to proton diffusion in bulk water[33] (**Figure 1.3b**). The involvement

of water as the proton transfer bridge between an acid and a base during a proton transfer process is also proved experimentally.[37] The study of ionic conductivity to monitor mobility of protons and hydroxide ions in water is also proved to be a helpful technique.[38-40]

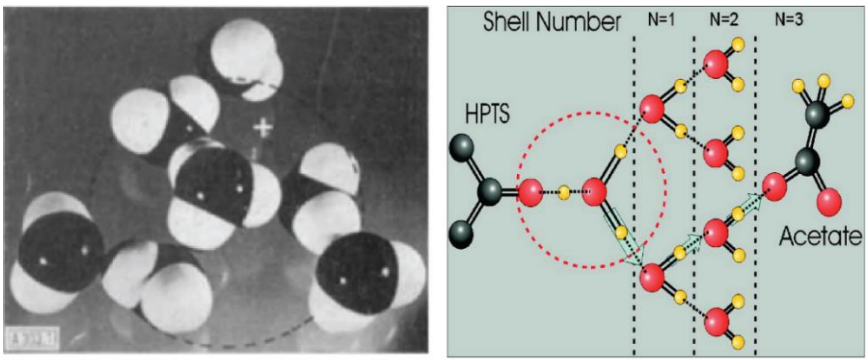

(a) Hydrated proton species, as $H_9O_4^+$ (b) Grotthuss hopping model of PT in aqueous solution

Figure 1.3: Schematic representation of proton exchange in aqueous solution (a) Eigen hydration cation: a H_3O^+ ion strongly H-bonded to three water molecules; (b) Grotthuss hopping model: H-transfer from HPTS to acetate via H-bonded water network.[30,33]

Kinetic isotope effect (KIE) is a convenient way to show whether fluorescence modulation of a fluorophore is linked with ESPT process. Stryer reported[41] observation of large isotope effect on fluorescence emission spectra of fluorophores in the presence of proton donor or acceptor group. The ESPT behaviour of HPTS also shows isotope sensitivity.[42] The rate constant of the excited state proton transfer (ESPT) of HPTS to water, k_{PT}, is $\approx 10^{10} s^{-1}$ (τ_{PT}= 100ps) becomes smaller by about factor of 3; when dissolved in D_2O (k_{PT}, is $\approx 3.3 \times 10^9 s^{-1}$, τ_{PT}= 300ps) and thus the KIE is ~3.[42]

1.2.2. ESPT of HPTS in solvent mixture:

Stronger photo-acids ($pK_a^* < 0$) are capable of transferring a proton to polar solvents like alcohols and dimethyl sulfoxide (DMSO) within the excited state lifetime.[9] However, HPTS with pK_a^* within the range 0.5-1.3 is unable to proceed proton transfer to these solvents. Interestingly, introduction of these organic polar solvents in the aqueous solution of HPTS can control the ESPT rate and the intensity ratio of the two forms, $r = I_{protonated}/I_{deprotonated}$, is found to be proportional to the alcohol to water molar ratio.[43] From the **Figure 1.4** it is clearly revealed that the variation of relative ratio of emission of the deprotonated and protonated form of HPTS as the mole fraction of DMSO is increase in the medium.[43] The ratio itself may be a convenient indicator of alcohol content in an unknown mixture of alcohol-water.[44,45]

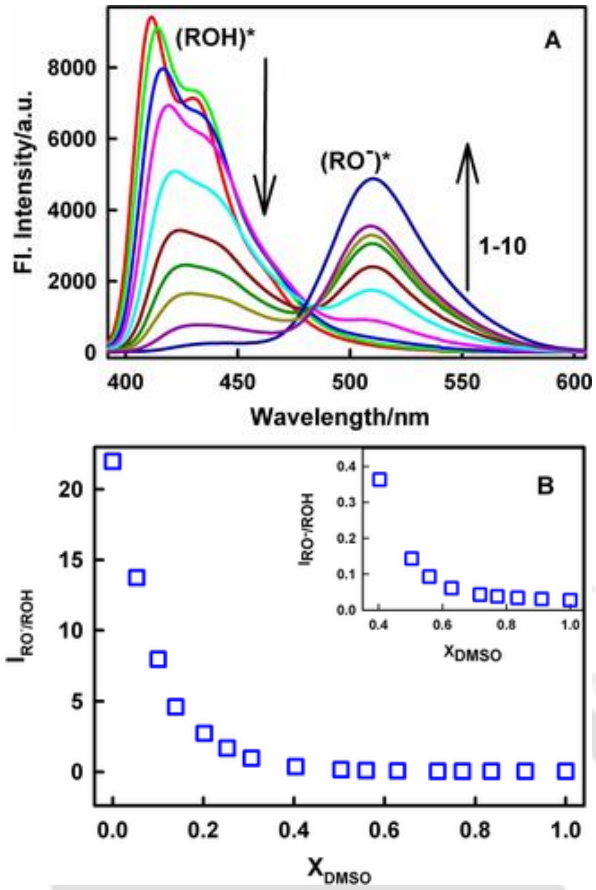

Figure 1.4: The relative intensity variation of protonated and deprotonated form of HPTS with decrease in mole fraction of DMSO in the solvent mixture. The intensity of protonated form of HPTS is deduced with concomitant increment of the de-protonated form of HPTS referring decrease in the amount of DMSO in the medium.[43]

1.2.3. ESPT of HPTS inside Confined Assemblies:

When a molecule gets encased inside a macromolecular or in a biological nanocavity, the physical and chemical properties of the molecule may change dramatically from those observed in solution.[46] This may arise from the decrease of degrees of freedom of the molecule in these confined media. This is applicable to water molecules under confinement. Interactions of water molecules with the confining surfaces can have strong effects on the proton mobility. It is to be noted that in a living organism, water molecules are present in a highly crowded environment and in a very less volume, more like a nano-pools.[47]

1.3. MACROCYCLIC HOSTS: CYCLODEXTRIN AND CURCUBIT[*N*]URIL:

Cucurbit-urils (CBs), are macrocyclic molecules composed of glycoluril monomers linked by *2n* methylene bridges.[48,49] They are highly symmetrical pumpkin-shaped hydrophobic cages of low polarity and polarizability with two identical dipolar portal ends composed of carbonyl functional groups (**Figure 1.5**).

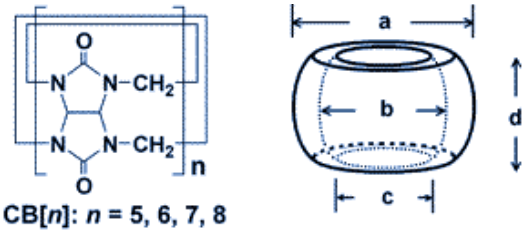

		CB[5]	CB[6]	CB[7]	CB[8]
outer diameter (Å)	a	13.1	14.4	16.0	17.5
cavity (Å)	b	4.4	5.8	7.3	8.8
	c	2.4	3.9	5.4	6.9
height (Å)	d	9.1	9.1	9.1	9.1
cavity volume (Å^3)	-	82	164	279	479

Figure 1.5: The cavity dimensions of CB[5], CB[6], CB[7] and CB[8] macrocycles.[48]

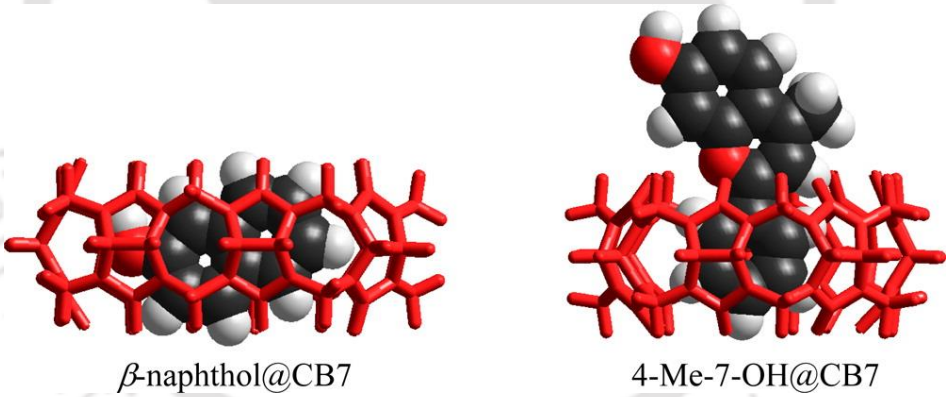

Figure 1.6: Effect of inclusion complex of cucurbit[7]uril with *β*-naphthol and 4-metyhl-7-hydroxyflavylium on ESPT dynamics.[54]

CBs, for example cucurbit[7]uril (CB7, with seven glycoluril units), have been established as a versatile and interesting host molecules. They can form stable inclusion complexes with small guest molecules like organic dyes,[48] metal cations, protonated amines[48] and cationic dyes such as rhodamines,[50,51] thioflavin T[52] via a combination of hydrophobic and ion-dipole interactions. The ESPT dynamics of *β*-naphthol and 4-metyhl-7-hydroxyflavylium display contradictory results upon inclusion complex formation with CB7.[53] No ESPT was observed for the CB7: *β*-naphthol inclusion complex.[54] This was attributed to the complete inclusion of the *β*-naphthol inside the CB7 cage and hence no access to water. However, 4-metyhl-7-hydroxyflavylium still undergoes

ESPT. It was suggested that only a part of the fluorophore is inside the CB7 and the acidic hydroxyl proton remains exposed to water environment allowing ESPT[54] (**Figure 1.6**). Thus, ESPT depends on the binding pattern and the local environment around the photoacid.

The *cyclodextrin (CD)* are macrocycles composed of D-glucopyranose monomer units interconnected by ether linkages in a cyclic manner.[55,56] Depending upon the number of monomer units involved, different CD homologues with varying cavity sizes are possible. For example, α-CD, β-CD and γ-CDs have 6, 7, and 8 D-glucopyranose units, respectively (**Figure 1.7**). These natural CDs are very important in the field of supramolecular host–guest chemistry. The presence of the hydroxyl groups at the portals of CD molecule makes their external surface fairly polar in nature and also makes them water soluble. However, the interior of the cavity is nonpolar in nature.[46,57] This unique geometric arrangement is very essential for the encapsulating nature of CDs.

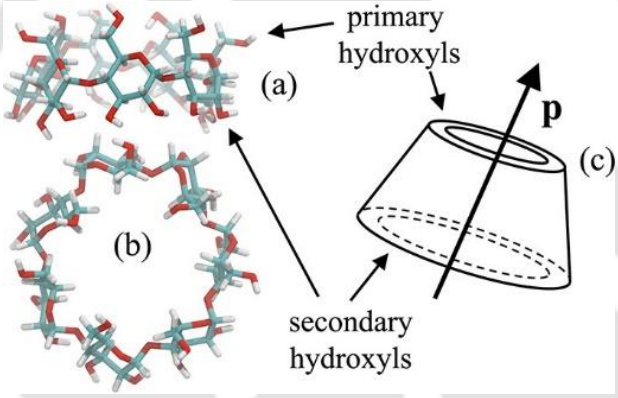

Typical cavity dimension of α-CD, β-CD and γ-CD hosts			
	α-CD (n = 6)	β-CD (n = 7)	γ-CD (n = 7)
Cavity depth	7.9Å	7.9Å	7.9Å
Wider rim diameter	5.7Å	7.8Å	9.5Å
Narrower rim diameter	5.3Å	6.0Å	7.5Å

Figure 1.7: Representative structures of β-CD: (a) side view and (b) front view (looking through the pore) and (c) a schematic representation as a truncated cone.[67] Cavity dimensions of α-CD, β-CD and γ-CD are also tabulated for a comparison.[56]

CDs can encapsulate a variety of guest molecules, through noncovalent interactions, resulting in the formation of well-defined host–guest complexes.[58-60] However, other specific noncovalent interactions like hydrogen bonding, dipole–dipole interaction, etc. can also contribute substantially to the extra stability of the host–guest inclusion complexes.[59,61,62] The ability of CDs to alter physical, chemical, and biological properties of guest molecules through the formation of inclusion complexes have made them a potential candidate for carrying and delivering drugs to a targeted site for a necessary period of time.[63] This encapsulation enhances the solubility, stability, and bioavailability of drug molecules.[64-66]

HPTS also serves as a guest to *γ*-CD (the height of the *γ*-CD cavity is about 8 Å, and the maximum inner diameter is 9.5 Å[68].) but not the smaller CDs. It was found that the ESPT dynamics modulates significantly upon encapsulation within *γ*-CD; the initial proton transfer and the dissociation of geminate ion pair becomes retarded while the rate of recombination of the geminate ion pair enhances.[69]. The slowing down of the overall proton-transfer rate was attributed to the rigidity of the water hydrogen bond network and slower solvation inside the cavity.[69] The excited state proton transfer dynamics from HPTS to acetate also gets slower in *γ*-cyclodextrin (*γ*-CD) and 2-hydroxypropyl-*γ*-cyclodextrin (HP-*γ*-CD) cavities (90 and 200ps) than in the bulk water (0.15 and 6ps) due to confinement effect and rearrangement of hydrogen bond network inside the cavity, where the acetate molecule is separated from the -OH group of HPTS by water bridges.[53] Notably, the ESPT dynamics is even become slower in substituted *γ*-CD than that in the unsubstituted one. This was attributed to the hydroxyl-propyl groups which prevent close approach of acetate to HPTS.[53]

1.4. PROTEIN AND PROTEIN-SURFACTANT COMPLEX:

Proteins offer a unique confined medium for proton transfer and plays an important role in the transport and distribution of various complex chemical and biological systems, such as fatty acids, drugs, and steroid hormones.[70] Mostly when a photo-acid binds to the protein surfaces, it senses water molecules whose properties and dynamics are very different from bulk water.[71] When bound to human serum albumin (HSA, the most abundant blood plasma protein) HPTS undergoes proton transfer in a large time window, spanning from 150fs to ~1.2ns.[72] The shortest component was attributed to the direct ESPT reaction within the probe-protein complex while the slower components were indicative of the slower dynamics of the biological water molecules that are involved in the proton transfer reactions.[72]

Very recently, it has been demonstrated that if the protein itself possesses a proton accepting domain, the ESPT process may become even faster than bulk water.[73] In the protein protamine, an ESPT component of 65ps was observed which was significantly faster than the ESPT component (95ps) of HPTS in aqueous buffer. This component was assigned to direct proton transfer to proline (pro8) amino acid residue at the binding site of the protamine protein (**Figure 1.8**).[73]

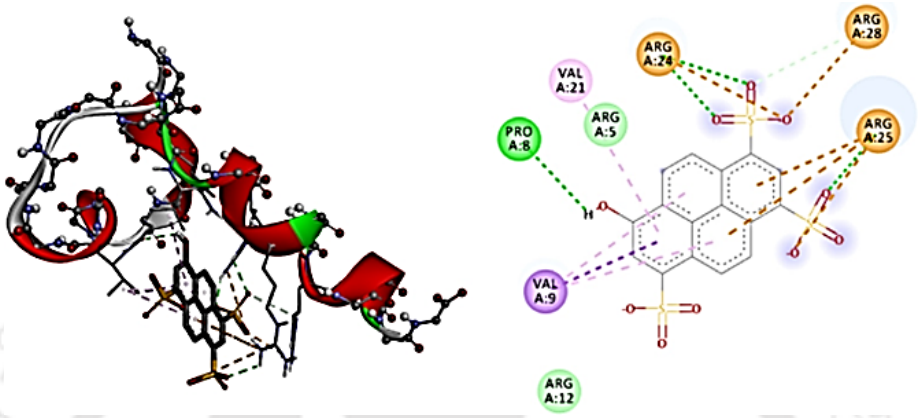

Figure 1.8: The HPTS-protamine protein complex. HPTS can directly transfer proton to proline (pro8) amino acid residue at the binding site even faster than in bulk water.[73]

The structural and conformational changes of proteins are of great concern and several spectroscopic methods e.g. circular dichroism,[74-76] Fourier-transformed infrared spectroscopy (FTIR),[77,78] NMR,[79] small-angle X-ray scattering (SAXS)[80] and electron paramagnetic resonance[81] have been used. For fluorescence probing, the polarity sensitive nature of the tryptophan (Trp) residue is widely used.[82] The basic idea is that if the Trp is buried deep inside the hydrophobic protein moiety, it normally displays an emission maximum at 308 nm but whenever the protein becomes unfolded and the Trp residue is exposed to water and undergoes a red shifting to 355 nm.[83,84] However, all the proteins do not contain Trp residue and many proteins contain multiple Trp residues making interpretation difficult. HPTS may be a good alternative to track structural transition of proteins at different pH and concentration.[85]

The protein BSA may exist in as many as five reversible conformations depending on pH: “normal” form (N-form) at a neutral pH (pH = 4.3−8), “expanded” form (E-form) below a pH 2.7, “fast” form (F-form) between a pH of 2.7 and 4.3, “basic” form (B-form) between a pH of 8 and 10, and “aged” form (A-form) above a pH of 10.[86,87] The F → E structural transition of BSA disrupts its tertiary structure.[88,89] However even after this conformational change, BSA possesses active sites which can successfully bind HPTS (BSA-HPTS protein binding site is not evaluated[85]). At this pH (~2) addition of BSA leads to increase in emission from protonated band

like that at pH 7. This slower ESPT of HPTS inside BSA was attributed to the limited accessibility to water molecules upon binding to BSA.[85] But interestingly, only at pH 2 after a threshold protein concentration (~ 0.75-1%), the protonated emission intensity starts to fall up to a concentration of 8%. These emission behaviour of HPTS clearly reveals occurrence of second structural transition at ~ pH 2 apart from the reported F → E structural transition. This pH and concentration induced conformation transition can cause significant changes to the configuration of active binding site that may even result in release of HPTS from the bounded state.[85] The SAXS study also suggested protein structural transition from unfolded to globular conformation at pH 2 for 1% BSA concentration.[90]

Another antibacterial human enzymatic protein, lysozyme is widely used as a model biological system for the understanding of folding and dynamics, structure–function relationships and ligand–protein interactions.[91,92] Higher stability, high natural abundance in tissues, saliva, tears, milk, mucus etc. and smaller size than serum albumin protein have magnified its beauty.[93,94] When HPTS is bound to this protein at pH 7[95], in the electronic ground state the anionic form of HPTS becomes thermodynamically more favourable than the protonated form (**Figure 1.9a**). and both the p*K*a and p*K*a* values are downshifted by a factor of ~ 0.4 (**Figure 1.9b**).[95]

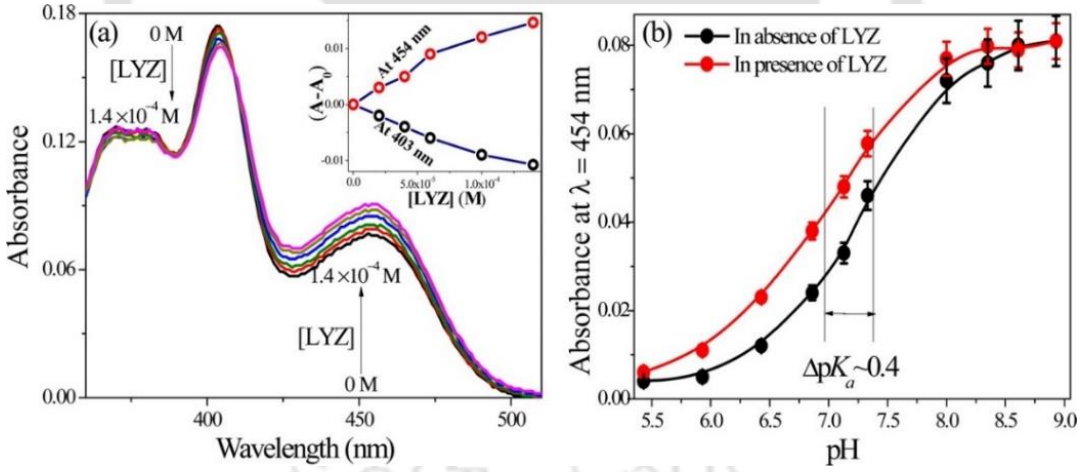

Figure 1.9: (a) Absorbance spectra of HPTS with increase of lysozyme concentration at pH 7. The inset shows the absorbance variation upon addition of lysozyme. (b) Determination of ΔpK_a of HPTS.[95]

On the contrary, excited state proton transfer rate gets slower with ESPT time constant of ~140 and ~750ps[95] than in bulk water (~95ps[96]). This slower time constant 750ps clearly refers to the presence of highly confined water molecules nearby HPTS-lysozyme binding which are reported to be responsible for this slower proton transfer.[97] The slower solvation of ~530ps for eosin[98] bound to lysozyme also revealed its restricted environment for water molecules with

disrupted H-bonding network. However, the other component of 140ps ascribed to presence of water molecules loosely associated to the protein.[95]

This protein-surfactant interaction plays an important role in protein folding,[99] modifies the surface charges and thereby enhances biological activities and aggregation properties of the protein.[100] The ESPT dynamics of HPTS can also be employed in exploring *protein- surfactant* (lysozyme-CTAB) *interaction* and to distinguish the surfactant protein complex from the micelle.[101] But at first sight this lysozyme- CTAB interaction seems quite unrealistic as both possess cationic properties at pH 6.5.[102] However, micro-calorimetric study revealed that the dominated hydrophobic interaction over the electrostatic repulsion[103] leads to the formation of lysozyme–CTAB aggregates at a critical association concentration (CAC) of ~0.4mM for CTAB.[101] The ESPT behaviour of HPTS in this medium is quite interesting as the anionic HPTS binds strongly to the cationic CTAB and lysozyme; leading to slower proton transfer.[71,101] However, HPTS undergoes faster deprotonation ($5 \times 10^3 ps^{-1}$), recombination ($4.2 \times 10^3 ps^{-1}$), and dissociation ($1.6 \times 10^3 ps^{-1}$)of geminate ion pair inside the lysozyme–CTAB aggregate compared to in the CTAB micelle ($1 \times 10^3 ps^{-1}$, $0.14 \times 10^3 ps^{-1}$ and $1 \times 10^3 ps^{-1}$ respectively for deprotonation, recombination and dissociation of geminate ion pair).[101]

Now-a-days the fundamental goal in the battle against cancer is to design drugs that can selectively attack the cancer cells.[104,105] For this, it is important to recognize the morphological and physiological differences between malignant and normal tissues. The basis of altered intracellular distribution of molecules relies on the differences in intracellular pH gradients.[106,107] The proton transfer dynamics study of HPTS in live normal and cancer effected lysozyme region of lung cells is able to clearly differentiate their nature and properties.[108] The viscous nature of cancer cell is revealed by the slower rotational relaxation time of HPTS (~ 1330ps for cancer cell and ~ 470ps for normal cell) compared to normal cell. Additionally, the faster dissociation of geminate ion pair (τ_{diss}~ 80ps and ~ 120ps in cancer and normal cell respectively) and slower recombination time (τ_{rec}~ 25ps and ~ 30ps in cancer and normal cell, respectively) refer to more crowded and less polar environment in cancer cells.[108]

Thus, HPTS is a successful intracellular pH indicator that can even able to provide insight of protein interior and surfaces.

1.5. MEMBRANES, SURFACES AND POROUS MATERIALS:

To understand the accessibility of water at biological surfaces like insulin amyloid fibrils, cellulose etc. HPTS has been employed.[109,110] When it adsorbs on insulin amyloid membrane the

ESPT rate is decreased to k_{PT}~$10^9 s^{-1}$ (in bulk water k_{PT}~$10^{10} s^{-1}$)[25] revealing its hydrophobic nature.[109] On the other hand, the polysaccharide cellulose (**Figure 1.10a,**) behaves like a molecular sponge (can adsorb high percentage of water that can be easily removed by evaporation[111]) and ESPT from HPTS is dependent on the weight percentage of water adsorbed by it.

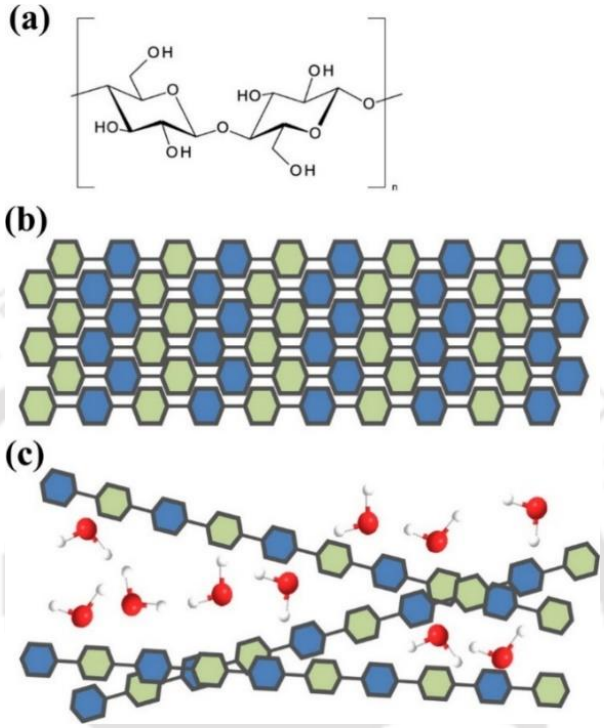

Figure 1.10: (a) Molecular structure of cellulose and a schematic representation of the molecular packing in (b) the dry (crystalline) and (c) hydrated states.[109]

When HPTS adsorbs on dry cellulose (**Figure 1.10b),** the emission spectrum mostly (~ 95%) composed of ROH emission and only ~ 5% was contributed by the RO^- emission. The de-protonated emission arises from the presence of humidity. The ESPT process remains slow (τ_{PT} ~ 3-10ns) for absorption of water molecules up to a certain extent (about three water molecules per glucose ring). These water molecules possess characteristics of bound water. However, with adsorption of more water molecules tends to create water pool with free-water like properties within the cellulose framework (**Figure 1.10c)**. At this water-rich condition, HPTS molecules move from the surface regions of cellulose to the water pool. Thus, HPTS provides information on the diffusion of water molecules and hydronium ions (protons) in biological systems.[109]

Porous materials like MCM-41 (i.e. Mobil Composition of Matter No. 41)[112] or zeolites have been intensively studied with regard to technical applications as catalysts and catalyst supports.[113-115] The study of proton transfer dynamics in this membrane has great importance for designing of electro-optic devices.[116-119] In absence of water, HPTS exists as aggregates in DCM suspension due to strong $\pi-\pi$ interactions (**Figure 1.11A**). This is manifested by broad emission band at 520

nm and multi-exponential emission decays ($\tau_{solid\ state/\ DCM}$ 120 ps, 600 ps and 2.2 ns).[120] After adsorption on MCM-41 membrane, population of these aggregates decreases and HPTS prefers to exist in monomeric form. When these HPTS and HPTS/MCM-41 complexes dispersed in DCM are exposed to water, HPTS undergoes slower recombination and proton transfer (τ_{rec} =7.5 Å ns^{-1}, k_{PT} = 13 ns^{-1} and τ_{rec} =2.2 Å ns^{-1}, k_{PT} = 5.4 ns^{-1} respectively) due to decrease of its photoacidity and the reduction of the diffusion space of adsorbed HPTS and water molecules (**Figure 1.11B**).[120]

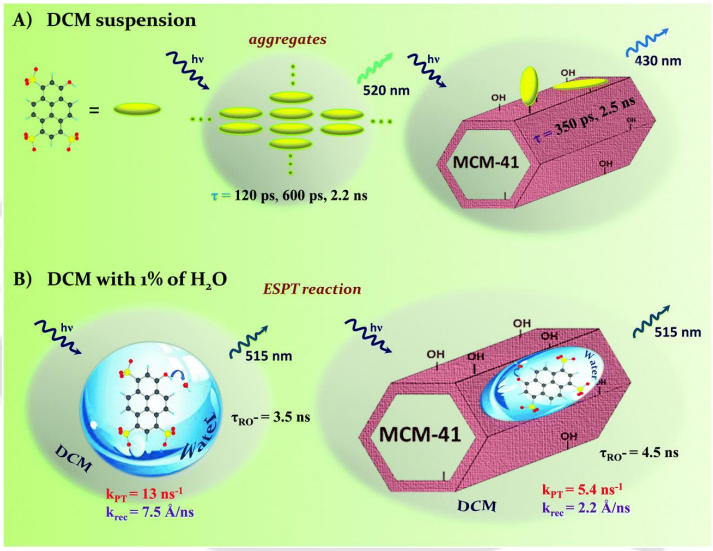

Figure 1.11: Schematic illustration of (A) HPTS and HPTS/MCM-41 in a DCM suspension and (B) HPTS trapped within a water droplet in a DCM suspension, and adsorbed on the MCM-41 surface.[120]

Nafion, a perfluorosulfonate polymer, is an another important membrane composed of teflon (polyfluoroethylene) backbone with fluoropolymer pendant chains and hydrophilic sulfonic acid headgroups (**Figure 1.12a**) which has been most extensively used as a proton transporter in fuel cell.[121,122] The difference in polarity between the backbone and headgroups creates hydrophilic domains with nanoscopic channels that swell up with level of hydration.[122] The level of hydration is usually defined in terms of a ratio of water to sulfonate molar concentration $\lambda = \frac{[water]}{[SO_3^-]}$.[122] These channels are thought to be responsible for proton diffusion through the membrane and can be controlled by the nature of the pendent chain and hydration level.[123]

Fayer group studied ESPT of HPTS inside the nanochannels of nafion to link the confinement and the proton transport nature[122-124] and also compared the ESPT dynamics inside nafion membrane with AOT (sodium dioctyl sulfosuccinate) reverse micelle.[122] The hydrophilic groups of AOT and Nafion are quite similar as they both contain sulfonate groups. For both

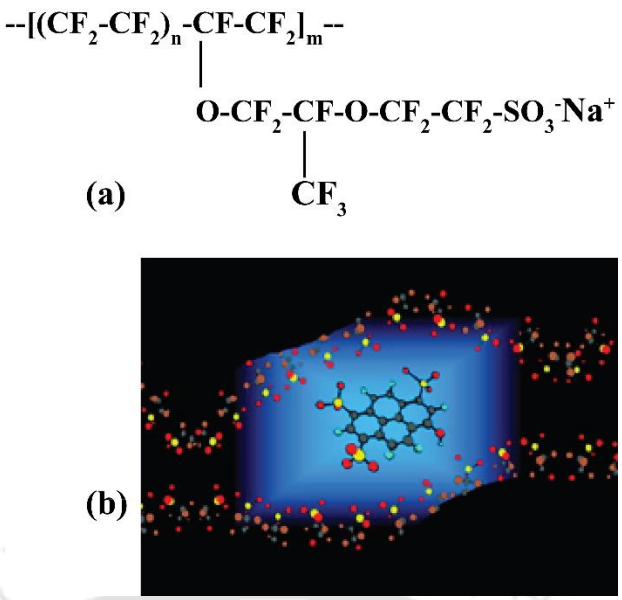

Figure1.12: (a) The repeating unit of nafion and (b) HPTS and nanoscopic water channels inside nafion membrane.[122,124]

systems, the proton transfer dynamics was observed to be slower with the decrease of water level.[122] But unlike AOT reverse micelle, Nafion membrane does not have a consistent interfacial structure and with increase in hydration level the pendent chain as well as sulfonic acid headgroups rearrange to stabilised water cluster.[125,126] The ultrafast IR pump-probe spectroscopic study [124] and solvation dynamics study[127] clearly reveal the orientation of water molecules in two ensembles inside the nafion membrane; viz., interfacial headgroup bound water and bulk like free water (**Figure 1.12b**).[124,127] These studies are quite important as the nature of proton transport and proton mobility in nafion nanoscopic channels is crucial in fuel cell operation.

The lipid-based lyotropic liquid crystalline (LLC) materials have received special attention because of their increasing utility in material science,[128] biomedical,[129] drug delivery,[130] protein crystallization[131] and food technology.[132,133] The materials can be prepared by binary mixture of an amphiphilic surfactant (especially lipid) and water.[134] 1-linoleoyl-rac-glycerol (GML), is often chosen as surfactant due to its excellent biocompatibility, outstanding phase behaviour and extensive applications in the scientific, industrial, and technical fields.[135] With slight variation of water content and temperature, different GML-based LLC materials can be prepared, e.g. reverse hexagonal (H_{II}), diamond (D) Pn3m, and gyroid (G) Ia3d phases. Topology of these materials have close resemblances to the architecture of biological membrane present in eukaryotic cells,[136] mitochondrial inner membrane in amoeba,[137,138] chloroplasts[139] etc. They also play a unique role in the controlled drug delivery,[140] enzymatic reactions,[141] size controlled material synthesis[142] and single crystallization process.[143] The H_{II} phase adopted inverted "water-in-oil" version

structure,[144] while Ia3d (gyroid type) and Pn3m (diamond type) phases exhibit inverse and bi-continuous structure.[145] In these phases, the number of free water molecules vastly reduces due to H-bonding with –OH group of GML, leading to decrease in proton transfer rate. The slower dissociation time constant in these phases (τ_{diss} ~ 1010, 980, and 735ps for Pn3m, Ia3d, and H_{II} phases respectively) compared to τ_{diss} ~ 350ps[146] in water support this scenario. Notably, the decay component of neutral form matches with the rise component of anionic form and appear two rise components (200ps and 1.3ns for Pn3m) much slower than in water. The two rise components refer to presence of two different types of water environments: quasi free and bound water. In these phases the ESPT dynamics vary following the sequence of H_{II} < Ia3d < Pn3m < H_2O even at the presence of equal content of water. This observation clearly reveals the topological influences in proton transfer dynamics.[147]

1.6. MICELLES AND REVERSE MICELLES:

Micelle and reverse micelles are well-known surfactant assemblies and often used as models of confined media.[148,149] The mono-glycerides and fatty acids combine with bile salts and phospholipids may form micelle and are used in the transport of the poorly soluble mono-glycerides, fatty acids, fat soluble vitamins and cholesterol to the surface of the enterocyte where they can be absorbed.[150-152] In vitro the micelle or reverse micelle are formed by the self-assembly of the surfactant molecules in a precise fashion, depending on the nature of the continuous phase.[153] At room temperature and in bulk water, surfactant molecules arrange as micelle (polar head-groups exposed to water molecules keeping the hydrophobic long alkyl chains away) upon exceeding a critical micelle concentration (CMC) of the surfactant molecule.[154] The ESPT probe can signify this critical point,[155-157] as the proton transfer dynamics changes in the micelle interfaces from bulk water (τ_{PT} in P123 micelle is 65ps, which is 10 times slower than that in water 5ps[158]).[159,160] Several ESPT studies also reveal the presence of surfactant aggregation before CMC.[161,162] However, the probe-surfactant binding depends on the length of the alkyl chain of the surfactant and nature of surfactant headgroup.[163] For the C_nTAB surfactant series, the intensity ratio of ROH and RO^- follows the order of CTAB > TTAB > DTAB > water.[164]

Interaction of polymer chains with surfactants has also received quite attention.[165-167] In aqueous solutions, polymers readily form aggregates with surfactants above a particular surfactant concentration, known as the critical association concentration (CAC) because of its hydrophobic effect.[168] The CAC for a polymer−surfactant system is often very much lower than the critical micellar concentration (CMC) of the surfactant[169], e.g. the CAC of P123 and CTAC is reported to be ~ 0.25mM[170] far lower than CMC of CTAC (~ 1.3mM[171]). The proton transfer dynamics can

reveal nature of these polymer-surfactant assemblies.[172,173] In P123-CTAC aggregate, HPTS displays three rise times: 30, 250, and 2400ps even longer than those in CTAC micelle (23, 250, and 1800ps), in bulk water (0.3, 3, and 90ps), and in P123 micelle (15 and 750ps).[173] The two rise times arise in the P123−CTAC complex (250 and 2400ps) suggest the presence of two precise locations, a "fast" and a "slow" site. The proton transfer rate (k_{PT}) in P123 micelle, in the two sites of the P123−CTAC complex are 1.52×10^{10} s^{-1}, 1.79×10^{10} s^{-1} and 1.37×10^{10} s^{-1}, which are much slower than in bulk water is 18.5×10^{10} s^{-1}.[173] These observations clearly refer to a different microenvironment for P123−CTAC aggregates from bulk water or P123 (or CTAC) micelle.[173]

On the other hand, in non-polar continuous phase surfactant molecules get assembled entrapping an aqueous (or other polar solvent) droplet suspended in a nonpolar solvent.[148,174] The size of the confined water pool as well as the reverse micelle depends on the w_0 value, where w_0 = [water]/ [surfactant].[175] As the w_0 increases, the surfactant molecules are exposed to more water molecules leading to the increase in the size of the water pool with concomitant increase in the reverse micelle size. The change in reverse micelle size leads to an instantaneous changes in the local environment inside the cavity.[175-178]

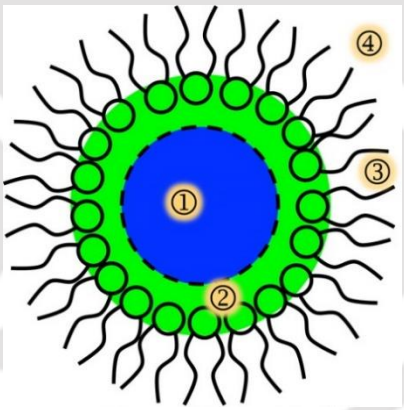

Figure 1.13: Schematic representation of a reverse micelle. It is composed of four heterogeneous regions, (1) intra-micellar water pool with bulk water character, (2) aqueous interfacial region. Charged particles, including H^+ and OH^- migrate to this region that change its local pH from the apparent pH in the reverse micellar core, (3) surfactant layer and (4) nonpolar phase.[179]

A lot of studies reported heterogeneity of the reverse micellar medium.[179-181] The water confined inside the reverse micelle can be separated into two regions: firstly, a few layers of water near to the negatively charged surfactant headgroups, i.e. in the interface region and secondly, water residing at the core of the water pool with relaxation time constants of 0.5−1.7 and 3.5−11.8 ns attributed to "free" and "bound" water reorganization, respectively.[179,182] The properties of these two broadly different regions bring changes in the H-bonding capability and dynamics. The

difference between the interface and the core water molecules becomes more prominent with increase of reverse micelle size and the properties of core water approaches more like bulk water (**Figure 1.13**).[179]

The polarity of water pool encased within the reverse micelle increases with increase in micellar radius followed by enhancement in the number of free water molecules, e.g. in AOT reverse micelle micro-polarity of water increases up to w_0 = 10.[183,184,185] Molecular dynamics simulation study also revealed that the ions present in the interface can efficiently bind to the surfactant polar headgroups and also regulate the polarity of interfacial water.[186] These interfacial water molecules lead to increase in the effective dielectric constant at the water/surfactant interface that reached a plateau at w_0 = 12.[187] Not only polarity, the solvation dynamics also increases with increase of reverse micelle size, yet they cannot achieve the bulk like faster solvation dynamics due to strong binding of interfacial water molecules to the polar surfactant headgroup.[188]

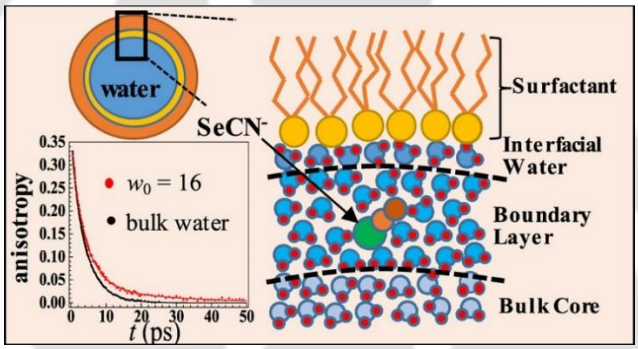

Figure 1.14: Orientation of the water molecules inside AOT reverse micelle. The H-bonding of the water molecules in the interfacial region is interpreted by their binding to surfactant polar headgroups and the boundary layer is also perturbed by the interfacial water molecules.[189]

The IR pump–probe measurements on large RMs ($w_0 \geq 16$) suggested the presence of two HODs populations, which have distinct vibrational lifetimes and reorientation dynamics.[181] This observation can be described by a core-shell model. The "core" region is separated from the interface and has bulk water properties and displays faster vibrational lifetime of 1.8ps and an orientational relaxation time of 2.6ps. The interface region exhibits a slower dynamics with vibrational life time of 4.3ps and orientational relaxation time constant of 18ps.[181] Interestingly, use of $SeCN^-$ (**Figure 1.14**) as vibrational probe in reverse micelles ($w_0 \geq 16$) shows presence of a slower orientational relaxation time constant of ~13ps in addition to faster bulk water like relaxation time constant of 1.4 and 4.5ps.[189] This slow component indicates presence of an intermediate transition region between interfacial and core water (**Figure 1.14**). Water molecules of this boundary region are perturbed by the interface but are not directly associated with it. This

is the transition layer between water in direct contact with the interface and bulk water in the large RM core.[189]

The large interface of reverse micelle allows reactants that prefer different phases to be brought together. For example, most enzymes, being highly polar molecules, are much more soluble in aqueous phases, but many substrates are soluble only in nonpolar solutions, so that reactions between the two will only occur if there is a sufficient interface between the phases[190-192] (**Figure 1.15**).

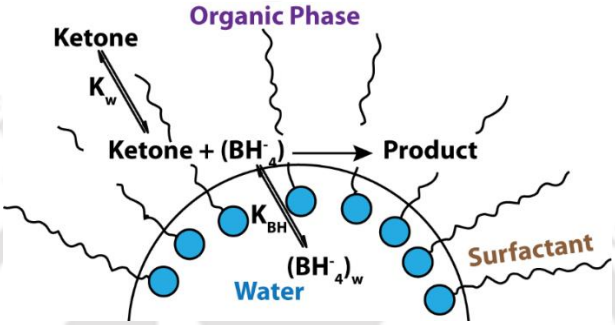

Figure1.15: The reduction of hydrophobic ketone by water soluble sodium borohydride ($NaBH_4$) occur at the reverse micellar interfaces.[190]

The unique confinement effect of reverse micelle made it a good model system of various biological phenomenon and elementary processes such as enzymatic reactions[193], chemical catalysis[190,194,195], solvation dynamics[149,196], photo-induced electron transfer[197], excited state proton transfer (ESPT), etc.[9,198] and a widely used system in photo-physics. Noted if the surfactant molecule composed of particular functional group like the oxygen atoms (and OH) of TX-100 in RTIL/TX-100/benzene reverse micelle, HPTS undergoes ESPT (the deprotonated form exhibits three rise components of 0.3, 14, and 375ps) even in the absence of water.[199] Interestingly, the first two rise components are even faster than the proton transfer rate in bulk water (ESPT time scale of ~95ps[96]).

The proton transfer dynamics is controlled by the availability of the proton acceptor, solvation of the proton, dissociation of the geminate ion pair, and diffusion of the ion pair.[200,201] The size of reverse micelle is related to availability of proton acceptor, polarity of its confined medium.[148,14,202] Interestingly, this ESPT dynamics of HPTS can also explore the nature and properties of confined water inside the reverse micelle.[203,204] The ESPT dynamics revealed that both the dielectric relaxation of the free water,[203] and proton transfer rate is significantly slower in smaller reverse micelle than bulk water regardless of surfactant type (At w_0 = 8 for AOT RM, k_{PT} = 221 ps^{-1}).[205] However they approaches to bulk like behaviour with the increase in reverse

micelle size (at w_0 = 15 for AOT RM, k_{PT} = 85 ps^{-1})[205].[149,159] The proton transfer dynamics in a confined medium can also be regulated by location of the photo-acid.[72,180,206]

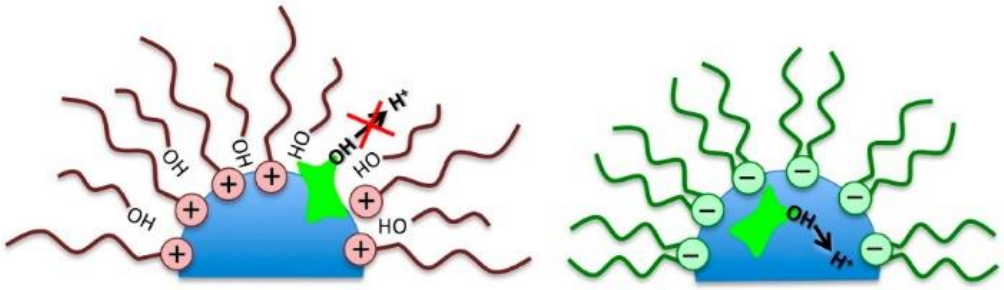

Figure 1.16: The localization of the HPTS molecule in reverse micelle water is regulated by the electrostatic nature of the surfactant molecules. HPTS localised in the reverse micelle core water in the anionic water/AOT/cyclohexane reverse micelle that favours the ESPT dynamics unlike the hydrophobic interfacial region of the water/CTAB/*n*-octanol/cyclohexane reverse micelle.[180]

Levinger group investigated this phenomena for HPTS in anionic AOT RM and cationic CTAB RM, using ultrafast time-resolved transient absorption and two-dimensional NMR spectroscopies.[180] The 2D NMR results show strong interaction of probe with the surfactant headgroups in cationic CTAB RM, no interaction is arise in ionic AOT RM and thus ensured distribution of the probe in two different locations. The ultrafast study revealed presence of ESPT in AOT RM and unable to detect ESPT at the interface of CTAB reverse micelle, suggesting presence of dry interface (**Figure 1.16**).[180] But molecular dynamics simulation study clearly revealed penetration of significant amount (~30%) of water into the CTAB/hexanol/*n*-pentane/water quaternary RM[207]. Moreover increases in ESPT for HPTS located at the interface of neutral Igepal CO-520 reverse micelle with the increment of reverse micelle size suggests penetration of water content into the interface.[208]

The single tail surfactants like cetyltrimethylammonium bromide (CTAB), sodium dodecyl sulphate (SDS), Triton-X etc. need contribution of another co-surfactant e.g. medium or long chain alcohol to satisfy the necessary geometric condition $^{v}/_{al} > 1$, where v refer to volume and l is the chain length of the hydrocarbon tail, a polar headgroup area of the surfactant molecule to form a stable reverse micelle.[209,210] The co-surfactant is usually assumed to be inserted in-between the surfactant molecules at the interface of the quaternary reverse micelle and introduced a new parameter (p_0 = [co-surfactant] / [surfactant]) in addition to prevalent parameter, w_0 (= [water] / [surfactant]). The capability of this new parameter to control the size and properties of the RM like flexibility and applicability of the RM enhance the importance of this quaternary RM.[211]

Interestingly, compared to neutral, anionic or cationic surfactant, zwitterionic surfactant: combining two opposite charges in its headgroups exhibits many intriguing features, e.g. excellent biocompatibility and biodegradability, good water solubility, and can even withstand higher temperature.[212-215] In aqueous medium these sulfo-betaine surfactant assembled in L-shaped geometry within the micelle interface; exposing the cationic ammonium group towards water.[214] Due to this behaviour sulfo-betaine micelles behave more like cationic micelle, even after the presence of an anionic headgroups.[214]

1.7. OBJECTIVES OF THE THESIS:

The ESPT of HPTS depends critically on the nature and dynamics of water inside an organized assembly. Being highly negatively charged, HPTS behaves like an organic anion and its location inside an assembly is often dictated by the electrostatic feature of the assemblies. Thus, it is of great promise to utilize this photoacid to probe selectively a region of a reverse micelle and micelle. We establish the connection between the ESPT dynamics and the local hydration inside a cationic surfactant, subtle change in interfacial hydration can be sensed. How the hydration can be effected by the presence of co-surfactant or with the overall change of the reverse micellar shape. We also applied the ESPT as indicator of alcohol solubilisation and established that the solubility properties of confined water may differ greatly from that of normal (bulk) water. We can also selectively compare the interfacial properties of two micelles of two different classes.

Chapter-2

Materials and Experimental Methods

CHAPTER 2:

EXPERIMENTAL AND ANALYSIS METHODS

In this chapter, we have mentioned specifications of all the instruments used in our works including UV-Vis, steady-state and time-resolved fluorescence (TCSPC), nuclear magnetic resonance (NMR) and dynamic light scattering (DLS). We also added sources of all chemicals used and all sample preparation procedures including various data analysis methods, models and so on.

2.1. STEADY-STATE MEASUREMENTS:

Absorption spectroscopy is one of the most useful spectroscopic tools. UV-visible absorption study provides important information about the wavelength of transition and the corresponding molar extinction coefficient (ε) of a chromophore under investigation. Throughout the studies, we have recorded the UV-Vis spectra of our samples in either Perkin-Elmer Lamda-35 or Lamda-750 spectrophotometers. Lamda-750 spectrophotometer consists of deuterium, tungsten and halogen lamps as light sources, a double holographic grating monochromators and a high sensitivity R928 PMT.

Steady-state fluorescence spectra of all the samples were recorded using a Jobin Yvon Fluoromax4 spectrofluorometer. For all the steady-state measurements, we have used standard quartz cuvette of path length 1 cm. The spectrofluorometer used a high-pressure 150W xenon (ozone free) arc lamp as light source. Fluorescence is collected at right angles with respect to the incident beam while the emitted light is detected through a monochromator by a R928P photomultiplier (PMT).

2.2 TIME CORRELATED SINGLE PHOTON COUNTING (TCSPC)

Time-correlated single-photon-counting (TCSPC) is a well-established and very standard method to record fluorescence lifetime in hundreds of picoseconds and nanosecond time scale. The actual time resolution and time window depends on the nature of the light source and electronic components of the spectrometer. We used a TCSPC setup Life Spec II from Edinburgh Instruments, UK or Ultrafast-01-DD from TCSPC Horiba Scientific Instruments to record fluorescence decays. In this technique, the sample to be analysed is excited with a short pulse (~50 ps) from a periodic light source. In our case, light sources were picosecond laser diodes (EPL-375 nm from Edinburgh and DeltaDiode-375L from Horiba Scientific with maximum repetition rate

of 10 MHz and 100 MHz, respectively). The full width at half-maximum (FWHM) of these setup was typically ~100 ps measured using a liquid scatter. We measured the decay at magic angle (55°) with respect to the analyser and polarizer to avoid the contribution of rotational diffusion and anisotropy on the intensity decays.

2.1.1. Single wavelength decay of the protonated and deprotonated emission transients of HPTS:

The simplest way to look at the ESPT dynamics is to monitor the fluorescence decays at a particular wavelength representing the protonated or the deprotonated emission. We measured fluorescence decays for HPTS at 425 nm and 570 nm, respectively for the two forms. 425 nm is slightly at the blue side of the emission maximum of the protonated from whereas the 570 nm was at the red side of the emission maximum of the deprotonated form. These two emission wavelengths were intentionally chosen to avoid mixing of the two forms.

We analysed the fluorescence decays by a multi-exponential (bi or tri) following proper convoluting with the instrument response function (IRF) using FAST or DAS6 software. The quality of the decay fit was ensured by reduced χ^2 value, the distribution of the weighted residuals among the data channels and the autocorrelation function of the residuals. The fit function can be represented as:

$$[ROH^*(t)](or\ [RO^{-*}(t)]) = \sum_i a_i e^{-t/\tau_i},\ i = 2 \text{ or } 3 \qquad (2.1)$$

2.2.2. Bimodal distribution of HPTS: Matching decay of the protonated form with the rise of the deprotonated form:

In some cases, we obtain a very good matching between one of the decay components of the of protonated (425 nm) form with the rise component of the deprotonated form (570 nm). To justify the occurrence of this pattern, we propose a bimodal distribution of HPTS into two different regions: hydrated and less hydrated. In this scenario one fraction of the HPTS ([AH1*]) may reside in a relatively hydrated region and thus, can undergo ESPT. Another fraction ([AH2*]) may be at

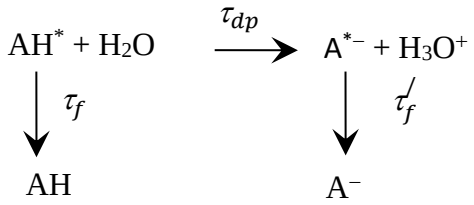

Scheme 2.1. Proposed ESPT scheme. This model involves single step de-protonation and ignore of ion-pair formation or recombination.

a location devoid of water and hence, cannot undergo ESPT. Interestingly, a very simple scheme (**Scheme 2.1**) involving single step de-protonation without ion-pair formation or recombination can justify the observed ESPT dynamics qualitatively.

From the **scheme 2.1** we further evaluated [AH1*] and that remain in protonated form [AH2*]. According to **scheme 2.1**, the fraction of probe that undergoes proton transfer [AH1*] should follow the following differential equation:

$$\frac{d[AH1^*]}{dt} = -\frac{1}{\tau_{dp}}[AH1^*] - \frac{1}{\tau_f}[AH1^*] \tag{2.2}$$

Integrating we obtain that the population of [AH1*] should decay as

$$[AH1^*] = [AH1^*]_0 e^{-\left(\frac{1}{\tau_{dp}}+\frac{1}{\tau_f}\right)t} \tag{2.3}$$

The fraction [AH2*] that does not undergo ESPT should follow the differential equation

$$\frac{d[AH2^*]}{dt} = -\frac{1}{\tau_f}[AH2^*] \tag{2.4}$$

Thus, the population of [AH2*] should decay as

$$[AH2^*] = [AH2^*]_0 e^{-\frac{t}{\tau_f}} \tag{2.5}$$

Thus, the fluorescence decay of protonated form should follow bi-exponential decay.

$$[AH^*] = [AH1^*]_0 e^{-\left(\frac{1}{\tau_{dp}}+\frac{1}{\tau_f}\right)t} + [AH2^*]_0 e^{-\frac{t}{\tau_f}} \tag{2.6}$$

The kinetics of the deprotonated form can be written as

$$\frac{d[A^{-*}]}{dt} = \frac{1}{\tau_{dp}}[AH1^*] - \frac{1}{\tau_f'}[A^{-*}] \tag{2.7}$$

$$\Rightarrow \frac{d[A^{-*}]}{dt} + \frac{1}{\tau_f'}[A^{-*}] = \frac{1}{\tau_{dp}}[AH1^*]_0 e^{-\left(\frac{1}{\tau_{dp}}+\frac{1}{\tau_f}\right)t}$$

$$\Rightarrow \frac{d[A^{-*}]e^{\frac{t}{\tau_f'}}}{dt} = \frac{1}{\tau_{dp}}[AH1^*]_0 e^{-\left(\frac{1}{\tau_{dp}}+\frac{1}{\tau_f}-\frac{1}{\tau_f'}\right)t}$$

$$\Rightarrow [A^{-*}]e^{\frac{t}{\tau_f'}} - [A^{-*}]_0 = \frac{1}{\tau_{dp}}[AH1^*]_0 \frac{1-e^{-\left(\frac{1}{\tau_{dp}}+\frac{1}{\tau_f}-\frac{1}{\tau_f'}\right)t}}{\frac{1}{\tau_{dp}}+\frac{1}{\tau_f}-\frac{1}{\tau_f'}}$$

$$\Rightarrow [A^{-*}] = -\frac{\frac{1}{\tau_{dp}}[AH1^*]_0}{\frac{1}{\tau_{dp}}+\frac{1}{\tau_f}-\frac{1}{\tau_f'}} e^{-\left(\frac{1}{\tau_{dp}}+\frac{1}{\tau_f}\right)t} + \left([A^{-*}]_0 + \frac{\frac{1}{\tau_{dp}}[AH1^*]_0}{\frac{1}{\tau_{dp}}+\frac{1}{\tau_f}-\frac{1}{\tau_f'}}\right) e^{-\frac{t}{\tau_f'}} \quad (2.8)$$

In the scheme, the shorter decay component of the protonated emission that arises due to deprotonation, should match with the rise (negative) component of the deprotonated emission.

Experimentally the decays could be fitted as

$$[AH^*] = a_1 e^{-\frac{t}{\tau_1}} + a_2 e^{-\frac{t}{\tau_f}} \quad (2.9)$$

$$[A^{-*}] = -a_3 e^{-\frac{t}{\tau_2}} + e^{-\frac{t}{\tau_f'}} \quad (2.10)$$

Comparing the bi-exponential decays from the model (eq 2.6 and 2.8) with the fitted bi-exponential decays (eq. 2.9 and 2.10), we obtain

$$\frac{[AH2^*]_0}{[AH1^*]_0} = \frac{a_2}{a_1} \quad (2.11)$$

$$\frac{[A^{-*}]_0}{[AH1^*]_0} = \left(\frac{1}{a_3} - 1\right)\frac{\frac{1}{\tau_{dp}}}{\frac{1}{\tau_{dp}}+\frac{1}{\tau_f}-\frac{1}{\tau_f'}} = \left(\frac{1}{a_3} - 1\right)\frac{\frac{1}{\tau_1}-\frac{1}{\tau_f}}{\frac{1}{\tau_1}-\frac{1}{\tau_f'}} \quad (2.12)$$

Using these ratios, we obtain the fraction of each excited state populations, using the fact

$$[AH1^*]_0 + [AH2^*]_0 + [A^{-*}]_0 = 1 \quad (2.13)$$

2.2.3. Time Resolved Emission Spectra (TRES) and Time Resolved Area Normalized Emission Spectra (TRANES):

The fluorescence decays measured at two fixed wavelengths representing the protonated and deprotonated forms usually provide only a qualitative idea about excited state proton transfer dynamics. Significant overlap of the emission bands of the two forms, dynamic Stokes shifts and any addition quenching processes may complicate the analysis of these fixed wavelength decays. Thus, measurement of fluorescence decays for a set of wavelengths across the whole emission band (at a regular interval of 5nm) followed by reconstruction of the time resolved emission spectra (TRES, following *eq.2.15*) is preferable. These are more informative to monitor ESPT dynamics since it reports spectral modifications during the ESPT event. To resolve the mixing of the protonated and de-protonated forms in the emission spectra, we de-convoluted their contributions with a bi-lognormal fit function (*equation 2.14*) and observed considerable overlap between the emission spectra of the two forms over a significant wavelength range (**Figure 2.1**).

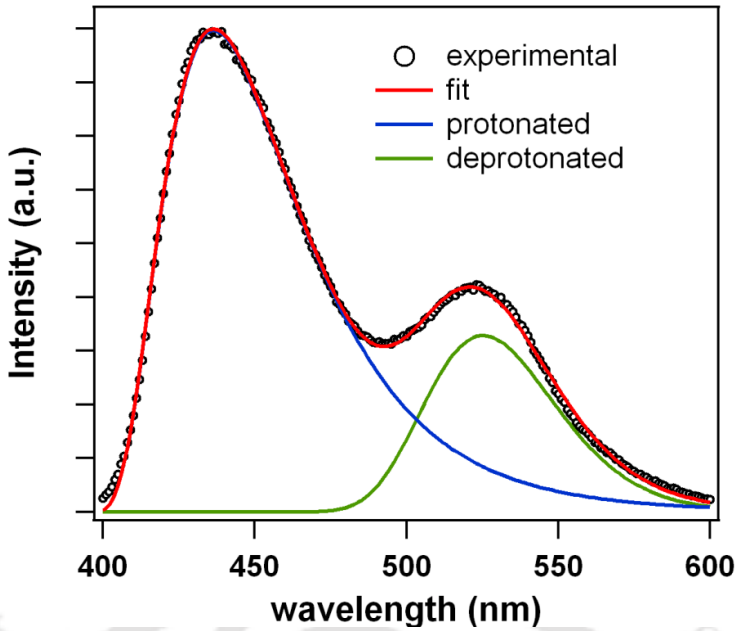

Figure 2.1: Decomposition of the observed emission spectrum of HPTS at w_0 = 10 (open circle) into emission contribution of the protonated (blue line) and de-protonated (green line) forms in water/BHDC/benzene reverse micelle. The red line denotes the fitting by a superposition of two lognormal functions.

The emission spectra were fitted by a bi-lognormal function:

$$I(\nu) = (I_0^1)\exp\left\{-\ln(2)\left[\frac{\ln\left(1+\frac{2b_1(\nu-\nu_p^1)}{\Delta}\right)}{b_1}\right]\right\}^2 + (I_0^2)\exp\left\{-\ln(2)\left[\frac{\ln\left(1+\frac{2b_1(\nu-\nu_p^2)}{\Delta}\right)}{b_2}\right]\right\}^2 \quad (2.14)$$

Where I_0 denote peak height, ν_p peak position, b asymmetry factor and Δ for width parameter.

TRES provides information on the excited state kinetics and heterogeneity of emissive species in a system. The relation used to construct TRES can be given as:

$$I(\lambda, t) = \frac{I_{ss}(\lambda)}{\sum_i a_i \tau_i} \sum_i a_i e^{-t/\tau_i} \quad (2.15)$$

We have also constructed area of TRES against their respective time and evaluated the lifetime of free HPTS molecule.[208,216] We can further constructed time resolved area normalized spectra (TRANES) by normalising each spectrum of TRES by their respective spectrum area.[217,218]

2.2.4. Time Resolved Fluorescence Anisotropy Decay:

Fluorescence anisotropy decay provides information of local environment around the probe. To measure fluorescence anisotropy decays, the analyzer was rotated at regular intervals to obtain

parallel ($I_{\parallel}$) and perpendicular ($I_{\perp}$) decay components of a fluorescence decay separately. The anisotropy function, r (t) was constructed using the expression:

$$r(t) = \frac{I_{\parallel}(t) - GI_{\perp}(t)}{I_{\parallel}(t) + 2GI_{\perp}(t)} \quad (2.16)$$

The G value of the set up was determined at 440 nm emission wavelength of HPTS and was found to be 0.68. Fluorescence anisotropy decays were fitted using DAS6 software, using bi-exponential fitting function, retaining a constant residual anisotropy(r_∞):

$$r(t) = (r_0 - r_\infty)\left[a_s\, e^{-t/\tau_s} + (1 - a_s)\, e^{-t/\tau_f}\right] + r_\infty \quad (2.17)$$

Where r_0 is initial anisotropy; τ_s and τ_f are the slow and fast rotational time constants, respectively and a_s is the amplitude of the slow component.

2.3. WOBBLING IN CONE MODEL (WIC):

The anisotropy decays of fluorophores bound to micelle or the reverse micellar interface is often analysed by a popular "wobbling in cone model". According to this model, a fluorophore may undergo a wobbling motion tracing a cone with a semi-cone angle of θ along with lateral diffusion of the probe along the interface (**Figure 2.2**).[219-221] The observed anisotropy decay, r (t) is a product of three motions:

$$r(t) = r_w(t) r_D(t) r_M(t) \quad (2.18)$$

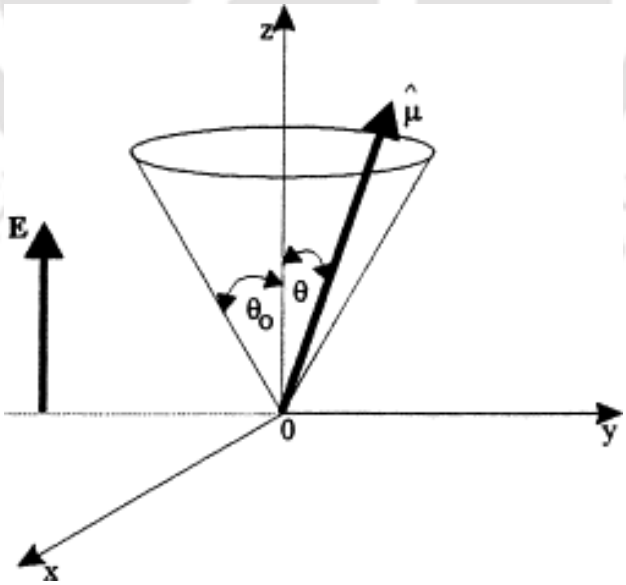

Figure 2.2: Wobbling-in-cone model. $\hat{\mu}$ represents the symmetry axis of the chromophore, which forms an angle θ with the z-axis.[222]

$r(t)$ may also be written in terms of the order parameter S

$$r(t) = r_0\left[S^2 + (1 - S^2)e^{-t/\tau_D}\right]\exp\left(-t\left(1/\tau_D + 1/\tau_M\right)\right) \quad (2.19)$$

The time constant (τ_M) of the overall rotation of the micelle is given by

$$\tau_M = \frac{4\eta\pi r_h^3}{3k_BT} \quad (2.20)$$

Where, η = viscosity of solution and r_h is the hydrodynamic radius of the micelle. We used dynamics light scattering (DLS) measurements to obtain the hydrodynamic diameter of the micelles.

However, the overall time scale is expected to be very long compared to the life time of HPTS. Thus, we did not explicitly include the overall rotation in our analysis and rather assumed that the effect of the very slow overall motion may be reflected in the observed residual anisotropy except in case of micelle, *chapter 7*. Using this model and assigning time constants of these motions as τ_W, τ_D respectively, the anisotropy decay may be modelled as

$$r(t) = (r_0 - r_\infty)\left[S^2 + (1-S^2)e^{-\frac{t}{\tau_W}}\right]e^{-\frac{t}{\tau_D}} + r_\infty \quad (2.21)$$

Where S is an order parameter and is related to the semi-cone angle θ as

$$S = \frac{1}{2}\cos\theta\,(1+\cos\theta) \quad (2.22)$$

Equating (2.4) and (2.8) one obtains

$$a_s = S^2 \quad (2.23)$$

$$\frac{1}{\tau_s} = \frac{1}{\tau_D} \quad (2.24)$$

$$\frac{1}{\tau_f} = \frac{1}{\tau_W} + \frac{1}{\tau_D} \quad (2.25)$$

Finally, we obtained the diffusion coefficient for wobbling (D_w) of HPTS at the DDAB RM interface using the relation[27,223-225]

$$D_w = \{\tau_w(1-\beta)^{-1}\left[\frac{x^2(1+x)^2}{2(x-1)}\left\{\ln\left(\frac{1+x}{2}\right) + \left(\frac{1-x}{2}\right)\right\} + \left(\frac{1-x}{24}\right)(6+8x-x^2-12x^3-7x^4)\right] \quad (2.26)$$

Where x = cos θ.

2.4. NUCLEAR MAGNETIC RESONANCE SPECTROSCOPY:

The ^{1}H NMR spectra of BHDC reverse micelles incorporated with HPTS probes were recorded using a Bruker 600 MHz NMR spectrometer (*chapter 4*). The 2D-NOSEY NMR spectra

were recorded in the 600 MHz NMR spectrometer; the 90 degree pulse width was 6.5μs; the spectral window was 12 kHz in both t_1 and t_2, the acquisition time was 13.09s, digital signal processing and frequency shifted quadrature detection were used.

All NMR measurements were carried out in deuterated benzene solvents (Sigma Aldrich, 99.96 atom% D) solvent containing 0.03% (v/v) TMS as the chemical shift reference.

2.5. DYNAMIC LIGHT SCATTERING (DLS) MEASUREMENTS:

To measure size of micelle and reverse micelle we have recorded dynamic light scattering (DLS) measurements in a Malvern Nano ZS90 instrument. The He-Ne Laser (λ = 632.8 nm) was used as excitation source. The scattering was collected at a fixed angle of 90°. The solutions were filtered with PTFE syringe filters having 0.2μM pore size prior to DLS measurements. All measurements were performed at 298K.

For the DLS measurement, of water/AOT/*n*-heptane reverse micelle (*chapter 3*) with addition of alcohols ethanol and *n*-octanol, we estimated the viscosity of the continuous phase comprising of the mixtures of *n*-heptane (η = 0.386cp) and the alcohol ethanol (η = 1.084cp) or *n*-octanol (η = 7.24cp) using the *equation 2.14*

$$\eta = (\eta_1^{1/3} X_1 + \eta_1^{1/3} X_1)^3 \qquad (2.27)$$

Where η_1, η_2 stand for viscosities and X_1, X_2, for mole fractions of *n*-heptane and the alcohol (ethanol or *n*-octanol), respectively.

In this calculation, partitioning of alcohol (ethanol or octanol) into the reverse micelle (in the core and/or interface) is neglected. Such partitioning is expected to be small compared to the octanol partition into *n*-heptane due to their high mutual miscibility. Note, *n*-heptane and octanol are completely miscible at all mole fractions.

2.6. MATERIALS USED:

8-Hydroxypyrene-1, 3, 6-trisulfonic acid trisodium salt (HPTS, pyranine), 8-methoxypyrene-1,3,6-trisulfonic acid trisodium salt (MPTS), cetyltrimethylammonium bromide (CTAB, 98%), cetyltrimethylammonium chloride (CTAC), dodecyltrimethylammonium bromide (DTAB, 98%), didodecyldimethylammonium bromide (DDAB,98%), 3-(hexadecyldimethylammonio)-propane sulfonate (SB-3-16 or SB16), and 3-(dodecyldimethylammonio)-propanesulfonate (SB-3-12 or SB12), benzylhexadecyl

dimethylammonium chloride (BHDC) and sodium bis(2-ethylhexyl) sulfosuccinate (AOT) were purchased from Sigma-Aldrich Chemicals.

HPLC grade cyclohexane, *n*-heptane, ethanol, benzene were purchased from Spectrochem India. Benzene-d_6, *n*-octanol and D_2O were purchased from Sigma-Aldrich Chemicals. Water (resistivity 18.2 MΩ cm) was obtained from a Millipore system.

2.7. PREPARATION OF REVERSE MICELLE AND MICELLE SOLUTIONS:

The reverse micelle solutions at various w_0s were prepared by adding a requisite amount of water (using the relation, $w_0 = [H_2O]/ [\text{surfactant}]$) into a non-polar surfactant solution. The concentration of surfactant was selected at concentrations remarkably higher than their respective critical micellar concentrations (CMCs).

Micelle solutions were prepared by dissolving an appropriate amount of the surfactants in water at concentrations significantly higher than their respective critical micellar concentrations (CMCs). We deliberately use high concentrations to ensure sufficient abundance of micelles to uptake all HPTS, thus eliminating any contribution from free fluorophores. To incorporate HPTS into the micelle or reverse micelle solution, a required amount of a stock solution of HPTS in water were injected into the requisite solution. In all of the experiments, the concentration of the HPTS was kept at ~10μM.

The pH of the medium was maintained at ~5.6 with the addition of 0.12 M HCl to suppress ground state proton transfer of HPTS whenever pH of the medium is more than 6. All the experiments were performed at room temperature.

Chapter-3

Confinement Induced Variable Solubility of *n*-octanol Inside the Aqueous Core of Water/AOT/*n*-heptane Reverse Micelle[#]

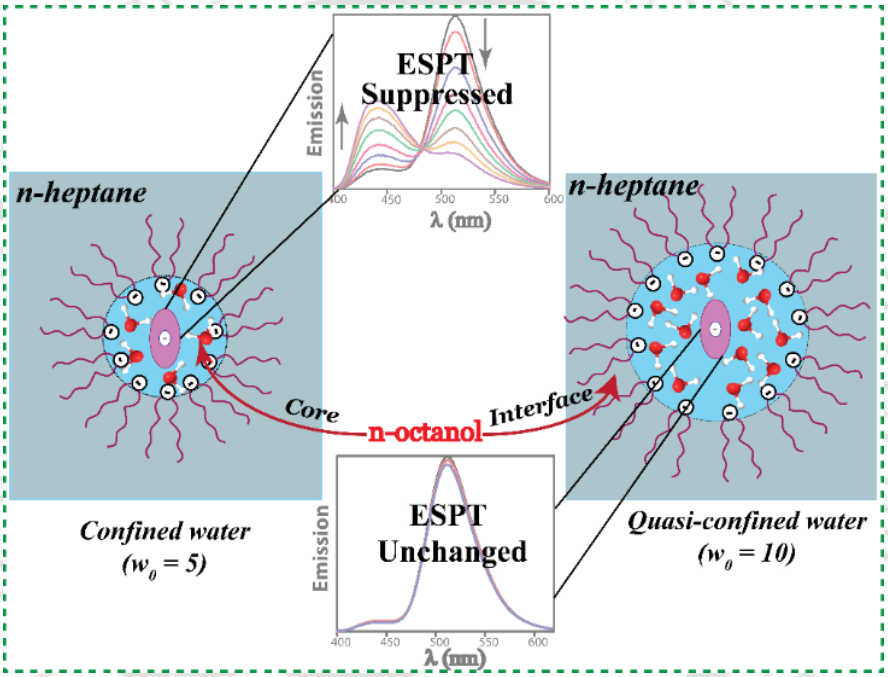

[#]This work has been published in *Chem. Commun.* **2015**, *51*, 14103-14106.

CHAPTER 3:
CONFINEMENT INDUCED VARIABLE SOLUBILITY OF N-OCTANOL INSIDE THE AQUEOUS CORE OF WATER/AOT/N-HEPTANE REVERSE MICELLE.[226]

3.1. INTRODUCTION:

Water is a well-known ubiquities solvent. It behaves as a lubricant of life, sustaining many natural and biological processes. The physical properties of water are strongly intertwined with the dynamics of its hydrogen bonding (H-bonding) network. The hydrogen bonding network of water molecule encased within self-organized assembly undergoes structural or chemical perturbation, consequently, altering the properties of water from the bulk water behaviour.[47,227] Water confined inside a reverse micelle (RM) is a popular model of confined water with the level of confinement easily adjustable from highly-confined (a very small water pool) to quasi-confined (a relatively large water pool) by simply tuning the water to surfactant ratio (w_0).[148,174] The infra-red spectroscopy[149,228] and molecular dynamics simulations[148,229] are widely used technique to investigate structure and dynamics of water within a RM at a different level of confinement. The orientation relaxation of water is markedly slower at low w_0 but becomes gradually faster with the increase of water content and ultimately approaches bulk-like dynamics.[228,229] These variable nature of trapped confined water has versatile applications, ranging from drug delivery, capturing inorganic salts or small organic molecules[194,230] to nanoparticle synthesis[231]. In the reverse micellar medium long chain alcohol plays a vital role as co-surfactant in stabilizing reverse micelle of single chain surfactant. Although the effect of different alcohols on the structure and properties of a reverse micelle has been studied for long,[232-234] but yet partitioning of alcohols into the water pool or at the interface was only analysed in terms of their bulk miscibility properties. The water-soluble short chain alcohols (methanol, ethanol, propanol), believed to be mixed within the water pool of the RM. But the water-immiscible long chain alcohols (e.g. *n*-heptanol, *n*-octanol and higher alkanols) would avoid the water pool and mainly act as co-surfactants partitioning into the interface.[235] Moreover, *n*-octanol was also used as continuous solvent in a water/AOT/*n*-octanol reverse micelle due to its water-immiscibility[236].

In this chapter we have compared the solubility of short and long chain alcohol (ethanol and *n*-octanol) in the reverse micelle core water and their dependence in the level of confinement of water pool in the water/sodium bis-(2-ethylhexyl) sulfosuccinate (AOT)/*n*-heptane reverse micelle. We deliberately choose two different levels of confinement – highly confined (at $w_0 = 5$) and quasi-confined (at $w_0 = 10$) and employed the well-known phenomena of excited state proton transfer (ESPT), and used steady-state and time-resolved emission spectroscopy and dynamic light

scattering measurement (DLS) to reveal the alcohol effect on the structure of reverse micelle. To focus our study in the water core we used 8-hydroxypyrene-1, 3, 6-trisulfonate (HPTS or pyranine) as molecular probe because of its high negative charge (−3 and −4 respectively, in the protonated and de-protonated forms) and thus, resides at the center of the water pool surrounded by the negative AOT headgroups (**Scheme 3.1**).

Here we observed breakdown of the usual proposition of water-immiscibility of *n*-octanol at certain degree of confinement in the reverse micelle encased water pool.

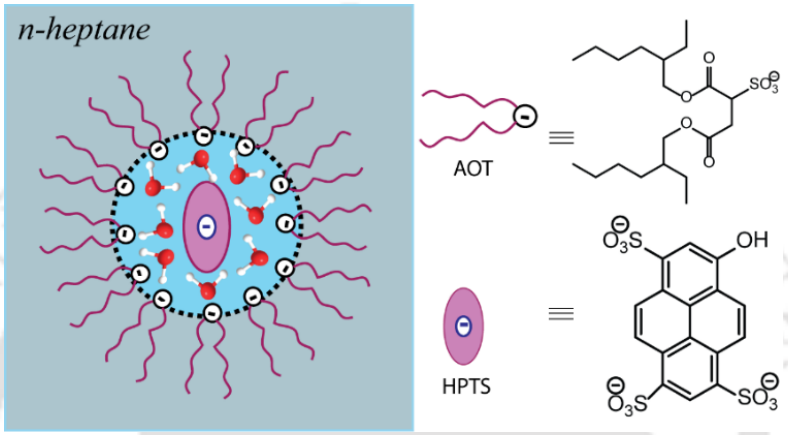

Scheme 3.1: Representation of a water/AOT/*n*-heptane reverse micelle with the molecular probe HPTS located at the center of the water pool. The highly negative HPTS is forced to stay at the center of the water pool due to repulsion by the negative AOT interface and is suitable for probing the microenvironment of the water pool selectively.

3.2. RESULTS

3.2.1. Steady-State Absorption and Emission Spectroscopy:

The fluorescent probe HPTS shows pH dependent absorption behaviour. We observed presence of only one absorption maximum for HPTS at lower pH at λ_{max}~403nm. However, a new absorption band for deprotonated form arise at λ_{max} ~450nm as the solution reach the pH ~7 (**Figure 3.1**). The measured pH of the anionic AOT reverse micelle without any pH adjustment was 7.8. However, the reverse micelle solution was made slightly acidic (pH ~5) by adding 2 μL of 1.2 M HCl into 2.5 ml of the reverse micelle solution to ensure that only the protonated form of dye remains in the ground state. Bulk pH measurement revealed a pH of 5.8 after this adjustment. The *n*-octanol (stock concentration ~ 6.29 M) was added gradually up to alcohol/ water mole ratio of 1.79 and 0.23 in w_0 = 5 and 10, respectively and after this concentration the phase separation occur.

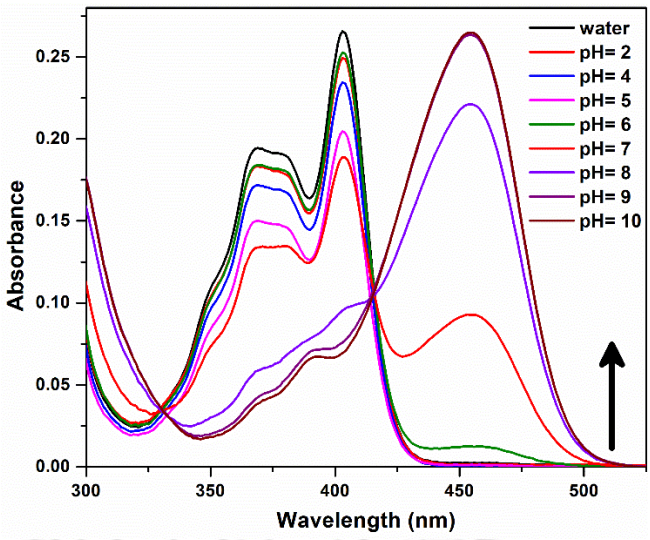

Figure 3.1: Effect of pH variation on the absorption spectrum of HPTS. At lower pH the absorption of the protonated form (absorption maximum ~ 403 nm) dominates but at higher pH the absorption of the de-protonated form (absorption maximum ~ 450 nm) becomes gradually prominent.

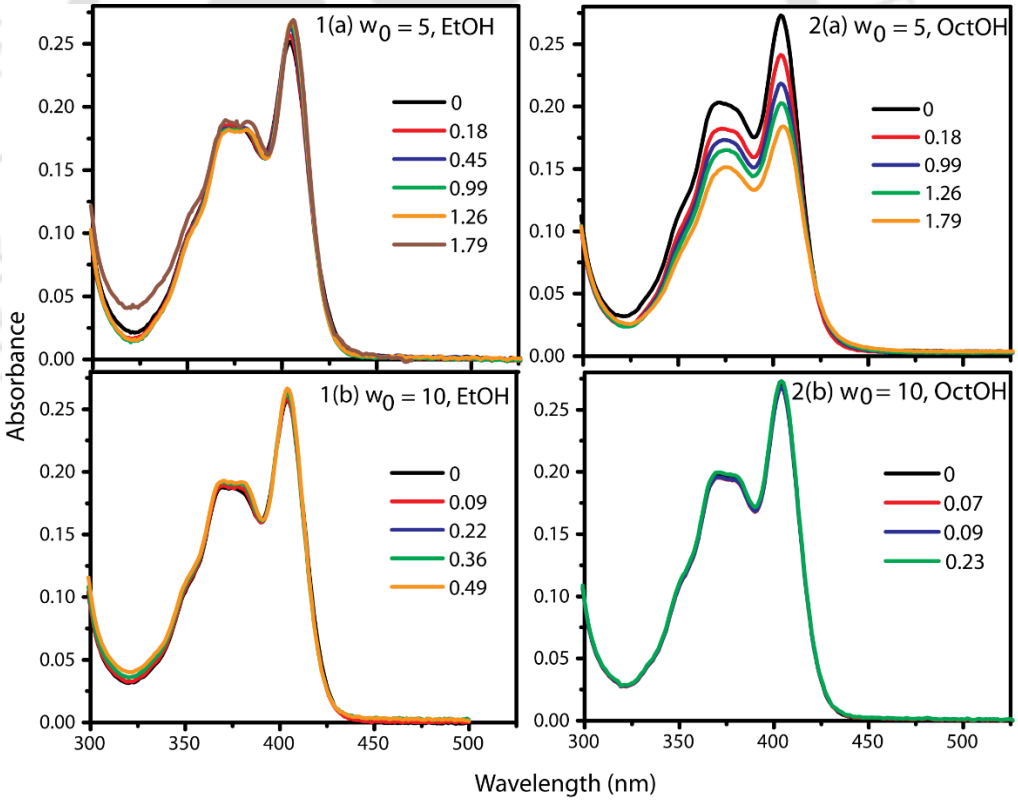

Figure 3.2: Absorption spectra of HPTS in the water/ AOT/ *n*-heptane reverse micelle for (a) w_0 = 5 and (b) w_0 = 10 at various *ethanol/water (left panel) and octanol/water* (right panel) mole ratios. The water wool was made slightly acidic (pH ~5-6) to suppress the de-protonated absorption. Addition of *alcohol* was performed after this pH adjustment.

In the reverse micelle water pool HPTS absorption band appears at λ_{max} ~405nm whereas in the bulk water it appears at ~ 403nm. The overall absorption decreases slightly with addition of *n*-octanol at w_0 = 5 but no change observed at w_0 = 10 (**Figure 3.2**). Here we represented concentration of alcohol as alcohol to water mole ratios. Similarly, for short chain water soluble ethanol, we observed gradual shift in the position of absorption maximum to 405nm from that arise in bulk water (403nm, **Figure 3.2**). The emission characteristics of HPTS governed by the excited state proton transfer (ESPT) process and depend greatly upon the degree of confinement.[122,205,208] The ESPT process is dramatically masked inside the confined water of the water pool at very low w_0 values, but gradually approaches the ultrafast bulk-like dynamics at high w_0 (≥10).[180,205,208] The Emission spectrum of HPTS consists of two well-separated bands centered at ~440 nm and ~515 nm, representing the protonated (ROH) and deprotonated (RO^-) emission, respectively.

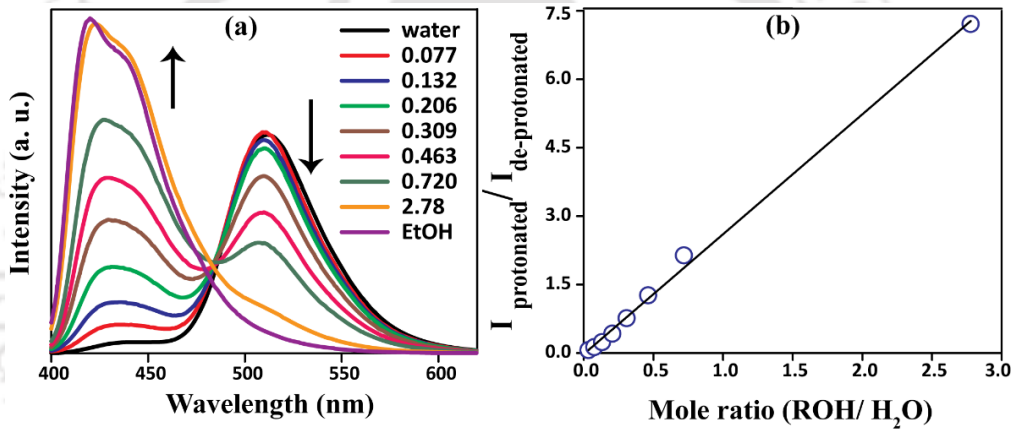

Figure 3.3: Emission spectra of HPTS in *water–ethanol mixtures* at various alcohol to water molar ratios. The ratio of the protonated emission (ROH, 440 nm) and de-protonated emission (RO^-, 510 nm) varies linearly with alcohol.

The ESPT process of HPTS can be modulated strongly by the presence of alcohol[237]. In neutral water, the ESPT dynamics is fast (~90ps) and the emission is mostly dominated by the de-protonated form.[27,224] However, in an ethanol–water mixture, the ESPT process becomes strongly retarded (**Figure 3.3a**) and consequently, the emission contribution of the protonated form (at λ_{em} ~ 440 nm) increases with the concomitant decrease of the de-protonated emission (at λ_{em}~515 nm) with increase of the amount of ethanol.[237] The dynamics of ESPT process is quite complex; a series of events (recombination and dissociation of the geminate ion pair) are generally associated with the ESPT process.[28] However, the intensity ratio of the two forms, r = ($I_{protonated}/I_{de\text{-}protonated}$), is found to be proportional to the alcohol to water molar ratio, and hence, may be a convenient indicator of alcohol content (**Figure 3.3b**) in an unknown alcohol-water

mixture. A similar variation of HPTS emission was also reported for the methanol–water mixture and the slowing down of the ESPT may be ascribed due to the breaking of the H-bonding network of water or blocking of the hydroxyl group of HPTS by the alcohol.[10] Note that no ESPT occurs in neat alcohol.

We adopted the ratio metric sensing ability of HPTS to check the miscibility of two alcohols, ethanol and *n*-octanol, in the water pool at two different w_0 values of 5 and 10 as the representative of highly-confined and quasi-confined water. The emission spectra clearly show enhancement in the intensity of the protonated emission (at 440 nm) band with concomitant decrease of the de-protonated emission (at 510 nm); gradually with the increase of the molar ratio of alcohol to water for both water confinement (w_0 = 5 and w_0 = 10 reverse micelle) with incorporation of medium chain alcohol (ethanol) into the reverse micelle (**Figure 3.4, left panel**).

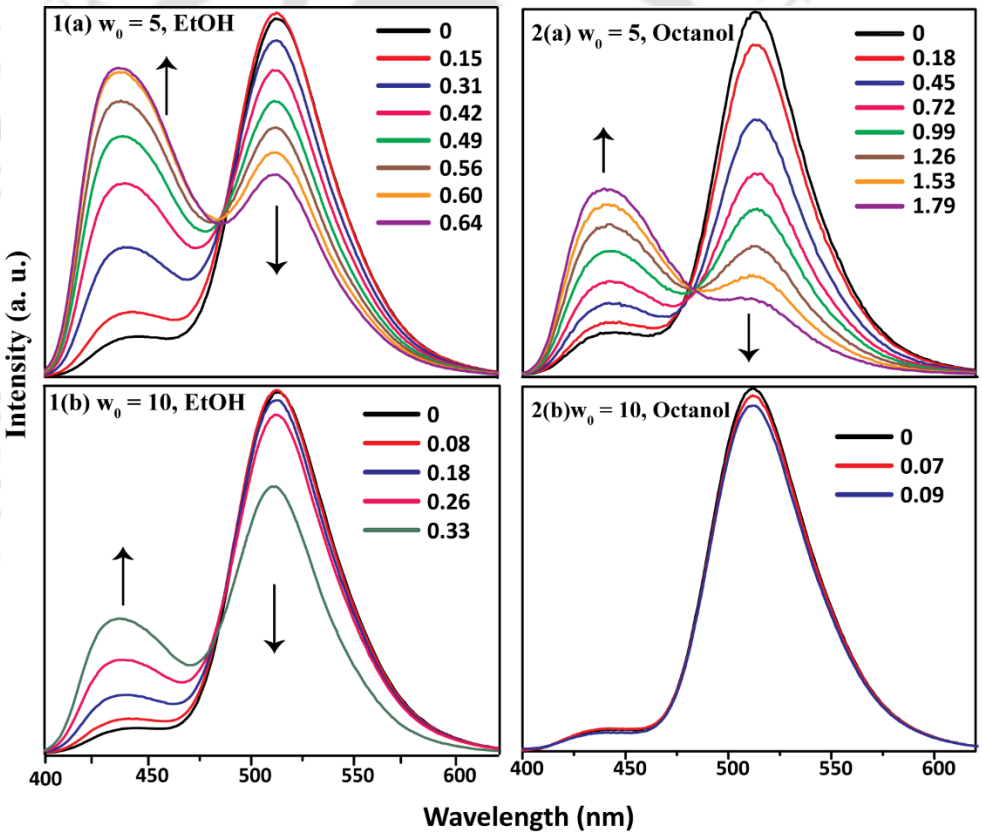

Figure 3.4: Emission spectra of HPTS displaying effect of ethanol (left panel) and *n*-octanol (right panel) addition into the water/AOT/*n*-heptane reverse micelle at (a) w_0 = 5 and (b) w_0 = 10.

But incorporation of *n*-octanol has effect on ESPT modulation similar to ethanol partition only at highly confined water, w_0 = 5 and no significant change in emission was observed at quasi-confined water, w_0 = 10. Intensity of the protonated emission (at 440 nm) increases while that of the de-protonated emission (at 510 nm) decreases gradually with the increase of the molar ratio of alcohol to water at w_0 = 5, but no significant change in emission was observed at w_0 = 10,

indicating similar partitioning of both alcohol at the two w_0s, even after variation in polarity. Noted octanol shows no significant effect on emission at $w_0 = 10$. Thus, the added *n*-octanol suppresses the ESPT of HPTS considerably when the size of the water pool is small but leaves the ESPT virtually unperturbed for a relatively large size reverse micelle (**Figure 3.4 right panel**).The remarkable ESPT modulation by *n*-octanol selectively at low w_0, but not at high w_0 can be interpreted in two different ways. First, we may believe conventionally that octanol resides at the interface of the AOT RM, and does not encroach into the core. The equilibrium (maximum) mole fraction of water soluble in *n*-octanol at 25°C is 7.03×10^{-5}.[238] Thus, if the solubility limit persists for the water pool, the probability of partitioning of octanol into the core is negligible. Another possibility is that the water-immiscible *n*-octanol actually becomes miscible within the highly confined water of the water pool (at $w_0 = 5$), but remains immiscible with the quasi-confined water (at $w_0 = 10$). In that case, partitioning of *n*-octanol into the core directly perturbs the H-bonding network of the water present in the water pool similar to the case of ethanol (highly water soluble). We observed the emission intensity ratio of HPTS changes linearly with the amount of externally added ethanol (relative to the amount of water) at both $w_0 = 5$ and 10 (**Figure 3.5**)

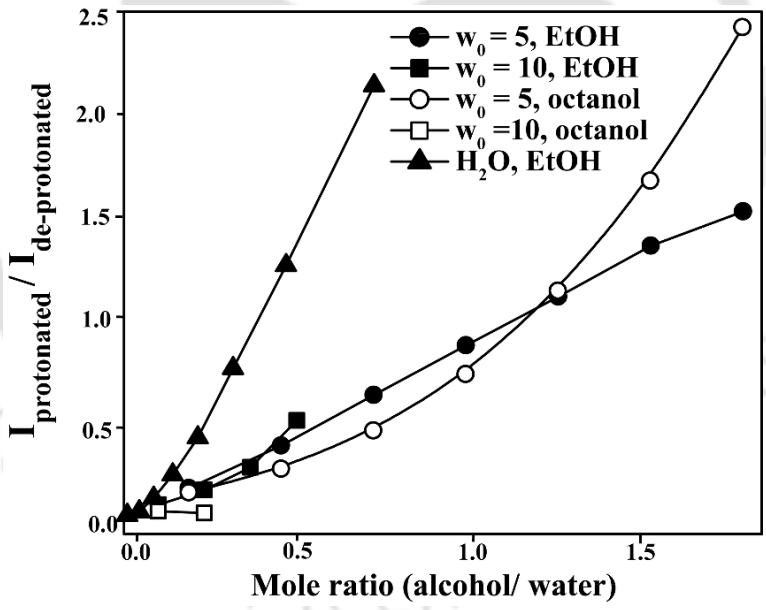

Figure 3.5: Comparison of the extent of HPTS intensity modulation (ratio of $I_{protonated}/ I_{deprotonated}$) upon alcohol (ethanol or *n*-octanol) addition in different systems.

. As expected from the good water solubility of ethanol, we may infer that ethanol indeed partitions into the water pool and disturbs the H-bonding network or reduces the availability of water around HPTS. The slope of the line representing the extent of variation of the HPTS intensity ratio with the alcohol/water molar ratio is somewhat less inside the reverse micelle than that of the bulk ethanol–water mixture. This may be because only a part of the ethanol is

incorporated inside the water pool, while the remaining stays in the continuous non-polar phase and/or at the interface.

3.2.2. Time-resolved fluorescence:

The fluorescence transients of HPTS, representative of the protonated (425 nm) form provided more insight about interaction of alcohol and the probe. Note that 425 nm is slightly higher in energy compared to the protonated emission maxima ($\lambda_{em}^{max} = 430\,nm$), we intentionally pick this wavelength to avoid undesirable mixing of the contribution from the deprotonated form[239,69] The fluorescence transients of HPTS monitored at 425nm becomes slower with increasing alcohol (ethanol and *n*-octanol) incorporation in the w_0 = 5, but *n*-octanol has no effect on HPTS life time at w_0 = 10 AOT reverse micelle (**Figure 3.6**).

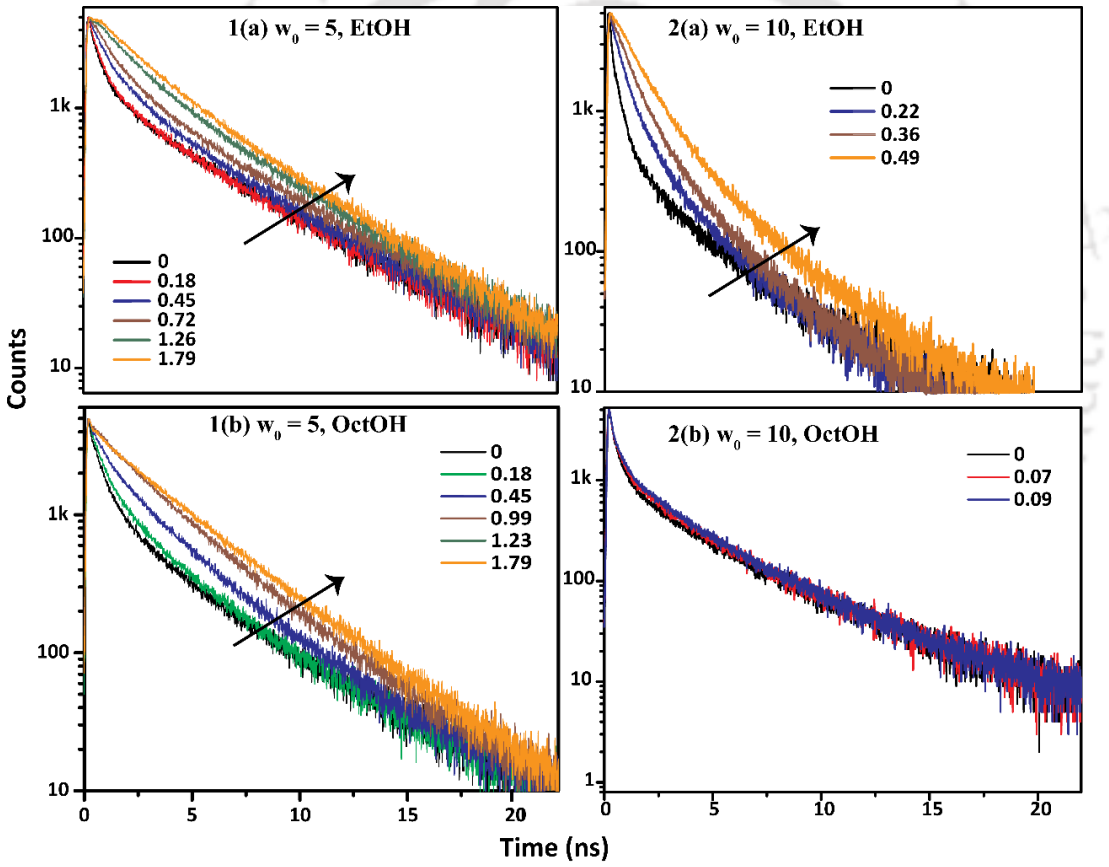

Figure 3.6: The effect of ethanol (1a, 2a) and *n*-octanol (1b, 2b) on the fluorescence transients of HPTS (at emission wavelength of 425 nm) inside the water/AOT/*n*-heptane reverse micelle at w_0 = 5 and w_0 = 10. A dramatic slowing down of the fluorescence decay was observed upon *n*-octanol addition at w_0 = 5 but almost no change is noticed among the transients at w_0 = 10. However, ethanol incorporation leads to slow down of the fluorescence decay for both the confinement (w_0 = 5 and w_0 = 10).

3.2.3. Dynamic light scattering:

To dissect between the two contradictory interpretations about *n*-octanol partition in the interface or encroachment into the core water pool; we have measured the effect of alcohol on the size of reverse micelle at different water confinement using dynamic light scattering. We found significant swelling of the RM size (up to 16–17 nm) upon ethanol addition at both w_0 = 5 and 10, confirming the inclusion of ethanol into the water pool (**Figure 3.7**). This supports the usual notion that water soluble species should be solubilized preferably inside the water pool. Fascinatingly, we observed swelling of the reverse micelle at w_0 = 5 upon *n*-octanol addition up to a certain extent (up to ~17 nm at *n*-octanol to water mole ratio of ~0.7), which then starts to shrink at a higher amount of *n*-octanol. However, only shrinking was observed upon octanol addition to the reverse micelle at w_0 = 10. Thus, we may affirm that *n*-octanol indeed mixes well with water in the water pool at a very high-confinement limit (w_0 = 5).

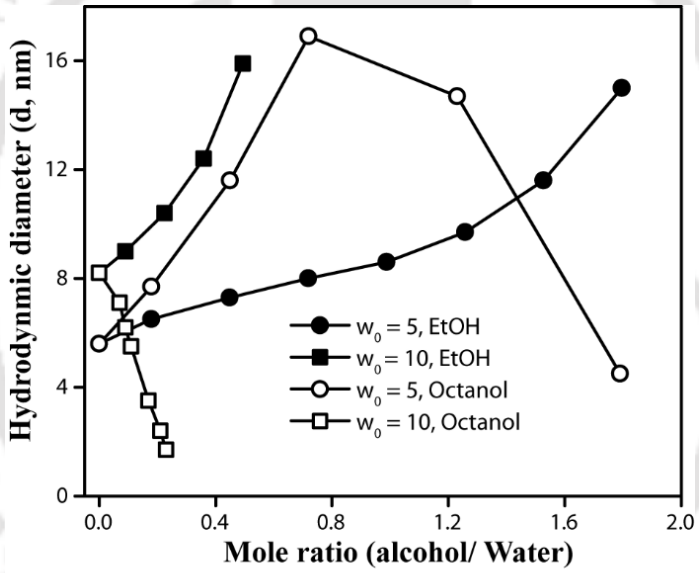

Figure 3.7: Variation of the hydrodynamic diameter (in nm) of the water/AOT/*n*-heptane reverse micelle with addition of alcohol at w_0 = 5 and 10. Upon *n*-octanol addition, the reverse micelle swells at w_0 = 5 up to a certain (0.8) alcohol/water molar ratio and thereafter, shrinks; but size of the reverse micelle monotonically shrinks at w_0 = 10. However, addition of ethanol swells up both the confinement.

At a lower amount of *n*-octanol core-partitioning dominates, but at a higher amount of *n*-octanol, interface-partitioning shrinks the overall reverse micelle size. Octanol partitioning at the interface may rigidify the interface and hence, may shrink the size to increase the interface curvature.[232] However, shrinking of RM size at w_0 = 10 notify predominant partition of *n*-octanol mainly into the interface and stays away from the core. We may estimate the approximate dimension of the water pool and more specifically, how far the HPTS molecule is from the

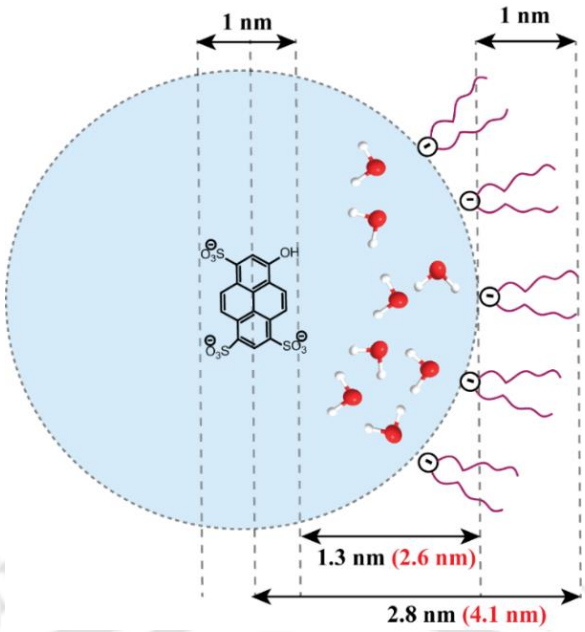

Scheme 3.2: A scheme showing approximate dimension of the reverse micelle systems at w_0 = 5 and 10 containing HPTS in the core.

Table 3.1: The variation of hydrodynamic diameter of water/AOT/*n*-heptane reverse micelle upon addition of ethanol obtained from dynamics light scattering (DLS) measurements at w_0 = 5 and 10. The estimated viscosities of the continuous phase are also included.

System	Overall concentration of ethanol, M	Ethanol/water mole ratio	Viscosity of continuous phase (cp)	Hydrodynamic diameter (d, nm)
w_0 = 5	0	0	0.386	5.6
	0.08	0.18	0.3914	6.5
	0.2	0.45	0.3997	7.7
	0.32	0.72	0.4078	8.0
	0.44	0.99	0.4157	8.6
	0.56	1.26	0.4235	9.7
	0.68	1.53	0.4311	11.6
	0.8	1.79	0.4386	15.0
w_0 = 10	0	0	0.386	8.2
	0.08	0.09	0.3914	9.0
	0.2	0.22	0.3997	10.4
	0.32	0.36	0.4078	12.4
	0.44	0.49	0.4157	15.9

interface. Our DLS measurements revealed that the diameters of the aqueous reverse micelles were 5.6 nm and 8.2 nm, respectively at w_0 = 5 and 10. Both the height and width of HPTS molecules are ~1 nm and the AOT length is also approximately ~ 1 nm.[208] Thus, considering that HPTS is occupying the center of the water pool, it stays approximately 1.3 nm and 2.3 nm away from the interface, respectively, at w_0 = 5 and 10 (**Scheme 3.2**). Hence, ESPT perturbation at low water content but no perturbation at high water content seems feasible. However, the extent of

ESPT suppression is quite high despite of the appreciable (~1.3 nm) separation between the HPTS and interface at w_0 = 5 and thus, the impact of octanol partition at the interface is not very easy to comprehend.

The change in hydrodynamic diameter and viscosity of the continuous phase (mixture of heptane and alcohol) was estimated from the bulk viscosities using **eq.2.27, *chapter 2***, with addition of ethanol and *n*-octanol and are tabulated in **Table 3.1** and **Table 3.2** respectively.

Table 3.2. The hydrodynamic diameters of water/AOT/n-heptane reverse micelles with addition of *n*-octanol obtained from dynamics light scattering (DLS) at w_0 = 5 and 10. The estimated viscosities of the continuous phase are also included.

System	Overall concentration of octanol, M	*n*-octanol/water mole ratio	Viscosity of continuous phase (cp)	Hydrodynamic diameter (d, nm)
w_0 = 5	0	0	0.386	5.6
	0.08	0.18	0.409	7.7
	0.2	0.45	0.444	11.6
	0.32	0.72	0.480	16.9
	0.56	1.26	0.551	14.7
	0.8	1.79	0.625	4.5
w_0 = 10	0	0	0.386	8.2
	0.06	0.07	0.403	7.1
	0.08	0.09	0.409	6.2
	0.09	0.11	0.412	5.5
	0.15	0.17	0.430	3.5
	0.18	0.21	0.439	2.4
	0.2	0.23	0.445	1.7

3.3. SUMMARY AND CONCLUSIONS:

The ratio metric alcohol sensing property of HPTS located inside the RM water pool notified different partitioning of *n*-octanol inside highly confined (w_0 = 5) and quasi-confine (w_0 = 10) environment. At low w_0, significant modulation of ESPT takes place signifying partitioning of *n*-octanol into the highly-confined water. However, no ESPT modulation was found at w_0 = 10, that support absence of *n*-octanol in the quasi-confined water. This was further supported by very different size modulation of the reverse micelle, depending on the initial state of water in the water pool of the reverse micelle. Thus, this study demonstrated the unusual variation of solubilisation properties of water with the degree of confinement. These results revealed that confined water behaves more like a hydrophobic solvent compared to quasi-confined or bulk water.

Chapter-4

Is the Interface of the Reverse Micelle Dry or Wet? Insights from ESPT of HPTS in the case of Cationic Water/BHDC/benzene Reverse Micelle[#]

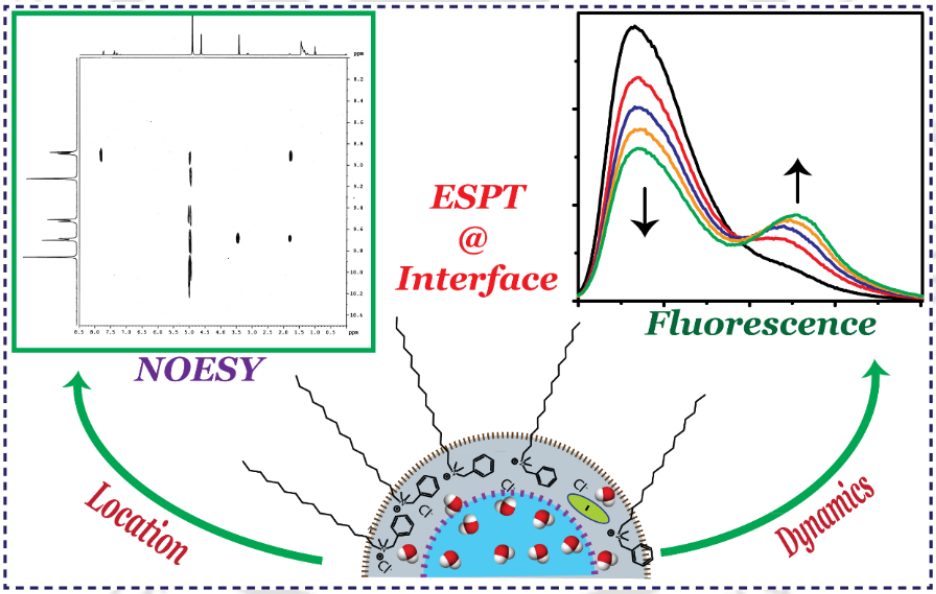

[#]This work has been published in *Langmuir* **2015**, *31*, 12587-12596.

CHAPTER 4
IS THE INTERFACE A REVERSE MICELLE DRY OR WET? INSIGHTS FROM ESPT OF HPTS IN CASE OF CATIONIC WATER/BHDC/BENZENE RM[240]

4.1. INTRODUCTION:

A lot of study mentioned about the heterogeneity of reverse micelle in the aspects of water distribution as discussed in *chapter1*. From ultrafast infrared spectroscopy, Fayer group clearly discussed the presence of two types of water ensembles in the reverse micelle assembly.[149] Moreover, the site selective solvation dynamics study unveiled the variation of interfacial water molecules from the bulk-like core water pool of the RM. The interfacial water undergoes slow orientation, unlike the faster bulk-like dynamics of water molecules present in the core of reverse micelle.[188,189,241] The behaviour of the interfacial water molecules are mostly effected by their tendency to form new H-bonding frame-work to the surfactant polar headgroup, e.g. to oxygen molecules on the sulfonate and succinate groups of AOT molecules;[188] even the nature and properties of these water molecules can be controlled by micro-polarity, micro-viscosity, molecular probe partition, and intramolecular electron-transfer processes.[242] But surprisingly, as discussed in *chapter 1* the interface of cationic water/CTAB/*n*-octanol/cyclohexane reverse micelle is water free.[180] Britton group attributed these observation to the presence of co-surfactant in the interface of CTAB reverse micelle.[210] These study influenced us to investigate presence of water molecules in the interface of co-surfactant free reverse micelle.

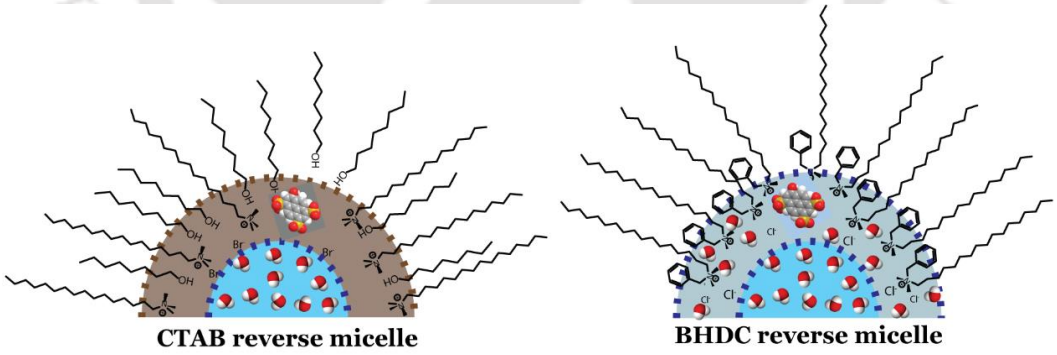

Scheme 4.1: Comparison of possible environment around HPTS in the interfacial regions of BHDC and CTAB reverse micelle. In the CTAB reverse micelle the co-surfactant *n*-octanol inserted in-between the CTAB surfactant.

We chose a tertiary medium, viz. water/BHDC/Benzene and explored with the interface localized probe HPTS and exposed the medium to different water level. A schematic representation of the interface of CTAB and BHDC reverse micelle is pictorialized in **Scheme 4.1**.

4.2. RESULTS

4.2.1. Steady-state Absorbance and Emission Spectroscopy:

The absorption spectra with λ_{max} ~ 406 nm, clearly revealed existence of only protonated form of HPTS in the RM (**Figure 4.1a**).

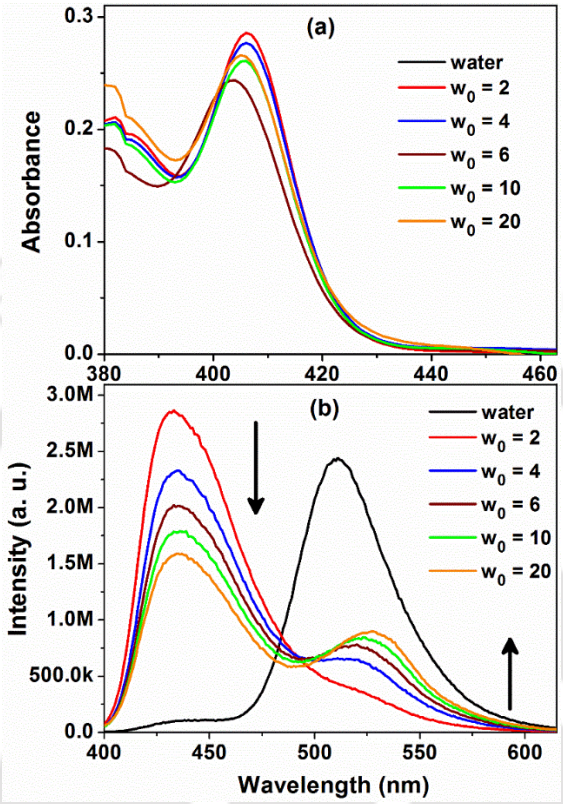

Figure 4.1. (a) Absorption spectra of HPTS in water/BHDC/benzene reverse micellar system at different w_0. Absorption spectrum of HPTS in water is also included for comparison. **(b)** Emission spectra of HPTS inside BHDC reverse micelle at various w_0 values (λ_{ex} = 390 nm). Emission spectrum in water is also included for comparison.

The emission spectrum of HPTS in water is largely dominated by a strong emission band centered at ~512 nm and a very faint emission band at ~440 nm (**Figure 4.1b**) representing the de-protonated and protonated form. The relatively faster ESPT of HPTS (~ 90ps) in water compared to its fluorescence lifetime (~5.5ns)[27] support this observation. On the contrary, inside the BHDC reverse micelle, the emission spectrum is rather dominated by the protonated form for low w_0 (= 2) and with a very minute hump at ~525 nm (**Figure 4.1b**). This observation revealed absence of significant ESPT inside BHDC at low w_0. However, with increasing water content, the emission intensity of the protonated emission decreases gradually with a concomitant development of the de-protonated emission band. To get more insight into the emission characteristics of the protonated and deprotonated forms, we decomposed the total emission spectrum at respective w_0 values into two emission bands as described in *chapter2* and then

generated the two emission spectra from the fit parameters. An example of the analysis is given for the emission spectrum at w_0 = 10 (**Figure 4.2a**). The fitted emission maxima of the protonated and de-protonated emission bands were at 436 nm and 525 nm, respectively and most importantly, we observed that the overlap between the emission spectra of the two forms extends over a significant wavelength range.

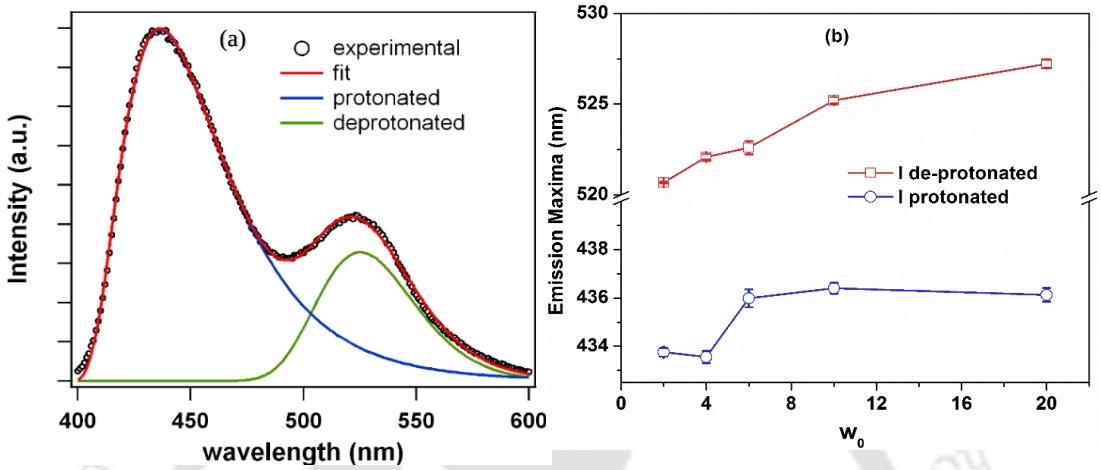

Figure 4.2: **(a)** Decomposition of the observed emission spectrum at w_0 = 10 (open circle) into protonated (blue line) and de-protonated (green line) emissions. The red line denotes the fitting by a superposition of two lognormal peak functions. **(b)** Variation emission maxima of the protonated and de-protonated emission of HPTS against w_0 inside water/BHDC/benzene reverse micelle.

From the decomposed spectra (**Figure 4.2a**), it is also clear that not only the intensity ratio of the two emissive forms but their peak positions are also changing with water content. The RO^{*-} emission maxima shifts from 521 nm to 527 nm as the w_0 values vary from 2 to 20 (**Figure 4.2b**). Interestingly, these values are much different from the emission maximum of the de-protonated form in water (512 nm) or other RM (AOT or Igepal[208]). Such red-shifted emission of RO^{*-} was reported for HPTS absorbed to CTAB micelle[239] or in lysozyme-CTAB aggregate.[101] The red-shifting of emission spectra may be a general feature of HPTS residing in a positive interface and may arise from the efficient electrostatic interaction and solvation by opposite charged headgroup. Cation-π interaction between the quaternary ammonium headgroup of BHDC and the aromatic ring of HPTS or π-π interaction between the benzyl group of BHDC and HPTS may also contribute to the red-shifting. Huppert and co-worker reported a red-shifted emission for HPTS linked to alumina surface via a covalent linkage.[243]

4.2.2. Time-resolved emission measurements:

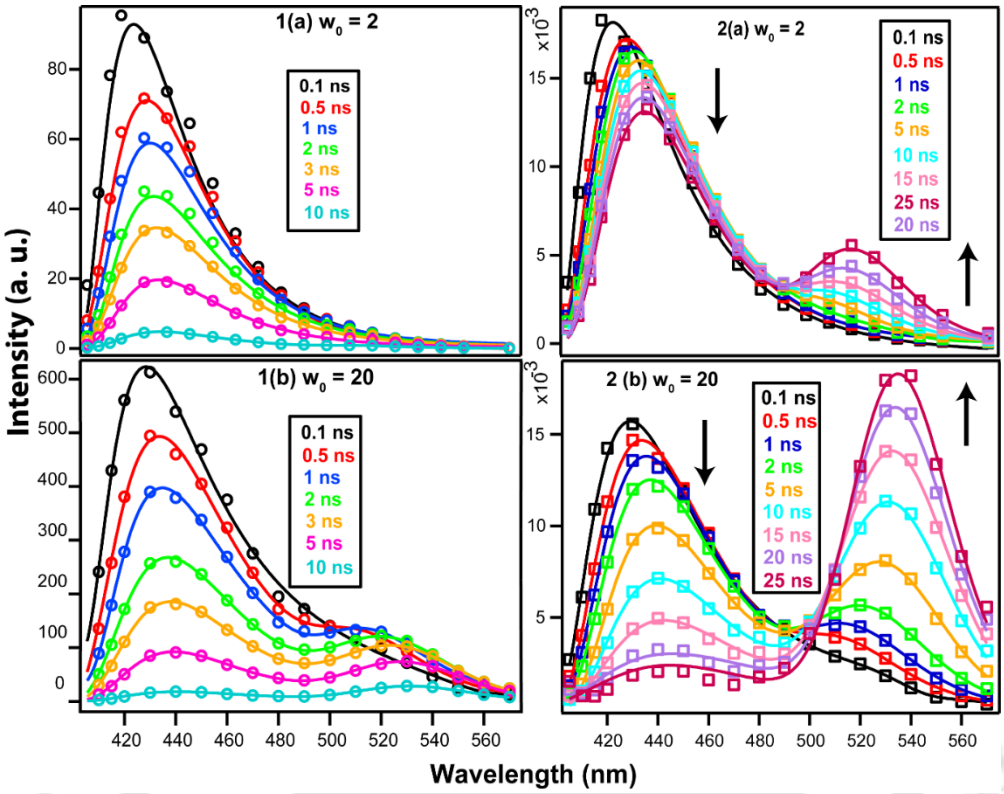

Figure 4.3: TRES (left panel) and TRANES (right panel) of HPTS inside BHDC reverse micelle at w_0 = 2 and 20, respectively. The ESPT process is obviously more prominent at higher w_0.

The fluorescence transients of HPTS were recorded at 10 nm wavelength intervals across the steady state emission spectrum and subsequently, time-resolved emission spectra (TRES, **eq. 2.15, *chapter 2***) and time-resolved area-normalized emission spectra (TRANES) were reconstructed accordingly (**Figure 4.3**). This is often considered as a better method of probing ESPT dynamics over single wavelength approach especially under strong overlap between protonated and de-protonated emissions and time dependent spectral relaxation.[208, 218, 220, 244] We clearly observed domination of protonated emission at short time for both TRES and TRANES. And with lapse of time, the de-protonated form appears at the expense of the protonated emission. Comparing TRANES of different w_0s, it can be stated that the ESPT process becomes more prominent with increase of w_0.

The decay of the integrated total emission intensity (integrated area of the entire TRES) shows an exponential decay with time constant of 3.2±0.2 ns (**Figure 4.4, right panel**). This time constant denotes lifetime of HPTS inside the BHDC reverse micelle free from ESPT[208] which is not vary significantly with w_0. The lifetime is very different from the reported lifetime in water

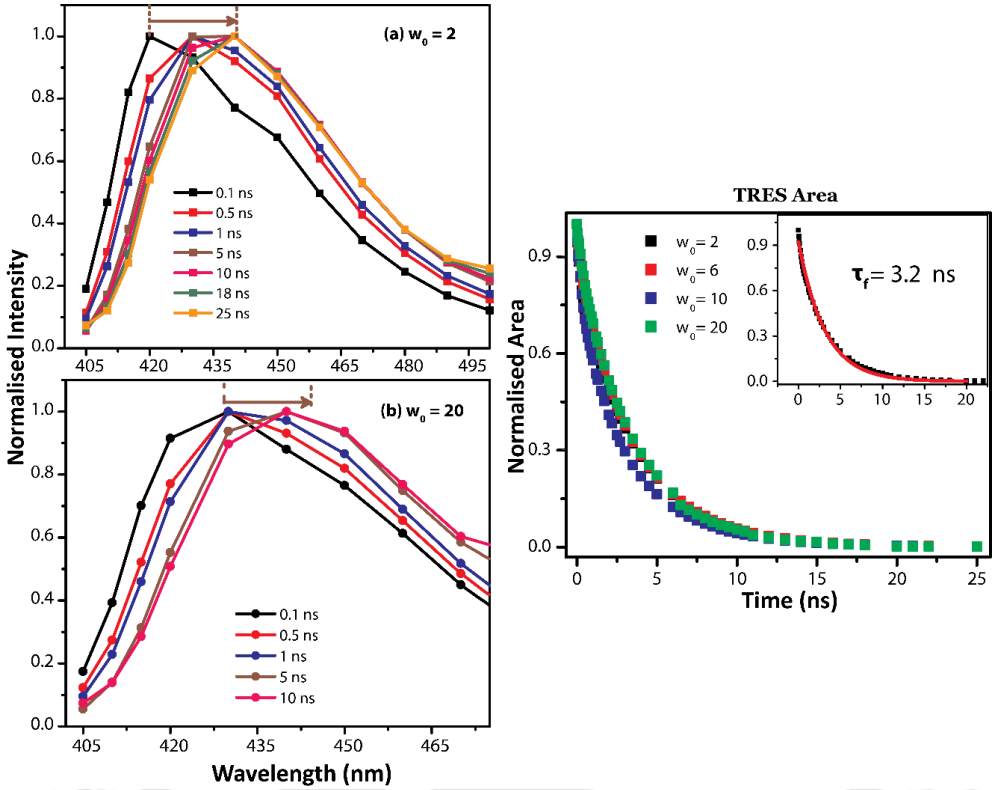

Figure 4.4: The normalized TRES (protonated form only, left panel) of HPTS inside BHDC reverse micelle at w_0 = 2 and 20, respectively. In the right panel, integrated area vs. time plot of the entire TRES of HPTS inside water/BHDC/benzene reverse micelle at w_0 = 2, 6, 10 and 20, respectively. The inset shows the average decay of the all four w_0 values, fitted to single exponential.

(5.4 ns)[27] and more closely resemble to the lifetime of HPTS in methanol (3.4 ns).[245] These life time variation implied change of the microenvironment of HPTS inside BHDC RM from that of bulk water. The lifetime of HPTS inside AOT RM was found to be 5.0 ns by the same method while a w_0 dependent distribution of lifetime (1.8-2.1 ns and 5.0-5.4 ns) was obtained for neutral igepal RM.[208]

Moreover, the normalized TRES of the protonated emission displays significant spectral relaxation in the shorter times mostly within ~ 1 ns (**Figure 4.4, left panel**). This time dependent Stokes shift (characteristics of solvation dynamics) may be due to solvation of the initially excited HPTS (protonated form) by the positive head-groups, counter ions and water prior to ESPT process. Thus, three different processes are evident from the TRES measurements: solvation dynamics accounting for spectral shift in the faster time scale followed by excited state proton transfer and relaxation back to the ground state (lifetime).

We also compared the fluorescence decays for different w_0 at two fixed wavelengths- 425 nm and 570 nm, respectively for the protonated and de-protonated forms. From the **Figure 4.5a**,

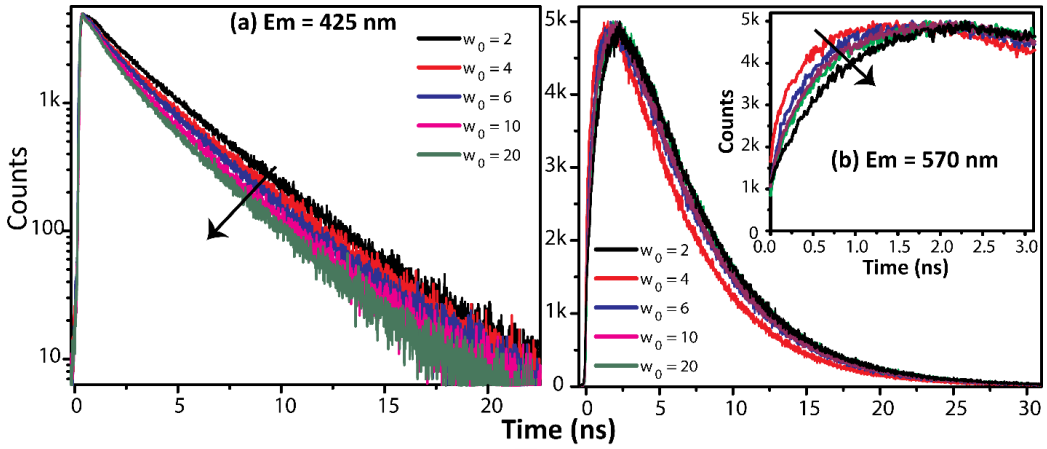

Figure 4.5. The fluorescence transients of the (a) protonated, ROH*(t) and (b) de-protonated, RO^{*-} forms of HPTS at different w_0 values. The emission transients were measured at 425 nm and 570 nm, respectively upon excitation at 375 nm. The initial portion of de-protonated transients (inset) clearly shows the systematic variation of rise of the emission decay at different w_0s are displayed in the inset to show clearly.

a moderate variation among emission transients of the protonated form at different w_0 is visible. Although the decays of the protonated form become progressively faster with increase of the w_0 values; yet even at the highest w_0 value is markedly slower than that of bulk water. The decays at 425 nm (ROH* emission) and 570 nm (RO^{-*} emission, **Figure 4.5b)** can be best fitted by a tri-exponential and bi-exponential function respectively (**eq. 2.1** ***chapter 2***). This is consistent with three processes extracted from the TRES measurement. Thus, we may assign the first component to solvation dynamics while the longest component represents the lifetime and the intermediate component may be due to ESPT process. Note that there is only very little variation among the components at various w_0s but a clear variation of the amplitude of the components can be noticed (**Table 4.1**).

Table 4.1. Fluorescence decay parameters of protonated, ROH*(t) and de-protonated, RO^{*-} emissions of HPTS inside BHDC reverse micelle, respectively measured at 425 nm and 570 nm. The decay parameters of the D_2O containing RM are also added for comparison.

w_0	Protonated, ROH*(t)			De-protonated, RO^{*-}(t)	
	τ_1 (ps)	τ_2 (ps)	τ_3 (ps)	Rise (ps)	τ_f (ps)
2 (H_2O)	330 (0.20)	1435 (0.25)	3450 (0.55)	1240 (-0.90)	4770 (1.90)
2 (D_2O)	660 (0.14)	1565 (0.18)	3415 (0.67)	1275 (-0.45)	4570 (1.45)
4 (H_2O)	340 (0.28)	1550 (0.28)	3410 (0.44)	1700 (-1.80)	5000 (2.80)
4 (D_2O)	400 (0.24)	1725 (0.25)	3510 (0.51)	1770 (-1.37)	4990 (2.37)
6 (H_2O)	290 (0.30)	1340 (0.30)	3250 (0.41)	1640 (-2.20)	5100 (3.20)
6 (D_2O)	370 (0.24)	1540 (0.26)	3410 (0.50)	1810 (-2.16)	5150 (3.16)
10 (H_2O)	245 (0.32)	1250 (0.33)	3140 (0.35)	1500 (-2.78)	5200 (3.80)
10 (D_2O)	320 (0.24)	1490 (0.31)	3360 (0.45)	1826 (-2.61)	5270 (3.61)
20 (H_2O)	250 (0.31)	1180 (0.38)	3080 (0.32)	1480 (-2.30)	5230 (3.30)
20 (D_2O)	440 (0.30)	1730 (0.34)	3350 (0.37)	1820 (-3.07)	5365 (4.07)

Most notably, contribution (i.e. a_2) of the ESPT process increases with w_0. All the fluorescence transients (at 570 nm) of the de-protonated forms show distinct rise time matching with the ESPT component observed at 425 nm.

4.2.3. Kinetic isotope effect:

Kinetic isotopic effect is one of the convenient ways to test whether the photo-physical process of HPTS inside the BHDC reverse micelle involves solvation dynamics or ESPT phenomena.[246] We replicate the fluorescence measurements by replacing water with D_2O. The ratio of de-protonated emission intensity to the protonated emission is clearly smaller in D_2O containing BHDC RM compared to water analogue at all w_0 values (**Figure 4.6b**).

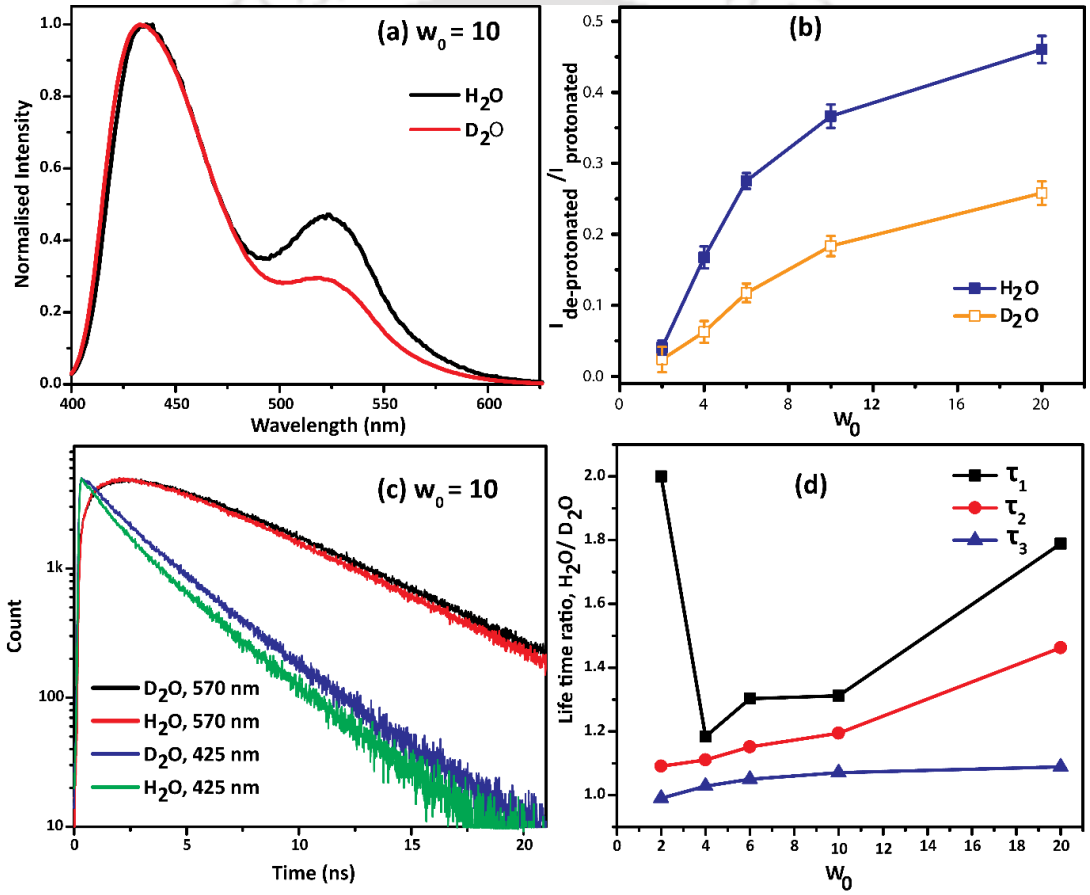

Figure 4.6: (a) Steady-state normalized emission spectra, (b) the ratio of intensity of de-protonated and the protonated emission band, (c) time-resolved fluorescence transients (at 425 nm and 570 nm) and (d) isotropic effect on the life time of HPTS inside the BHDC reverse micelle containing either water or D_2O.

A comparison of the emission spectra of HPTS inside BHDC reverse micelle containing water vs. D_2O at w_0 = 10 is given **Figure 4.6a**. The overall KIE is found to be 1.5-2 based on the steady-state fluorescence. Similarly, the fluorescence transients at both 425 nm and 570 nm differ significantly in D_2O from that in water. **Figure 4.6c** shows the fluorescence transients in water

and D_2O at w_0 = 10. The first two decay components (due to solvation dynamics and ESPT respectively) in the D_2O containing RM are significantly higher than the decay components in water containing RM (**Table 4.1**). We observed that the amount of KIE increases with increase of w_0 **(Figure 4.6b**).

However, KIE is significantly lower compared to that of bulk water vs. D_2O (KIE ~3).[246,247] Thus we may conclude that only a fraction of the HPTS is undergoing ESPT. The non-negligible KIE supports the assignment of the solvation dynamics and ESPT origin of the components. Note that similar small KIE (~1.7) was observed for HPTS absorbed onto the chitin surface in water vs. D_2O.[246]

4.2.4. Dynamic light scattering.

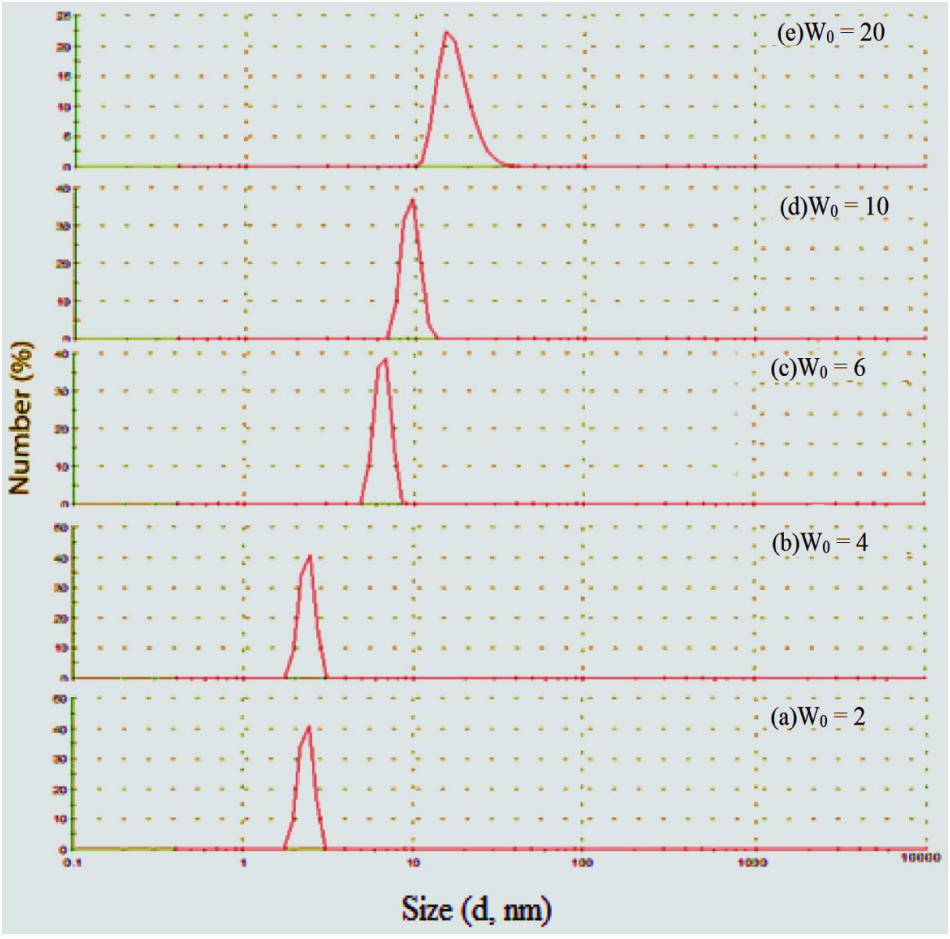

Figure 4.7. The size distribution obtained from dynamics light scattering (DLS) of water/BHDC/benzene reverse micelles at different w_0.

The size (diameter, nm) of the reverse micelle at various w_0 values were measured using dynamic light scattering. The size of the reverse micelle gradually increases with increase of w_0.

The measured sizes are listed in the **Figure 4.7** and **Table 4.2**. The values are consistent with an earlier report.[219]

Table 4.2. The hydrodynamic diameters of water/BHDC/benzene reverse micelles obtained from dynamics light scattering (DLS) at different w_0.

W_0	Hydrodynamic diameter (d, nm)	Reported size (d, nm)[a]
2	2.4	3
4	4.2	-
6	6.5	-
8	7.9	-
10	9.4	8.5
20	17.1	15

[a] From reference[247]

4.2.5. Fluorescence anisotropy decay:

Fluorescence anisotropy decays were measured to gain knowledge of the local environment around the probe. The anisotropy decays at various w_0 values are much slower compared to that in a fluid solvent (e.g. in methanol or water). The rotational relaxation time of HPTS in bulk methanol was found to be 240 ps.

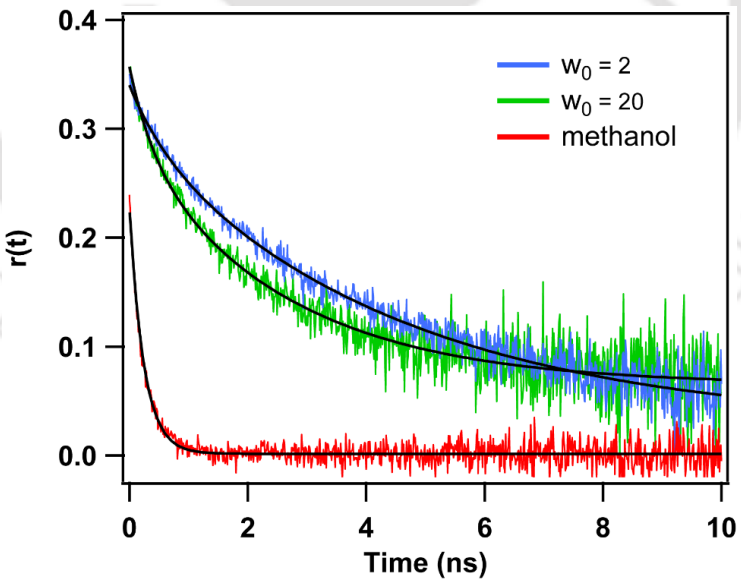

Figure 4.8. Fluorescence anisotropy decays of HPTS in bulk methanol (red) and in BHDC reverse micelle at w_0 values of 2 (blue) and 20 (green) measured at λ_{ex} = 375 nm and λ_{em} = 440 nm. The black line indicates a bi-exponential fit according to equation (2). It is evident that the anisotropy decays inside the RM are much slower compared to that in methanol and very less sensitive to water content.

The anisotropy decays in BHDC reverse micelle were found to be much slower compared to that of methanol indicating a very restricted rotation of the probe (**Figure 4.8**). Noted although they become relatively faster with increase of water content; yet remain much slower than in bulk water or inside AOT RM at same water content (or similar size of water pool). These may indicate that the interfacial arrangement becomes somewhat relaxed at higher w_0 due to higher level of hydration and still the probe retain in the interface.

The anisotropy decays maintain very small but finite residual fluorescence anisotropies that do not decay completely probably due to short fluorescence lifetime (~ 3.2 ns). The rotational anisotropy decays can be fitted with a bi-exponential function (**eq. 2.17** ***chapter 2***) having a constant residual anisotropy(r_∞). The anisotropy decay parameters are provided at **Table 4.3**. We analysed the anisotropy decays via wobbling-in-cone (WIC) model, used for interface-bound fluorescence probe in reverse micelles; discussed in ***chapter 2.*** The rotational times are usually very sensitive to the rigidity of the environment where the probe is located.

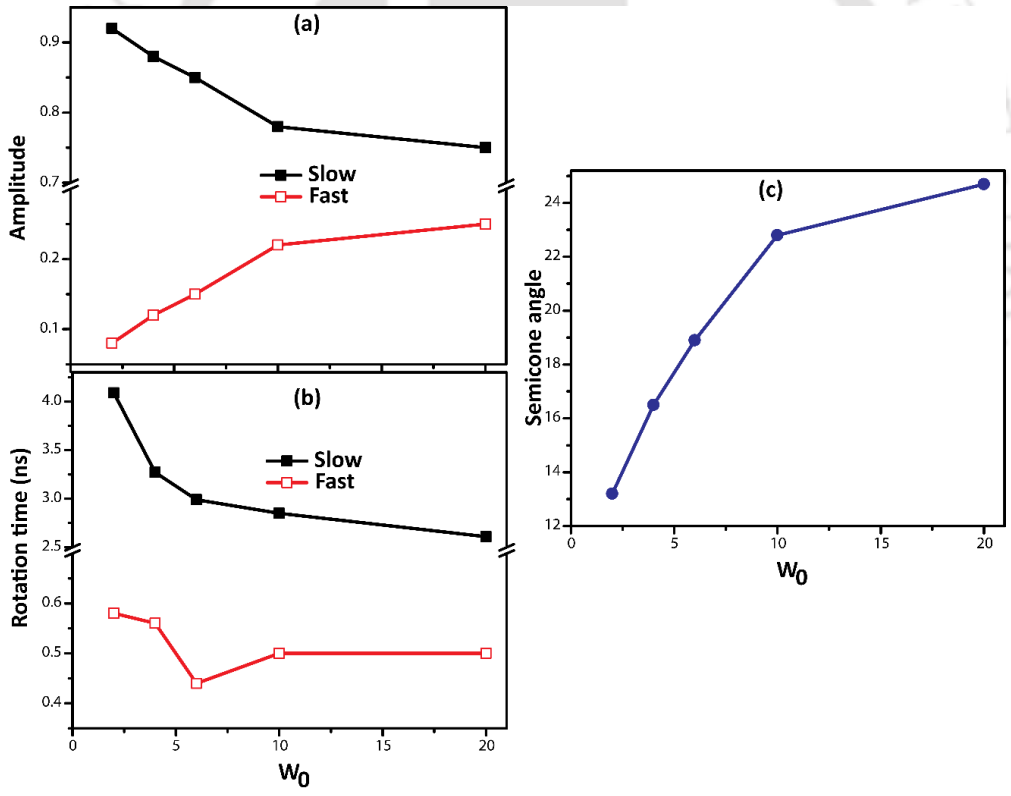

Figure 4.9. Variation of the amplitude and time constants of the anisotropy (left panel) and the semi-cone angles (right panel) of HPTS inside water/BHDC/benzene reverse micelle with w_0. It is clear that both the amplitude and time constant of slow rotational component decrease with increase of the water content.

Table 4.3. Anisotropy decay parameters of HPTS in water/BHDC/benzene reverse micellar system at different w_0 values.

w_0	r_0	r_∞	a_s	τ_s (ns)	τ_f (ns)	τ_W (ns)	$\theta\ (deg)$
2	0.33	0.03	0.92	4.09	0.58	0.67	13.2
4	0.33	0.03	0.88	3.27	0.56	0.67	16.5
6	0.34	0.04	0.85	2.99	0.44	0.51	18.9
10	0.39	0.08	0.78	2.85	0.50	0.60	22.8
20	0.35	0.07	0.75	2.61	0.50	0.62	24.7

If the probe is located in the core, the rigidity of the environment should change dramatically as the size of the water pool increases but much less effect should be observed if the probe is situated within the interface. Our data implied restricted rotation of the probe inside BHDC reverse micelle at all w_0s and a small but systematic w_0 variation is observed for the long component (lateral diffusion) and also for the amplitude of slow components (**Table 4.3** and **Figure 4.9a**). Note that the semi-cone angle is relatively small and increases with w_0 (**Figure 4.9c)**. This implies that probe may be tightly confined within the interface and experience strong electric field and with increase of w_0 the wobbling motion becomes somewhat facile because of higher hydration. The w_0 dependence of the anisotropy is much less dramatic compared to the HPTS analogue (MPTS) inside AOT reverse micelle or even for the neutral reverse micelle igepal.[208] These results lead to assumption that the probe may reside in the interface rather than in the core.

4.2.6. NMR spectroscopy:

Employing 2D NOESY experiments, we intend to measure interaction of HPTS protons with BHDC surfactant protons and water molecules, if exists. This may help us to locate the position of HPTS inside the RM. Such method was previously applied by Levinger and co-workers for locating HPTS inside CTAB and AOT reverse micelles.[180] We performed experiment at two different w_0 values- 5 and 10. **Figure 4.10a** shows several cross peaks in the 2D NOESY spectrum at $w_0 = 5$. Usually an off-diagonal or cross peak arises if the spatial separation between two protons is very small (typically <5 Å).[248]

Two cross peaks appear for the interaction of H_1 proton of HPTS with one of the proton (β) in the benzene ring and with the aliphatic β' protons of the BHDC surfactant. Another cross peak arises from the interaction of the H_5 or H_6 proton of HPTS with the protons of the two methyl groups attached to the quaternary amine headgroup of BHDC and also with the aliphatic β' protons of the surfactant. Along with these, all of the HPTS protons are found to be interacting with water molecules. The results strongly recommend that the HPTS is located inside the headgroup regions

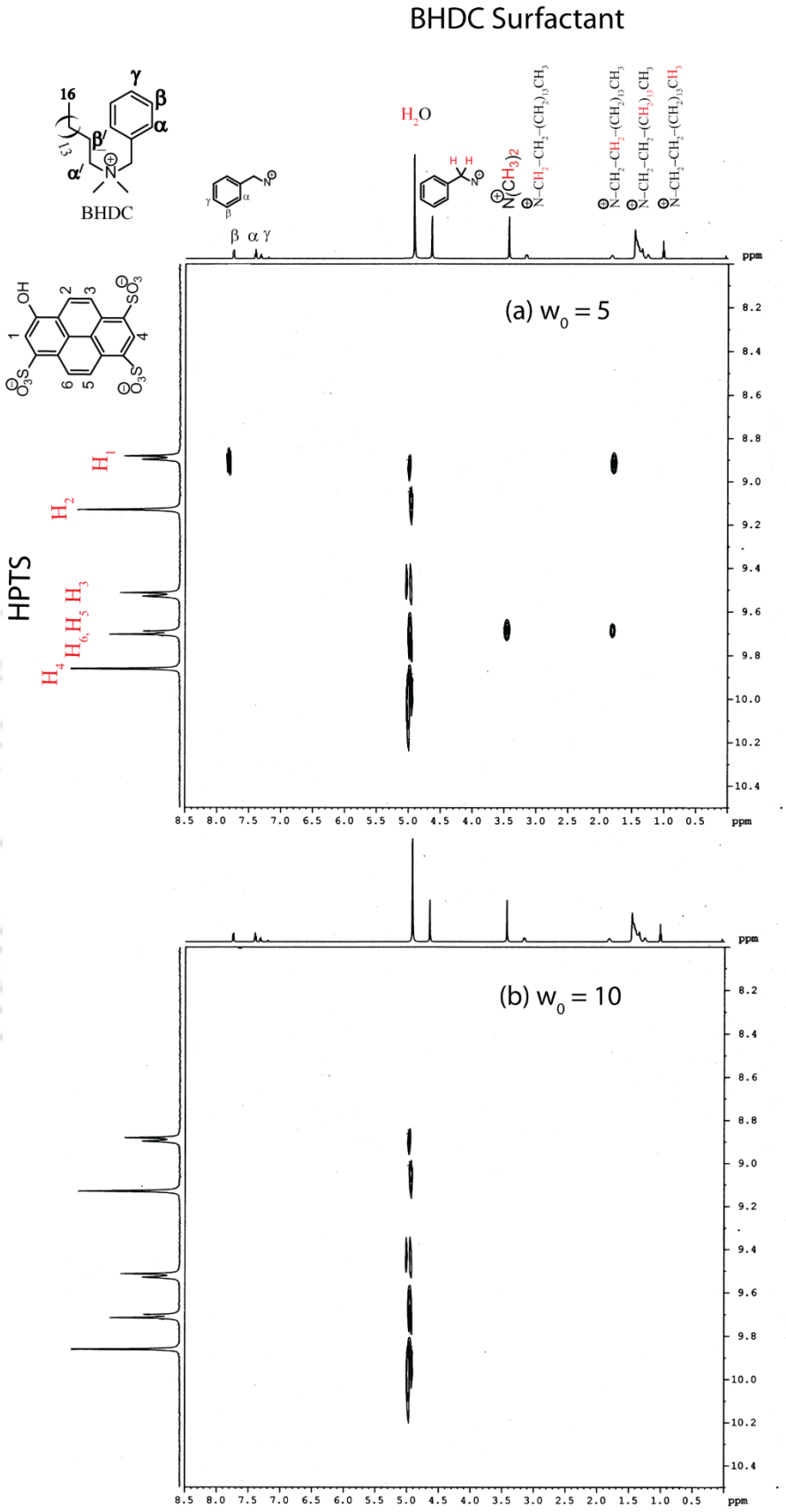

Figure 4.10. 2D NOESY spectrum of HPTS incorporated BHDC reverse micelles at (a) w_0 = 5. (b) w_0 = 10.

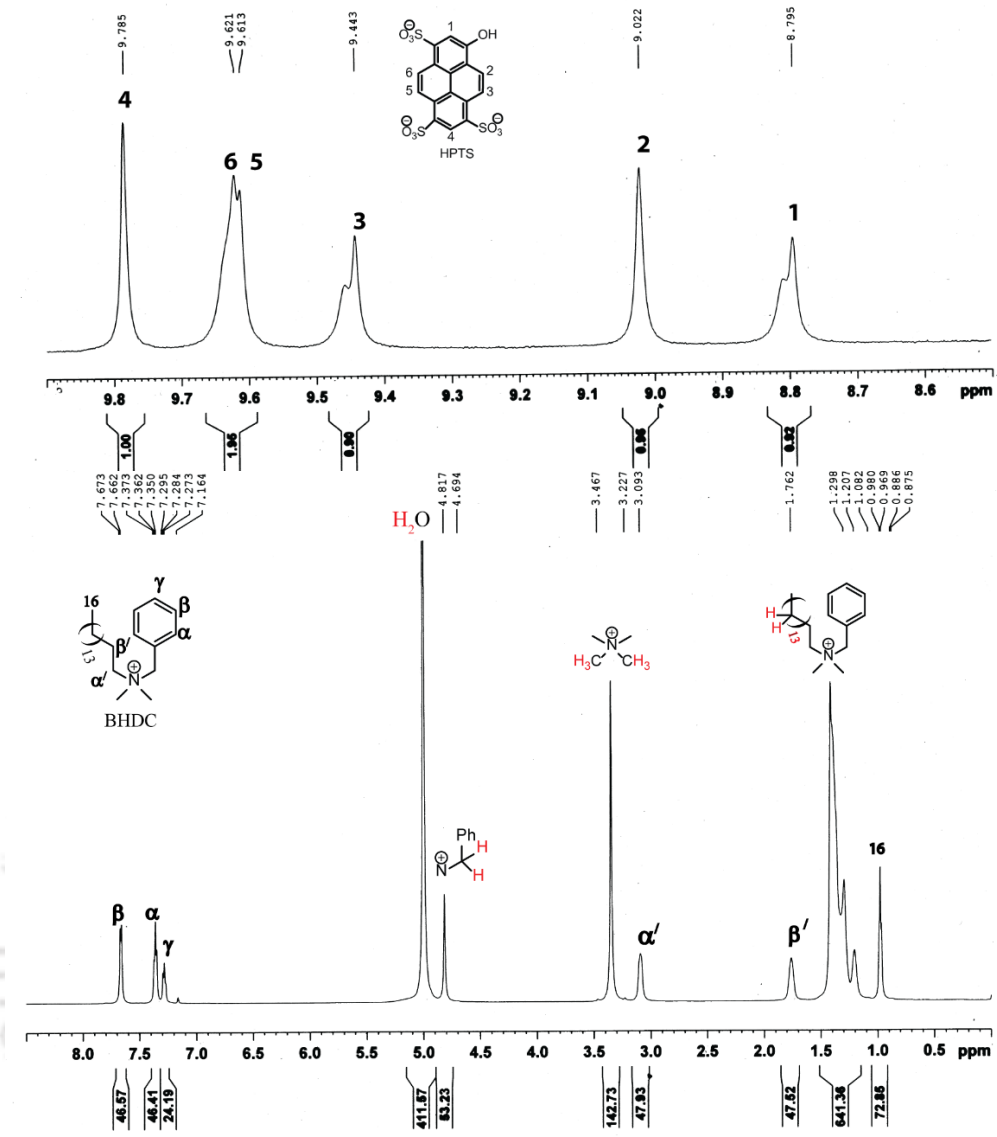

Figure 4.11 The ^{1}H NMR spectra of HPTS (top) and BHDC (bottom) in water/BHDC/benzene reverse micelle system.

of the BHDC RM supporting the electrostatic attraction between negatively charged probe and positively charged headgroup of the surfactants. In addition, several water molecules are present around HPTS supporting significant penetration of water molecules into the interface. These water molecules may be allowing ESPT even in this restricted position.

In the case of w_0 = 10 RM, the cross peaks are only observed with water; referring strong probe water interaction; that may suppressed the interaction of the probe with the surfactant BHDC.protons (**Figure 4.10b**). This may imply that the probe may move into the core or the interface is enriched with much more water so that interaction of the probe with surfactant gets suppressed. The NMR signals of all of the HPTS aromatic protons appear in the region ~ 8.8- 9.8 ppm. The signals were assigned to different protons of HPTS following Levinger and co-

workers.[180] These peaks are separated well from the peaks associated with the BHDC surfactants in the **Figure 4.11**.

4.3. SUMMARY AND CONCLUSIONS:

The ESPT of a negatively charged fluorophore HPTS has been investigated within a cationic BHDC reverse micelle using fluorescence spectroscopy. The location of the probe inside the RM was assigned by a combination of fluorescence anisotropy and NOESY measurements. The probe was found to be located at the interfacial region, similar to that of CTAB quaternary (*n*-heptane/CTAB/*n*-octanol/water) reverse micelle reported previously. However, the examined ESPT nature is very different from that of the CTAB reverse micelle; it undergoes detectable ESPT in BHDC RM whereas no ESPT was found inside CTAB RM. The difference in the ESPT trend in these two cationic interfaces may arise from difference in the interfacial properties of BHDC and CTAB reverse micelles; in the respect of co-surfactant. Our results qualitatively matches with that of the neutral igepal reverse micelle rather than in the cationic CTAB reverse micelle, where the presence of *n*-octanol at the interface may inhibit the ESPT completely at CTAB interface.[180] Moreover, the interfacial surfactant layer of BHDC is much less packed than conventional double chain surfactant like AOT, this may possibly help in water penetration from the core into the interface. The molecular dynamics simulation by Agazzi et al. also revealed high degree of water penetration into the BHDC RM interface; which enhanced with increase of water content and behave dynamically much restrained than water at the core.[249]

In summary, the interface of BHDC RM may be quite wet due to significant penetration of water from the core into the interface and it can serve as an excellent model for interfacial proton transfer at positively charged surface.

Chapter-5

The Impact of Co-surfactant on the Interfacial Hydration of Cationic Quaternary Water/CTAB/octanol/ cyclohexane Reverse Micelle[#]

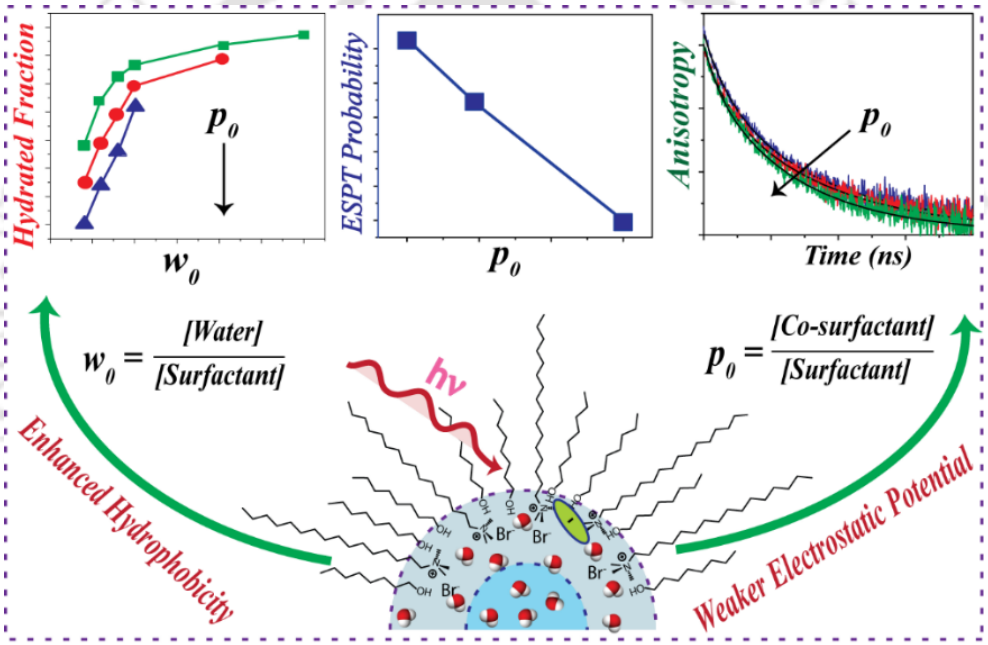

[#]This work has been published in *Langmuir* **2016**, *32*, 10659-10667.

भारतीय प्रौद्योगिकी संस्थान गुवाहाटी
Indian Institute of Technology Guwahati

CHAPTER 5
THE IMPACT OF CO-SURFACTANT ON THE INTERFACIAL HYDRATION OF CATIONIC QUATERNARY WATER/CTAB/OCTANOL/ CYCLOHEXANE REVERSE MICELLE[250]

5.1. INTRODUCTION:

Single tail surfactants like cetyltrimethylammonium bromide (CTAB), sodium dodecyl sulfate (SDS), and Triton-X, need assistance of co-surfactant e.g. medium or long chain alcohol to satisfy the necessary geometric condition $v / al > 1$, where v refer to volume and l is the chain length of the hydrocarbon tail, a polar headgroup area of the surfactant molecule to form a stable reverse micelle.[209,210] The co-surfactant is usually assumed to be inserted in-between the CTAB surfactants at the interface and introduced a new parameter p_0 (= [co-surfactant]/[surfactant]) in addition to prevalent parameter, w_0 (= [water] / [surfactant]). The capability of this new parameter to control the size and properties of the RM like flexibility and applicability of the RM enhances the importance of quaternary RM.[211] However, Levinger group reported absence of water content in this CTAB reverse micelle, through hydration sensitive ESPT dynamics, which may be due to participation of water repelling long chain alcohol, that acts as co-surfactant.[180] In another work they have investigated effect of the co-surfactant, 1-heptanol maintaining the ratio of 1:5 or 3:5 1-heptanol/AOT to retain the spherical structure of the water/AOT/isooctane tertiary RM.[232] They reported enhancement in the viscosity followed by slower solvation dynamics of the RM media. This co-surfactant effect even dominants over the influence of hydration level that increases with the w_0 value.[178,251]

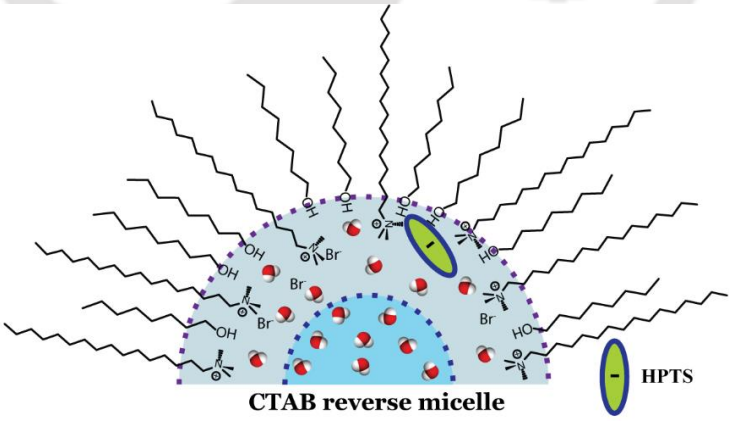

Scheme 5.1: Possible composition of the CTAB/Octanol/Water/Cyclohexane quaternary reverse micelle. Water is not only confined in the core but also penetrates into the interface and interfacial hydration depends on both parameters w_0 and p_0.

Following our work related to hydration response ESPT modulation of HPTS in the interface of BHDC RM, we get interest to investigate the complex interface of the quaternary

CTAB/Octanol/Water/Cyclohexane RM using the similar water sensitive ESPT technique. The interface of CTAB RM is quite promising, as they can successively entrap a large variety of proteins without disturbing their native state and activity compared with other RMs.[252,253] Moreover, Fuglestad et al. have reported penetration of significant amount (~30%) of water into the CTAB/hexanol/*n*-pentane/water quaternary RM[207] by molecular dynamics (MD) simulation study. The simulation result leads us to use nanosecond fluorescence spectroscopy technique to trace any slower ESPT dynamics in CTAB RM, remain unidentified in the pioneer work of Levinger and co-workers performed at ultrafast time domain. The composition of the reverse micellar medium is represented in **Scheme 5.1**.

5.2. RESULTS

5.2.1. Steady-state Absorbance and Emission Spectroscopy:

The absorption spectrum of HPTS in the CTAB/Octanol/Water/Cyclohexane reverse micelle shows a maximum at 407 nm at all w_0's (**Figure 5.1, left panel**). No absorption band persists at higher wavelength (> 430 nm) confirming exclusive existence of the protonated form in the ground state. Also the absorption spectrum is significantly red-shifted compared to the absorption maximum in water (403 nm) but similar to other cationic reverse micelles e.g. BHDC (406 nm) [240] and DDAB (405 nm).[254] This red-shift may be due to cation- π interaction of cationic headgroup of CTAB and π – electrons of aromatic ring of HPTS.

However, the emission spectra are dominated by a prominent band with emission maxima at 430 nm featuring the dominance of the protonated form in the excited state at all w_0's. Note that this emission band is slightly structured in nature having a clear shoulder at 440 nm; which may be assigned to the vibrionic transitions of the pyranine derivative commonly seen in less polar medium[198,223] under less solvent coupling. The position of the emission maximum and the shape of the emission spectra remain same for all w_0s, irrespective of the concentration of co-surfactant (**Figure 5.1, right panel**). With the increase of w_0, intensity of the protonated emission (at 430 nm) gradually decreases with a concurrent development of a new band at ~520 nm characteristics of the deprotonated emission (**Figure 5.1, right panel**). These observations are quite interesting in the context that Sedgwick et al[180] reported lack of ESPT for HPTS inside CTAB/octanol/cyclohexane/water reverse micelle from their ultrafast studies.

The emission maximum for the de-protonated form ($\lambda_{em}^{max} = 520\ nm$), undergoes gradual red-shift and may be due to solvatochromic behavior of HPTS and increase in the polarity of interface at higher w_0.[198] To monitor the role of the co-surfactant, we further varied the ratio of

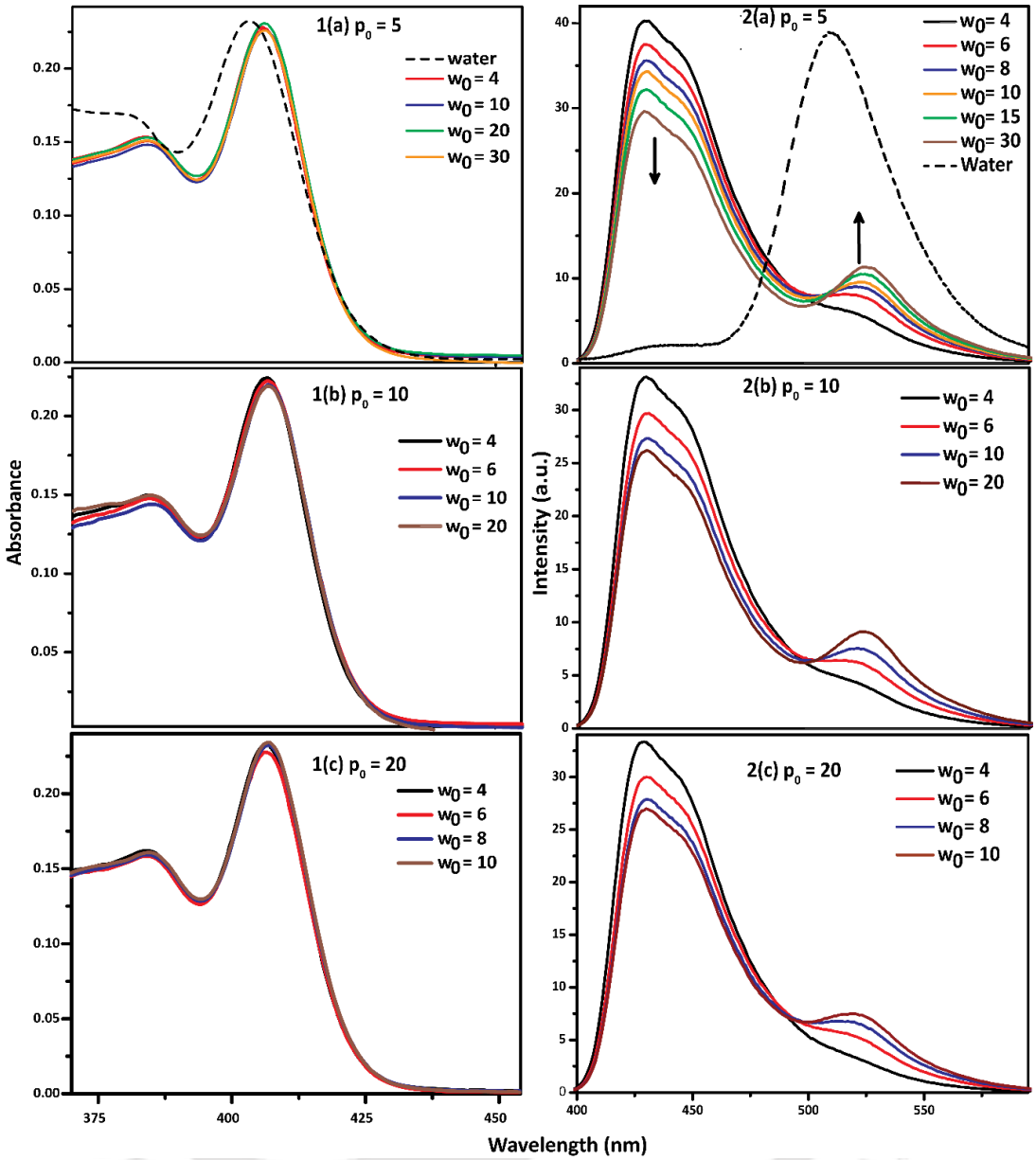

Figure 5.1: Absorption (left panel) and emission (right panel) spectra of HPTS in water/CTAB/cyclohexane/octanol reverse micelle at different w_0s for p_0 = 5, 10 and 20. The absorbance maxima of HPTS in the CTAB reverse micelle get red-shifted compared to the bulk water and only shows absorbance below 450 nm. The absorption emission spectra of HPTS in the water (dotted line) is also included for comparison.

co-surfactant to surfactant concentrations, p_0 = 5, 10, 20 and observed significant ESPT even at highest octanol concentration (p_0 = 20). However, any clear trend is not observed for the p_0 dependence from the steady state emission. Note that relative intensity of the protonated and deprotonated form not only depends on the rate or favorability of ESPT but also on the lifetime of the respective species. Decomposition of these two parallel processes is difficult from emission spectra.

5.2.2 Time-Resolved Fluorescence:

To get more insight about the ESPT nature we measured fluorescence transients of HPTS at 5 nm intervals across the steady state emission spectra and construct time-resolved emission spectra (TRES, **Figure 5.2, left panel**) and time-resolved area-normalized emission spectra (TRANES, **Figure 5.2, right panel**).[218,220]

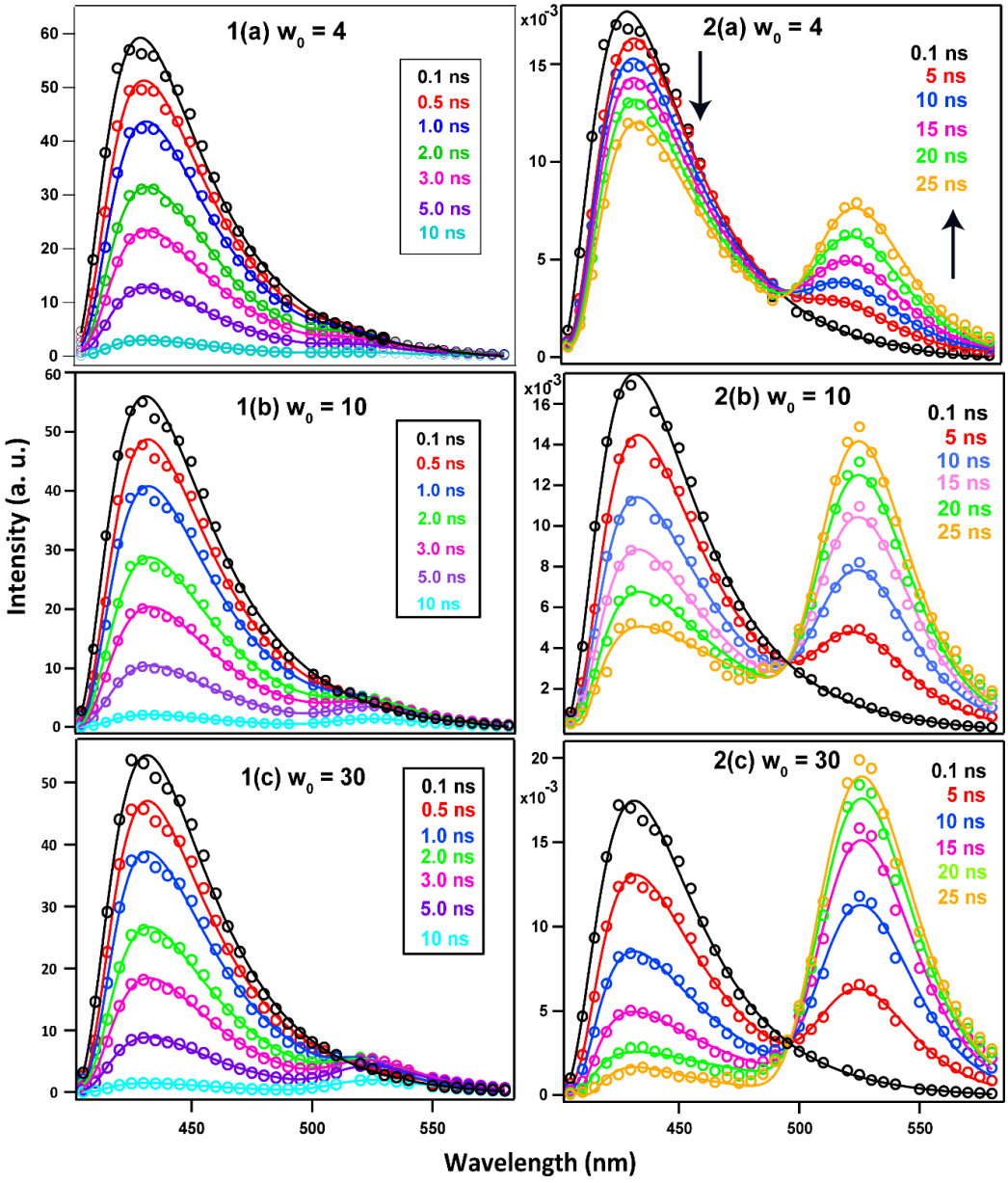

Figure 5.2: Time-resolved emission spectra (TRES, left panel) and Time-resolved area normalised emission spectra (TRANES, right panel) of HPTS inside the CTAB/octanol/cyclohexane/water (at $p_0 = 5$) quaternary reverse micelle at $w_0 = 4$, 10, and 30, respectively. Solid lines denote fit to a bi-lognormal function according to **eq. 2.14** at ***chapter 2***.

At early time (t = 0.1 ns) TRANES exclusively display only the protonated emission and no sign of deprotonated form. This confirms absence of any ultrafast component in the cationic CTAB

reverse micelle system that consistent with the results of Levinger and co-workers[180]. At longer times, the deprotonated band clearly manifests at the expense of the protonated band signifying ESPT process. It is also clear that at a fixed p_0 value ESPT is more facile with the increase of w_0.

We also compared TRANES at different p_0's at a longer time delay (25 ns) to appreciate the effect of alcohol on the ESPT dynamics (**Figure 5.3**). The plot reveals that the protonated form of HPTS becomes more prominent when alcohol participation increases in the interface suppressing the ESPT. The emission ratio of the deprotonated to protonated intensity against p_0 in the inset of **Figure 5.3** clearly shows the ESPT hindarence on increase in the p_0 value.

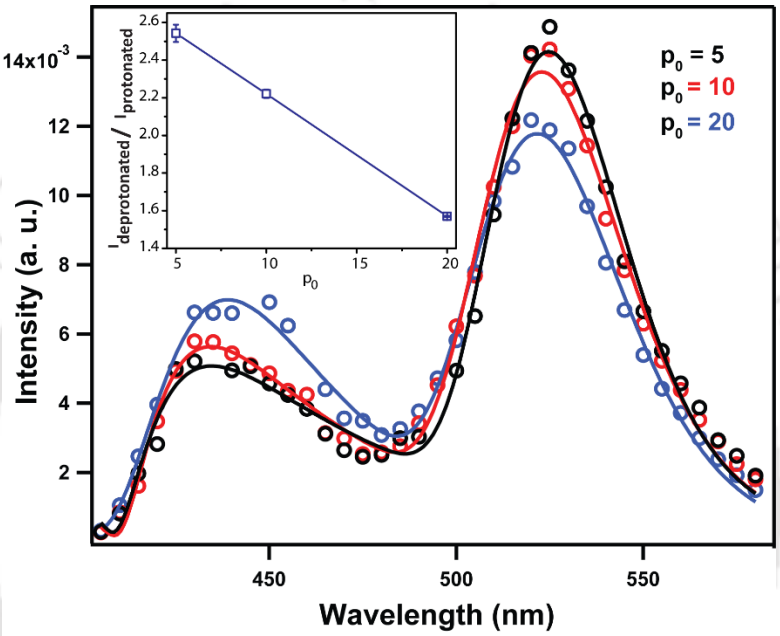

Figure 5.3: Comparison of 25 ns TRANES at fixed w_0 = 10 and at different p_0's. The ESPT probability seems to decrease when more alcohol is present at in the interface. The inset displays the ratio metric plot of the two peak intensities.

We have also recorded fluorescence transients of HPTS at two selective emission wavelengths representative of the protonated (425 nm) and deprotonated (570 nm) emission. Note that 425 nm is slightly higher in energy compared to the protonated emission maxima ($\lambda_{em}^{max} = 430\ nm$), whereas, 570 nm is lower in energy compared to the de-protonated emission maxima ($\lambda_{em}^{max} = 520 - 525\ nm$). We intentionally pick these wavelengths to avoid undesirable mixing of the contribution of the two respective forms.[239,69]

The fluorescence transients of HPTS monitored at 425nm becomes faster with w_0 variation, irrespective of octanol to CTAB ratio (**Figure 5.4, left panel**). We also observed that for a particular w_0, the effect of alcohol variation on the fluorescence transients of the protonated form is very small but systematic (425nm, **Figure 5.5, left panel**). The decay becomes slightly

slower with increase of p_0. However, the emission transients of the de-protonated form (at 570 nm, **Figure 5.5, right panel**) seemes to be significantly faster with the increase of p_0 values.

Table 5.1: Time transient fluorescence decays fitting parameters of protonated, ROH*(t), and deprotonated, RO^{*-}, forms of HPTS inside CTAB reverse micelle, measured at 425 and 570 nm, $p_0 = 5$. The faster decay time match to their respective rise time value. ([a] ± 0.1 ns)

W_0	$P_0 = 5$ [a]					
	ROH*= 425nm			RO^{-}*= 570 nm		
	τ_1 (ns)	τ_2 (ns)	χ^2	τ_1 (ns)	τ_2 (ns)	χ^2
4	2.1 (0.18)	3.5 (0.82)	1.02	2.1 (-2.28)	4.7 (3.28)	1.16
6	2.1 (0.37)	3.5 (0.63)	1.05	2.1 (-3.07)	5.1 (4.07)	1.15
8	2.1 (0.41)	3.5 (0.59)	1.03	2.1 (-3.67)	5.2 (4.67)	1.06
10	2.1 (0.46)	3.5 (0.54)	1.05	2.1 (-4.50)	5.3 (5.50)	1.03
20	2.1 (0.57)	3.5 (0.43)	1.09	2.1 (-5.75)	5.4 (6.75)	1.09
30	2.1 (0.60)	3.5 (0.40)	1.02	2.1 (-3.07)	5.5 (4.07)	1.12

The decays for both protonated and de-protonated form can be best fitted by a bi-exponential function (eq. 2.1, *chapter 2*).[254] The fitted results reveal that the contribution of faster component gradually increases on increasing the w_0 values, and so as their corresponding rise time irrespective of the alcohol to surfactant ratio (**Table 5.1 and Table 5.2**).

Table 5.2. Fluorescence decay fitting parameters of protonated, ROH^*(t), and deprotonated, RO^{*-}, forms of HPTS inside CTAB reverse micelle, measured at 425 and 570 nm, $p_0 = 10$ and 20. The faster decay time match to their respective rise time value.

w_0	$P_0 = 10$ [a]				$P_0 = 20$ [a]			
	ROH* = 425nm		RO^{-}* = 570 nm		ROH* = 425nm		RO^{-}* = 570 nm	
	τ_1(ns)	τ_2 (ns)	τ_1 (ns)	τ_2 (ns)	τ_1 (ns)	τ_2 (ns)	τ_1 (ns)	τ_2 (ns)
4	2.1 (0.20)	3.5 (0.81)	2.1 (-1.58)	4.6 (2.58)	2.1 (0.18)	3.5 (0.82)	2.1 (-0.82)	4.4 (1.82)
6	2.1 (0.33)	3.5 (0.67)	2.1 (-2.63)	4.7 (3.63)	2.1 (0.25)	3.5 (0.75)	2.1 (-1.58)	4.4 (2.58)
8	2.1 (0.39)	3.5 (0.61)	2.1 (-3.07)	4.9 (4.07)	2.1 (0.30)	3.5 (0.70)	2.1 (-2.28)	4.5 (3.28)
10	2.1 (0.44)	3.5 (0.56)	2.1 (-3.67)	5.0 (4.67)	2.1 (0.35)	3.5 (0.65)	2.1 (-3.07)	4.8 (4.07)
20	2.1 (0.56)	3.6 (0.44)	2.1 (-4.50)	5.3 (5.50)				

[a] ± 0.1 ns

The negligible contribution of the faster component at $w_0 = 4$ may be due to very less favourable ESPT at this low water content. It is remarkable that the de-protonated time transient decays can be fitted using rise time matching with that of the faster decay time constant of the protonated form at all w_0. On increasing p_0, the contribution of the slower component of protonated form

increases with concominent reduction of the contribution of the corresponding faster decay component (**Table 5.3**).

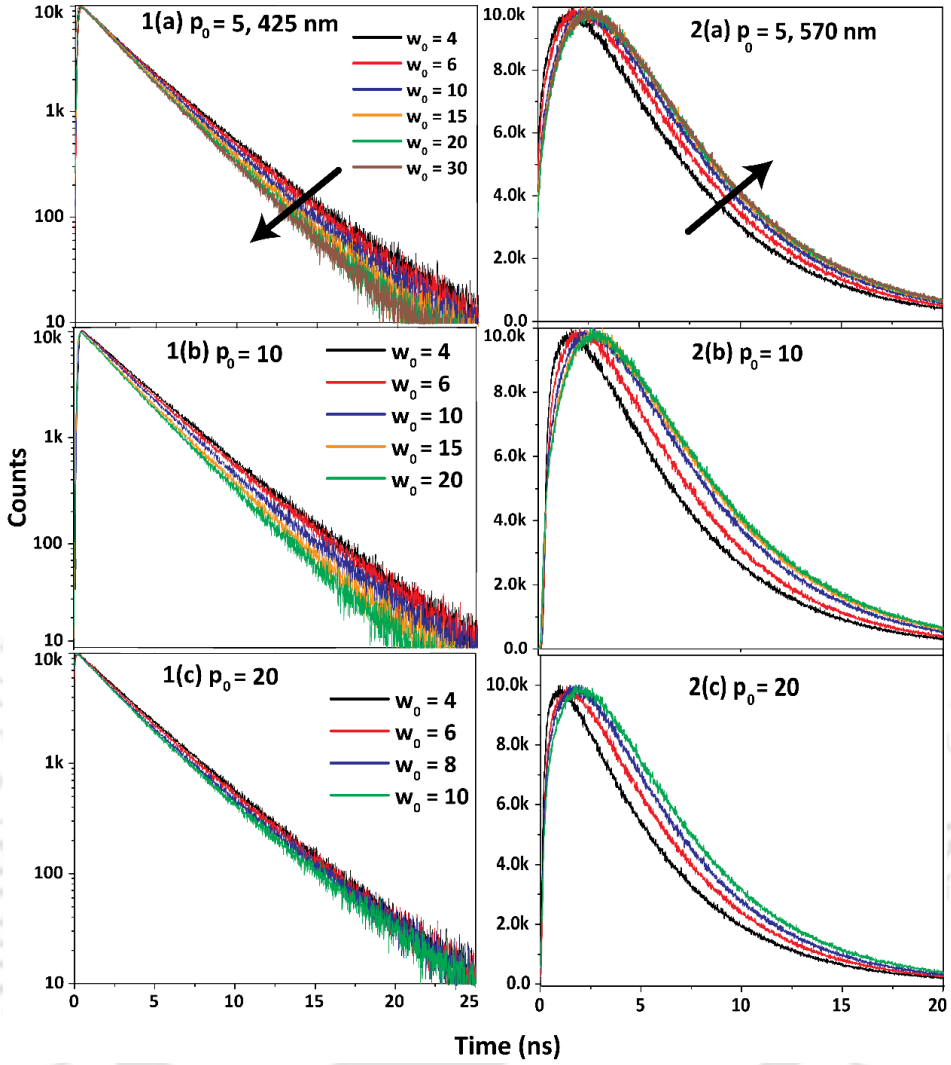

Figure 5.4: Fluorescence transients of the (left panel) protonated, ROH^* (λ_{em} = 425 nm), and (right panel) deprotonated, RO^{*-} (λ_{em} = 570 nm), forms of HPTS at p_0 = 5, p_0 = 10 and p_0 = 20 with variation of w_0s value (λ_{ex} = 375 nm). The protonated emission transients become faster with w_0 variation.

The fluorescence decays of both the protonated and de-protonated form can be reasonably fitted with a bi-exponential function (**eq. 2.1, *chapter 2***) with matching decay and rise times. However, this decay pattern could arise if we assume bimodal distribution of HPTS inside the interface. The fraction of probe which is localized inside the hydrated region may undergo ESPT. Another fraction might be present in the dehydrated region and hence, can not show ESPT and remains only in the protonated form. The ESPT kinetics of HPTS inside CTAB quaternary reverse micelle can be explained using our previously proposed ESPT model (**Scheme 2.1, *chapter2***)[254]. Applying this model the deprotonation rate constant of HPTS was found to be 5.3 ± 0.2 ns. We consider

Table 5.3: Fluorescence decay fitting parameters of protonated, $ROH^*(t)$, and deprotonated, RO^{*-}, forms of HPTS inside water/CTAB/cyclohexane/octanol reverse micelle, measured at 425 and 570 nm, respectively for p_0 = 5, 10 and 20 and w_0= 6 and 10

P_0	$W_0 = 6$ [a]				$W_0 = 10$[a]			
	ROH*= 425nm		RO^{-}*= 570nm		ROH*= 425nm		RO^{-}*= 570nm	
	τ_1 (ns)	τ_2 (ns)	τ_1 (ns)	τ_2 (ns)	τ_1 (ns)	τ_2 (ns)	τ_1 (ns)	τ_2 (ns)
5	2.1 (0.37)	3.5 (0.63)	2.1 (-3.07)	5.1 (4.07)	2.1 (0.46)	3.5 (0.54)	2.1 (-4.50)	5.3 (5.50)
10	2.1 (0.33)	3.5 (0.67)	2.3 (-2.63)	4.7 (3.63)	2.1 (0.44)	3.5 (0.56)	2.1 (-3.67)	5.0 (4.67)
20	2.1 (0.25)	3.5 (0.75)	2.2 (-1.58)	4.4 (2.58)	2.1 (0.35)	3.5 (0.35)	2.1 (-3.07)	4.8 (4.07)

[a] ± 0.1 ns

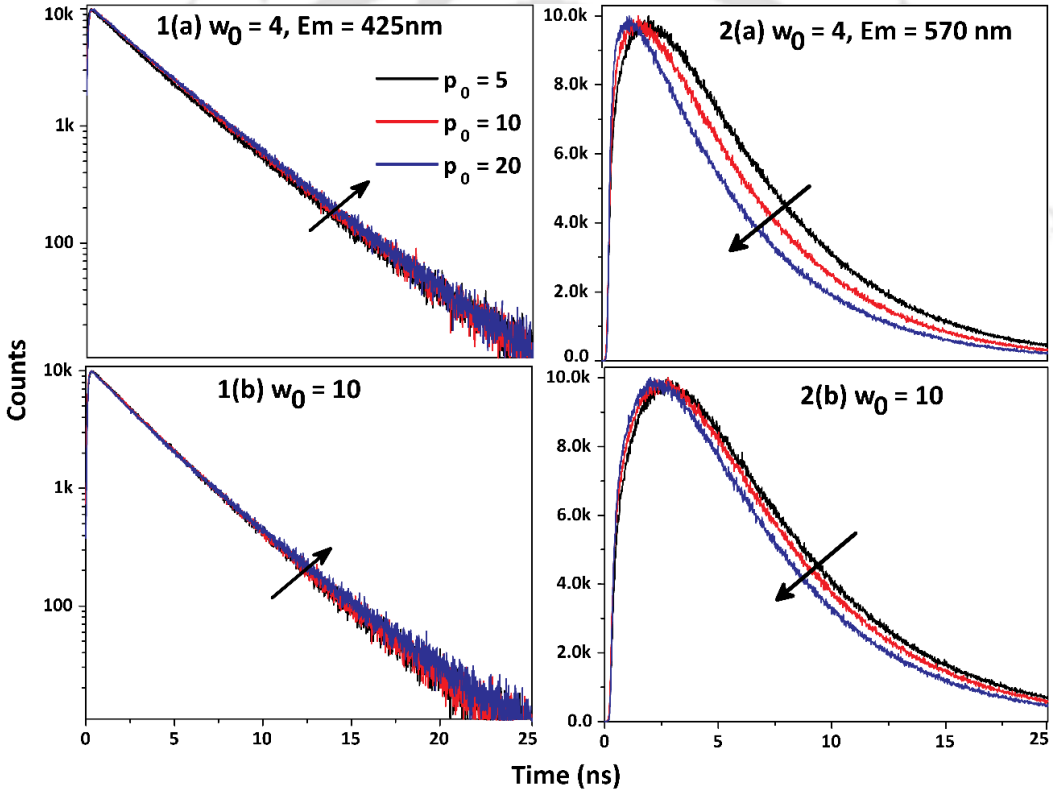

Figure 5.5: Fluorescence transients of the (left panel) protonated, ROH^* (λ_{em} = 425 nm), and (right panel) deprotonated, RO^{*-} (λ_{em} = 570 nm), forms of HPTS at w_0 = 4 and w_0 = 10 at different p_0 values (λ_{ex} = 375 nm).

$[AH_1^*]$ and $[AH_2^*]$ are concentrations for HPTS that undergoes and does not undergo ESPT, respectively. The subscript "0" indicates concentrations of species at t = 0. The plot of fraction of $[AH_1^*]_0$ (**Figure 5.6a**) and $[AH_2^*]_0$ (**Figure 5.6b**) displays that the hydrated HPTS fraction increases with water loading at a fixed p_0 value. Thus, we may conclude that increase of water loading in the core also enhances the amount of hydrated regions at the interface consistent with

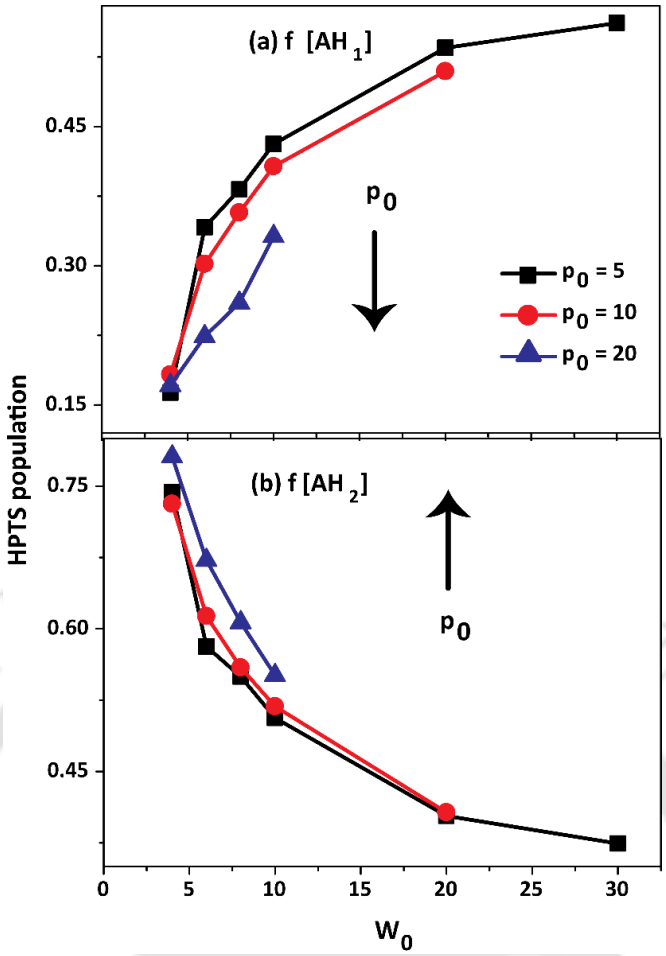

Figure 5.6: The variation of the initial populations of the (a) hydrated (f [AH_1]) and (b) dehydrated (f [AH_2]) fractions of HPTS with w_0 at different p_0 values. The hydrated HPTS fraction increases as water loading increases for a particular p_0 value, but decreases with increasing of alcohol concentration. The trend is exactly opposite for the dehydrated fraction.

our earlier observation with the DDAB reverse micelle.[254] On the other hand, the hydrated fraction decreases with the increase of p_0 and the dehydrated fraction increases with more alcohol loading and decreases with more water loading. These results are in accordance with the information acquired from TRANES measurement.

5.2.3. Fluorescence Anisotropy Decay:

The decay of fluorescence anisotropy of a probe is very sensitive to the local environment. The fluorescence anisotropy decays of HPTS is found to be very slow as the probe is expected to be bound strongly to the interface of the cationic CTAB reverse micelle by electrostatic attraction. We can also monitor the effect of co-surfactant in the interfacial region from the anisotropy decays. The anisotropy decays display that on increasing octanol concentration anisotropy becomes relatively faster (**Figure 5.7**). We have fitted the anisotropy decays by a bi-exponential function (according to **eq. 2.17**, ***chapter 2***) retaining a constant residual anisotropy(r_∞) and further analyzed with "wobbling-in-cone (WIC)" model (**Figure 2.2, *chapter2***). According to the model,

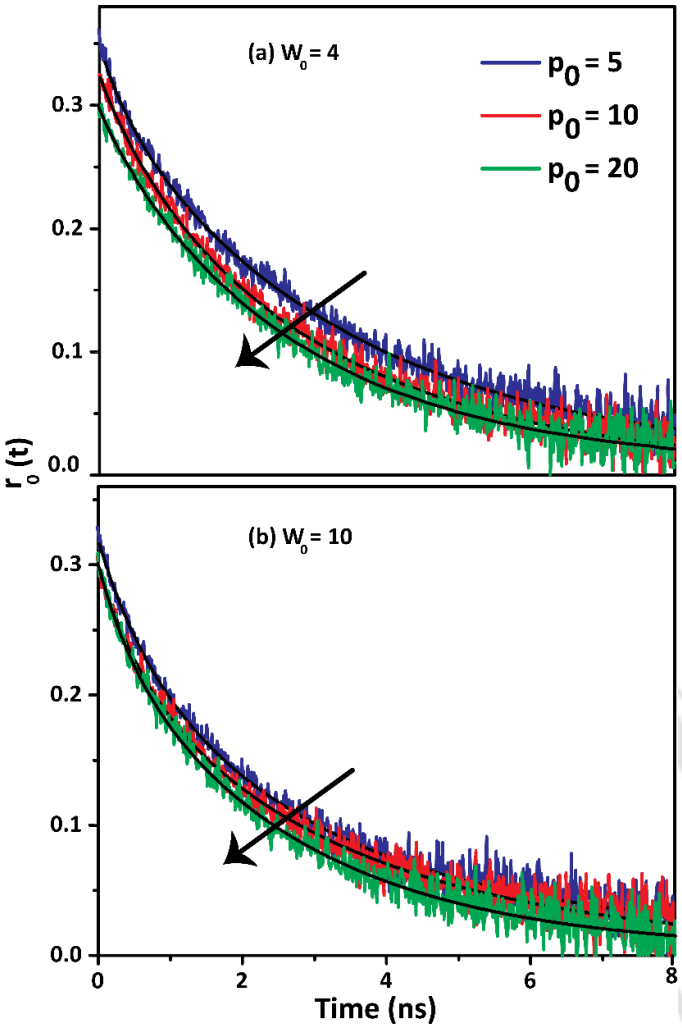

Figure 5.7: Fluorescence anisotropy decays of HPTS in CTAB RM at (a) w_0 = 4 and (b) w_0 = 10 with variation of p_0 values- 5 (blue), 10 (red) and 20 (green) measured at λ_{ex}= 375 nm and λ_{em} = 440 nm. The black lines indicates bi-exponential fit according to **eq. 2.17, *chapter 2***.

Table 5.4: Anisotropy decay parameters of HPTS in water/CTAB/cyclohexane/octanol reverse micellar system at different octanol concentrations at w_0 = 4 and 10.

System	P_0	r(0) [a]	r(α) [a]	a(s) [a]	τ_s (ns) [b]	τ_f (ns) [b]	τ_w (ns) [b]	θ (deg) [a]	D_w (ns^{-1}) [c]
w_0 = 4	5	0.34	0.011	0.89	3.34	0.45	1.90	15.9	0.011
	10	0.32	0.003	0.83	3.21	0.85	0.80	20.0	0.039
	20	0.33	0.004	0.82	3.03	1.03	0.64	20.7	0.057
w_0 = 10	5	0.32	0.013	0.73	3.19	0.75	1.00	25.9	0.055
	10	0.32	0.002	0.67	3.64	0.78	1.02	29.1	0.068
	20	0.32	0.004	0.61	3.52	0.93	0.80	32.2	0.105

[a]±0.01 [b]0.1 ns [c]0.01 ns^{-1}

the fluorophore may undergo a wobbling motion traversing a cone with a semi-cone angle of θ and may also diffusion along the interface[219,220,221] From the analysis of the fluorescence anisotropy data, it is very clear that both increase of w_0 and p_0 have significant effect on the

wobbling motion (**Table 5.4**). The relatively small semi-cone angle indicates strong binding of the probe with the interface supporting the view of Levinger and co-workers.[180] At a fixed p_0, the semi-cone angle and the diffusion coefficient increase with increase in w_0 indicating enhancement of fluidity at the interface. This is in agreement with concept that increase of w_0 not only leads to the increase of the size of the water core but also loosen the interface packing. It is also possible that increase of interfacial hydration may decrease the electrostatic potential experienced by the probe. Another point is also very clear that at a fixed w_0, the semi-cone angle and the diffusion coefficient increase with increase in p_0.The increasing values of semi-cone angle and diffusion coefficient imply that the probe experiences less hindrance for its rotational relaxation. These may be due to either octanol loosen the interface packing or alcohol reduce the electrostatic interaction between the cationic headgroup and the anionic HPTS. Khan et al[211] reported increase in the compactness of interface on increasing p_0 value.[211] Hence, reduction of electrostatic potential may be the prime reason.

5.3. SUMMARY AND CONCLUSION:

This chapter includes our investigation on the ESPT dynamics of HPTS within CTAB/octanol/water/cyclohexane quaternary reverse micelle using steady-state and time resolved fluorescence spectroscopy. In *chapter 4,* from the 2D-NMR and fluorescence anisotropy measurements we proposed presence of the negatively charged HPTS probe inside the surfactant interface. We found non-negligible signature of ESPT within the interface; that enhances gradually with the increase of water. These results can be conveniently analysed using bimodal distribution of HPTS into water-free and hydrated regions. Increase of w_0, favours the hydrated region over the water free region. Contrarily, on increasing octanol proportion, the fraction of HPTS undergoing ESPT decreases in the interfacial region and consequently the protonated emission becomes more prominent. This suggests that increase of octanol concentration as co-surfactant changes the regular packing of the interface as well as alter hydration level of this region. As a result the interface becomes more hydrophobic and ESPT becomes less favored. We also observed very slow rotational relaxation that may arise due to the strong electrostatic attraction between the cationic headgroup of CTAB and the anionic HPTS. However, with incorporation of more alcohol this probe- headgroup interaction may get weaken and the environment becomes comparatively free; allowing relatively faster anisotropy. Thus, the study successfully demonstrates the effect of co-surfactant in controlling the hydration level of the interface through the ESPT dynamics of HPTS.

भारतीय प्रौद्योगिकी संस्थान गुवाहाटी
Indian Institute of Technology Guwahati

Chapter-6

How does Interfacial Hydration Alter during Rod to Sphere Transition in DDAB/water/Cyclohexane Reverse Micelles?[#]

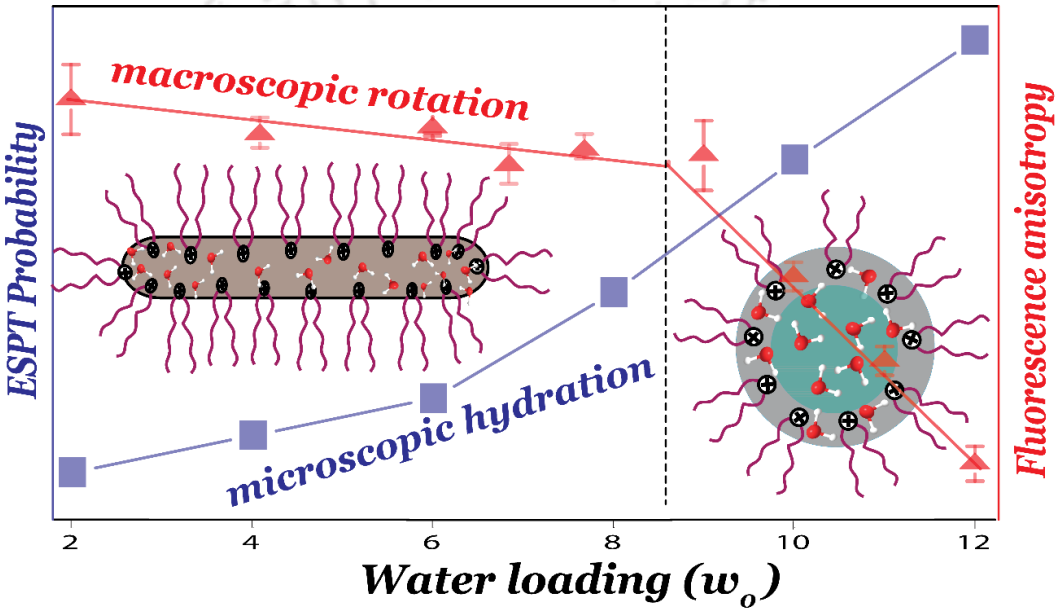

[#]This work has been published in *Langmuir* **2016**, *32*, 6656-6665

भारतीय प्रौद्योगिकी संस्थान गुवाहाटी
Indian Institute of Technology Guwahati

CHAPTER 6:
How Does Interfacial Hydration Alter during Rod to Sphere Transition in DDAB/Water/Cyclohexane Reverse Micelles?[254]

6.1. INTRODUCTION:

Micelle or reverse micelle possess different shape and structure depending on the nature and concentration of surfactant molecules.[206] For example, it is well-established that the AOT molecule acquire spherical orientation and swells up with increment of water content.[255] On the other hand sodium bis-(2-ethylhexyl) phosphate (NaDEHP) readily forms giant rod-like assembly.[256,257] Noted atom simulation studies suggest conformational changes of AOT reverse micelle from their original spherical shape to elliptical shape.[258,259] Interestingly, Didodecyldimethylammonium bromide (DDAB) provides an attractive reverse micelle assembly that undergoes structural transition from rod to spherical shape when amount of water loading, w_0= ([water]/ [surfactant]) exceeds a particular value (w_0 ~ 8)[260] A lots of study regarding involvement of structural impact on controlling hydration properties of these assemblies are investigated, as any change of these properties lead to modulation of structure or nature of molecule like protein.[188,261-263] It is also reported that the structure of DDAB micro-emulsion depends critically on the composition or volume fraction (ϕ) = ($V_{surfactant}$+V_{water})/ ($V_{surfactant}$ + V_{water} +$V_{non-polar}$), where the V_i term denotes the volume of the respective species of the polar components (**Table 6.2)**. Small angle neutron scattering (SANS) studies demonstrated that at low ϕ (~0.05) and at w_0 (<8), DDAB/water/cyclohexane micro-emulsion consists of discrete cylindrical RMs with a fixed radius of ~15 Å and varying lengths (~250 Å at w_0 = 2 to ~90 Å at w_0= 8, **Scheme 6.1**). However, at higher hydration (w_0 > 10), the micro-emulsion primarily contains spherical droplets with a core radius of ~19 Å **(Scheme 6.1).**[260] For more concentrated DDAB (ϕ ~ 0.20), the system exists as bi-continuous micro-emulsion at low water consisting of disordered connected cylinders (DOC) which at high water content transforms into spherical globules.[264] One of the objectives of this work is to investigate presence of any correlation between the degrees of hydration within the interfacial layer with nature of confinement. In this purpose the anionic HPTS is an appropriate ESPT probe, as it localized in the interface selectively. If the correlation exists, the ESPT dynamics may modulate differently at low range of w_0 values (cylindrical regime) from that at higher w_0 (spherical regime). On the other hand, SANS study described the interfacial layer by the hydrophobic interfacial film model;[265] and according to this model, ESPT should be masked as the probe HPTS is trapped within the interface. Thus, this study may provide valuable insight about the hydration behaviour of the interface layer at different water

content. As shown in the **Scheme 6.1**, in the smaller reverse micelle ($w_0 \leq 8$), water molecules so as our selected probe, HPTS distribute in two distinct regions, viz. less hydrated cylindrical and more hydrated hemispherical regions, unlike the homogeneously distributed water molecules in spherical reverse micelle ($w_0 = 12$).

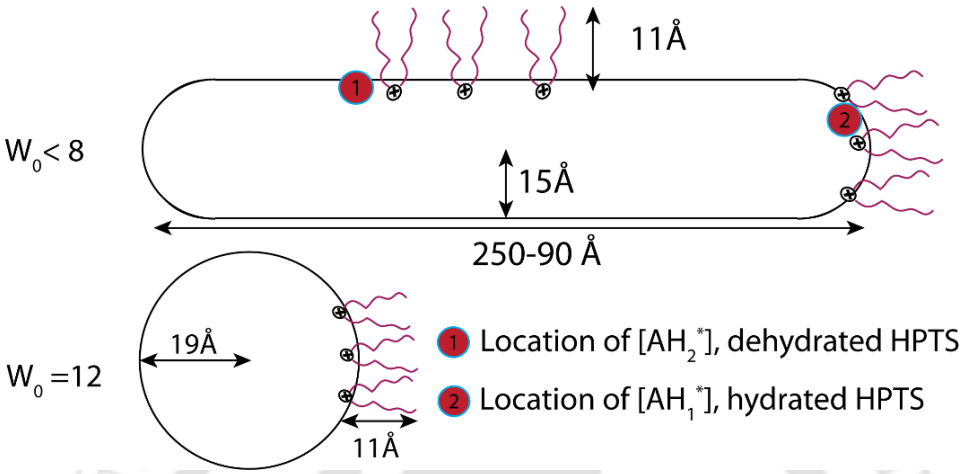

Scheme 6.1. Structures of DDAB/Water/Cyclohexane reverse micelle at low hydration ($w_0 \leq 8$) with two possible interfacial regions, i.e., less hydrated cylindrical and more hydrated hemispherical regions. In the higher (e.g. $w_0 = 12$) water content, spherical micelles are present and the two regions may be mixed together.

6.2. RESULTS

6.2.1. Steady-state Absorbance and Emission Spectroscopy:

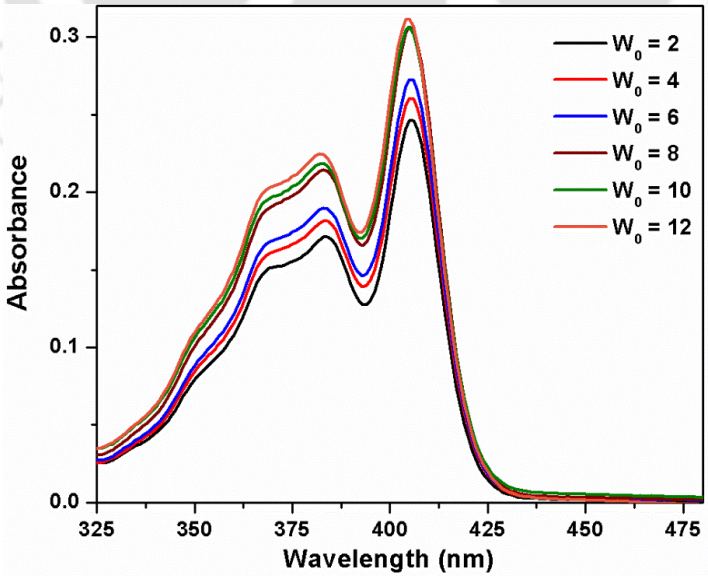

Figure 6.1. Absorption spectra of HPTS in water/DDAB/cyclohexane reverse micelle at different w_0s. The absorption spectra refer presence of probe mainly in the protonated form.

UV-Visible absorbance spectra: The absorption spectra of HPTS within the DDAB/cyclohexane/water reverse micelle show absorption band at ~405 nm, characteristics of the protonated form (**Figure 6.1**). There is no absorption band at ~450 nm indicating the absence of the deprotonated form in the ground state. Note that the absorption maximum (405 nm) inside the DDAB reverse micelle is slightly red-shifted compared to that of bulk water (403 nm) but is similar to the cationic BHDC RM (406 nm), discussed in *chapter 4*. The red shift of the absorption spectrum may be due to cation-π interaction between the cationic headgroup of the surfactant and the π-electrons of the aromatic ring of the HPTS.

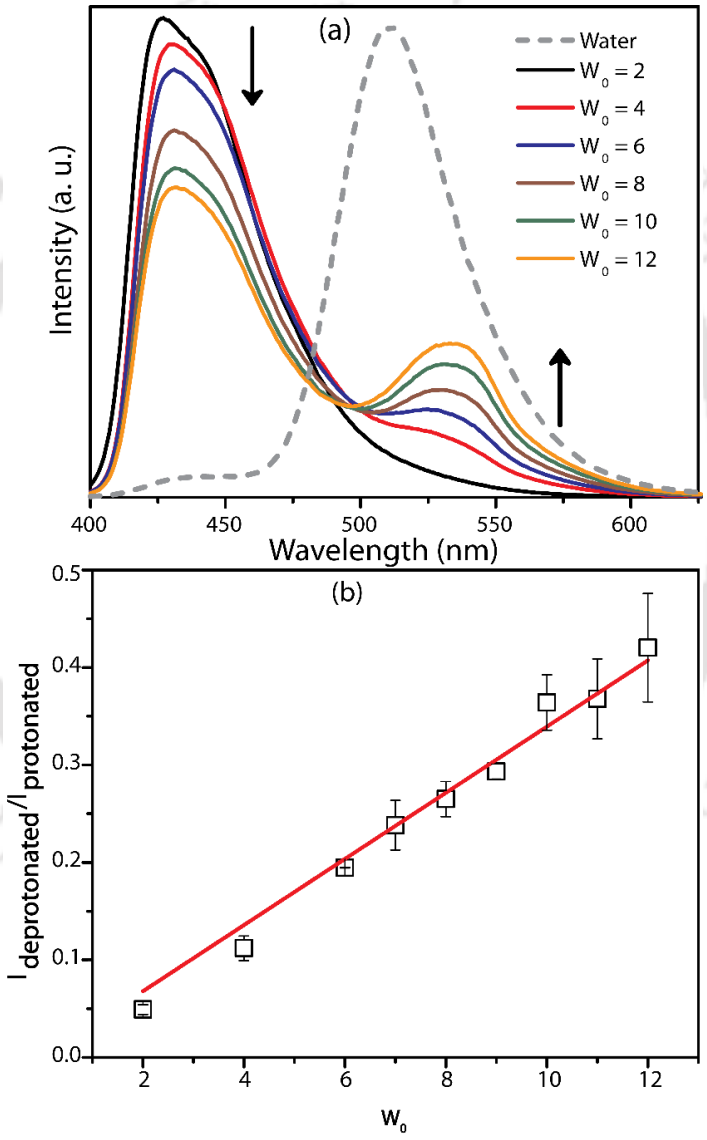

Figure 6.2: (a) Emission spectra of HPTS inside DDAB RM at various w_0 values (λ_{ex}= 390 nm). Emission spectrum of HPTS in water (dotted line) is also included for comparison. (b) The ratio metric plot of the de-protonated to the protonated emission intensity vs. w_0 inside the DDAB RM.

Observation from Emission spectra: In neat water, the emission spectrum of HPTS is greatly dominated by the emission from the deprotonated (λ_{em}^{max} = 512nm) form and a very weak emission band (at ~440 nm) is observed from the protonated state (**Figure 6.2a**). However, HPTS inside the cyclohexane/DDAB/water RM at w_0 = 2 exhibits only a single-band emission spectrum characteristics of the protonated emission with emission maximum at 426 nm (**Figure 6.2a**) and devoid of emission band characteristics of the deprotonated form referring negligible or ultraslow ESPT compared to the fluorescence lifetime of HPTS at this w_0. After that the emission spectra undergo clear systematic variation with w_0. With the increase of water content, the protonated emission intensity diminishes with the concomitant development of deprotonated emission intensity at ~535 nm (**Figure 6.2a**). Thus, gradual increase of water loading progressively promotes ESPT of HPTS located inside the cationic surfactant interface. Note that the shape of the emission spectrum, particularly that for w_0 = 2, possess a shoulder at ~450 nm, providing it slightly structured emission spectrum may be due to vibrionic transitions which are frequently observed for pyranine-derived fluorophores in less polar medium.[198,223]

The lack of ESPT at low water content may be assigned to the lower hydration or to the very high counter ion density near the surfactant headgroups; as ESPT process is feasible only in the aqueous medium and in presence of proton acceptor (water) and inhibited in the presence of high concentration of ion.[10,266-268] Thus, the lack of ESPT at low water content may be assigned to the lower hydration or to the very high counter ion density near the surfactant headgroups. With the increase of water content, the counter ions (bromide) may be displaced into the core and more water molecules may penetrate into the surfactant interface of the RM and thus, favour the ESPT opportunity. Another notable observation is that both the protonated and deprotonated bands shift towards higher wavelength with increase of the water content. This may be due to the solvatochromic behaviour of HPTS and increase of the polarity of the interface at higher w_0.[198] To illustrate the variation of ESPT upon w_0 more evidently, we plot the intensity ratio of the de-protonated to the protonated emission against w_0 (**Figure 6.2b**). It is clear that the ratio increases linearly with increase of w_0; without any distinct change of slope before and after w_0 = 8, the point where the reverse micelle is reported to undergo phase-transition from rod-shaped to spherical assembly. Thus, the morphological change of overall reverse micelle structure may have only a minor impact on the interface hydration.

6.2.2. Time-resolved fluorescence:

The fluorescence time resolved measurements are monitored at two selective emission wavelengths of 425 nm and 570 nm; representing the protonated and the de-protonated forms, respectively to monitor fluorescence kinetics associated with the ESPT process. (**Figure 6.3**). These two wavelengths were deliberately chosen to minimize the undesired mixing of contribution from the other form.[69,239] The fluorescence decays of the protonated form monitored at 425 nm become progressively faster with the increase of w_0 and the decay components for both forms were found to be bi-exponential with common decay constants of 2.1 ns and 3.6 ns, respectively (**Table 6.1**). The fitting function is described in the **eq. 2.1** ***chapter 2***.

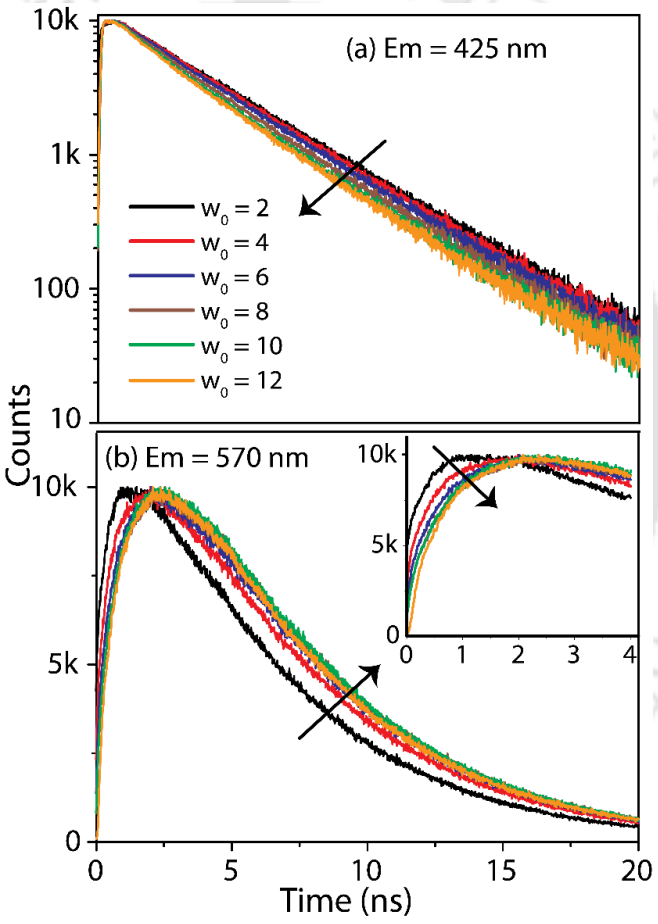

Figure 6.3. The fluorescence transients of the (a) protonated, ROH*(t) (λ_{em}= 425 nm) and (b) de-protonated, RO^{*-} (λ_{em}= 570 nm) forms of HPTS at different w_0 values at λ_{ex}= 375 nm. The initial portion of de-protonated transients are shown in the inset for clarity.

We observed a gradual increment of the contribution of the faster component with w_0 (**Table 6.1**). On the other hand, the fluorescence transients of the deprotonated form (measured at 570 nm) can be fitted bi-exponentially with a matching rise component of 2.1 ns followed by a decay component of 5.4 ns. Our proposed ESPT model support these observations (**Scheme 6.2**).

To interpret the decay components more convincingly, we have also measured fluorescence transients at different wavelengths with the interval of 5nm across the full emission spectrum and constructed time-resolved emission spectra (TRES, **eq. 2.15, *chapter 2* Figure 6.4, left panel**) and time-resolved area-normalized emission spectra (TRANES) at different times (**Figure 6.4, right panel**).

Table 6.1. Fluorescence decay fitting parameters of protonated, ROH*(t) and de-protonated, RO^{*-} forms of HPTS inside water/DDAB/cyclohexane reverse micelle, measured at 425 nm and 570 nm, respectively. Pre-exponential factors are added in the parenthesis.

w_0	Protonated, ROH*(t)			De-protonated, RO^{*-}(t)		
	τ_1 (ns)[a]	τ_2 (ns)[a]	χ^2	τ_3 (ns)[a]	τ_4 (ns)[a]	χ^2
2	2.1 (0.13)	3.6 (0.87)	1.08	2.1 (-0.46)	5.4 (1.00)	1.06
4	2.1 (0.20)	3.6 (0.80)	1.02	2.1 (-0.63)	5.4 (1.00)	1.08
6	2.1 (0.26)	3.6 (0.74)	1.05	2.1 (-0.71)	5.4 (1.00)	1.11
8	2.1 (0.39)	3.6 (0.61)	1.06	2.1 (-0.71)	5.4 (1.00)	1.05
10	2.1 (0.50)	3.6 (0.50)	1.08	2.1 (-0.71)	5.4 (1.00)	1.10
12	2.1 (0.57)	3.6 (0.43)	1.07	2.1 (-0.72)	5.4 (1.00)	1.18

[a]± 0.1 ns

The TRANES data ensured us about very insignificant ESPT process at lower w_0. For other w_0 values, the TRANES data clearly manifest decrease of the protonated emission band with simultaneous increase of the de-protonated emission intensity at longer time. Thus, ESPT is almost absent at low w_0 (=2) but is prompted dramatically at the higher w_0 values. On the other hand TRES data with dominated protonated band in the early time at all w_0s; confirmed absence of ultrafast component in our system. Moreover, Levinger and co-worker have already shown the absence of ultrafast component of ESPT inside another cationic reverse micelle (CTAB) interface.[180]

We have evaluated fluorescence lifetime of HPTS free from the associated ESPT process from the plot of area of TRES against the respective times; following Lawler et al method.[208] These data can be nicely fitted by a single exponential function with lifetime of 3.5±0.2 ns (**Figure 6.5**). This time constant is very similar to the time constant of the slower component of the decay of the protonated emission observed at 425 nm and may be assigned to the lifetime of HPTS inside the interface of the DDAB reverse micelle. Note that the lifetime is quite short compared to the lifetime of HPTS in water (~5.5 ns) but close to the lifetime of HPTS in methanol (~ 4 ns).[269] The bi-exponential nature of both protonated and the deprotonated emission transients with matching decay and rise time can be interpreted by assuming bimodal distribution of HPTS inside the

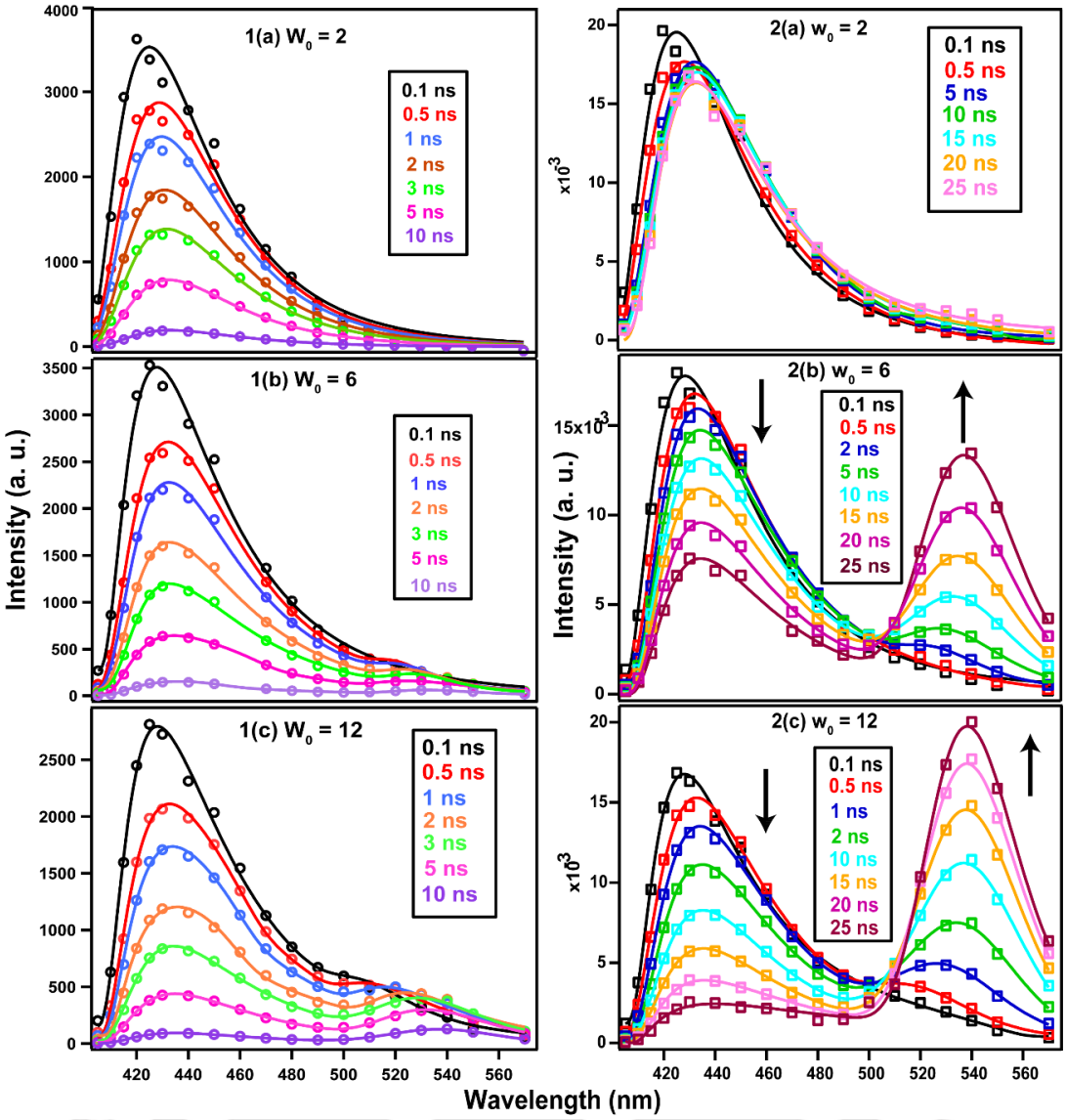

Figure6.4. Time-resolved emission spectra (TRES, left panel) and time-resolved area-normalized emission spectra (TRANES, right panel) of HPTS inside DDAB RM at w_0 = 2, 6 and 12, respectively. Solid lines denote fit to according to **eq. 2.14, *chapter 2***. The TRANES at w_0 = 2 do not show much variation except very small spectral shift of the protonated emission band and a very small contribution of deprotonated emission arises at long time (≥ 7 ns). However, for w_0 = 6 and 12 deprotonated emission band intensity undergo enhancement with time.

interface. The shorter component may be ascribed to the fraction of probe that is experiencing ESPT while the slower component to the fraction not experiencing ESPT. The fraction of HPTS that are at a location devoid of water cannot undergo ESPT. Interestingly, a very simple scheme (described in **Scheme 2.1 *chapter 2***) can justify the observed ESPT dynamics qualitatively constant as 5.04 ns. The lifetime of the protonated form of HPTS (τ_f) is found to be 3.6 ns which is consistent with the lifetime of 3.5± 0.2 ns obtained from the TRES area calculation involving single step de-protonation without involvement of ion-pair formation or recombination. From this scheme, we have calculated the deprotonation time (**Figure 6.5)**.

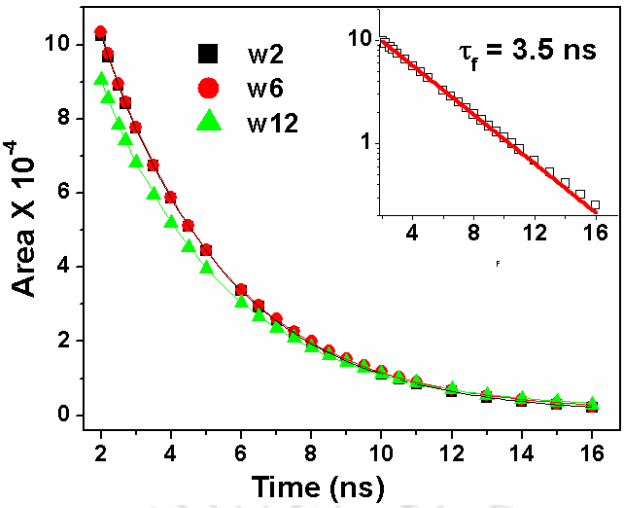

Figure 6.5. Integrated TRES area vs. time plot of HPTS inside DDAB RM at w_0 = 2, 6 and 12, respectively. The inset shows the average decay of the all three w_0 values, fitted to single exponential decay.

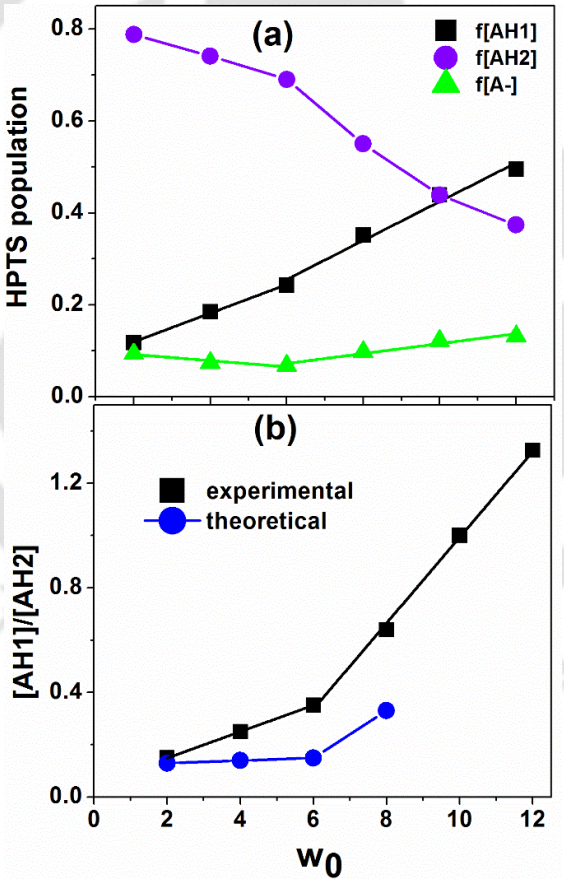

Figure 6.6. (a) Plot of the variation of the initial populations of HPTS with w_0. On increasing water loading, the hydrated protonated ([AH1]) and deprotonated ([A^-]) HPTS fraction increase, while the dehydrated protonated ([AH2]) HPTS fraction decreases. The initial population of the deprotonated species ([A^{-*}]) is very small at all w_0. (b) The plot of hydrated to dehydrated fraction of HPTS inside reverse micelles in experimental and theoretical (surface area $=2r/l$, where r for radius and l length of cylindrical reverse micelle, tabulated at **Table 6.2**) aspects.

The lifetime of the deprotonated form (τ_f') is given by the decay component (5.4 ns) of the deprotonated emission (**Table 6.1**). The obtained fraction of $[AH1^*]_0$ and $[AH2^*]_0$ and $[A^{-*}]_0$ are displayed in the **Figure 6.6a**. The very small values of $[A^{-*}]_0$ is consistent with the fact that the deprotonated species mainly originates from the hydrated protonated fraction, $[AH1^*]$ through the ESPT process.

With the increase of w_0, the fraction of $[AH1^*]$ increases while $[AH2^*]$ decreases (**Figure 6.6a**). The ratio of the two populations varies differently at low w_0 and high w_0 regimes. The population of the hydrated fraction relative to the dehydrated fraction increases marginally up to $w_0 = 6$ but thereafter, increases much more dramatically (**Figure 6.6b**). Interestingly, the break in the plot may correspond to the transition point where morphology of the RM changes from cylindrical to spherical shape. The two different populations of the protonated species may be realized in the following way. Assuming the cylindrical (or capsular) shape of the reverse micelle, the two regions may be ascribed to the tubular side region and the two hemispheres at edges (**Scheme 6.1**). If we take the dimension of the cylindrical micelles as that proposed by Eastoe and co-workers (**Scheme 6.1**),[260] the relative contribution of the two regions (inner surface area) can be given by $2r/l$ (**Table 6.2**) and this varies almost linearly with w_0 below $w_0 = 6$ but becomes significantly higher at $w_0 = 8$ **(Figure 6.6b**). In the side regions, surfactants may be well packed and remain free from water penetration while the end hemisphere regions may be hydrated. The two regions may be mixed together when the cylindrical RM transforms into sphere and their relative contributions may be equal. The ratio of the two HPTS fractions obtained from the fluorescence decay fit nicely correlated to this trend (**Figure 6.6b**).

Table 6.2. The volume fraction (ϕ) given by ($V_{surfactant} + V_{water}$)/ ($V_{surfactant} + V_{water} + V_{nonpolar}$), where V_i term denotes the volume of the respective species.and inner surface area representing relative contributions of the two regions (scheme 2) of water/DDAB/cyclohexane reverse micelle calculated using $M_{w\,(DDAB)} = 462$ g mol^{-1} and $\rho_{DDAB} = 1.1$ g cm^{-3}.

W_0	[DDAB], molL^{-1}	ϕ	Surface area, 2r/l
2	0.1	0.042	0.13
4	0.1	0.045	0.14
6	0.1	0.048	0.15
8	0.1	0.051	0.33
10	0.1	0.054	-
12	0.1	0.058	-

Although the applicability of this very simple kinetic scheme (**Scheme 2.1, *chapter2***) may appear to be strange yet could be justified as follows. The probe is located in the interfacial region where availability of water is expected to be very low and if present, such water molecules are probably isolated and normal hydrogen bonding network within water molecules may not exist.

Further, ion-pairing may not be stable due to strong electrostatic field of the positive quaternary ammonium headgroup. Moreover, once a hydronium ion is formed, it may be immediately pushed into the core by the positive charges of the surfactant headgroups and thus, eliminating the possibility of recombination of the dissociated proton (or hydronium ion) with the de-protonated species in the excited state.

Solvation dynamics: To ensure involvement of solvation dynamics in the ESPT process; we fitted the TRES at different times with a combination of bi-lognormal functions (**eq. 2.14, *chapter2***) to de-convolve individual contributions of the protonated and the deprotonated emissions at different times (**Figure 6.7**). The emission maxima of both the protonated and the deprotonated forms undergo significant red-shift with time. We can fit the dynamics of the spectral shift to estimate the dynamics of solvation inside the interface by the following equation[216,270]

$$\nu_t = (\nu_0 - \nu_\infty)\left[a_1 e^{-t/\tau_1} + a_2 e^{-t/\tau_2}\right] + \nu_\infty \qquad (6.1)$$

Where ν_0, ν_t, ν_∞ denotes emission frequency (in cm^{-1}) at 0, t and infinite time, respectively.

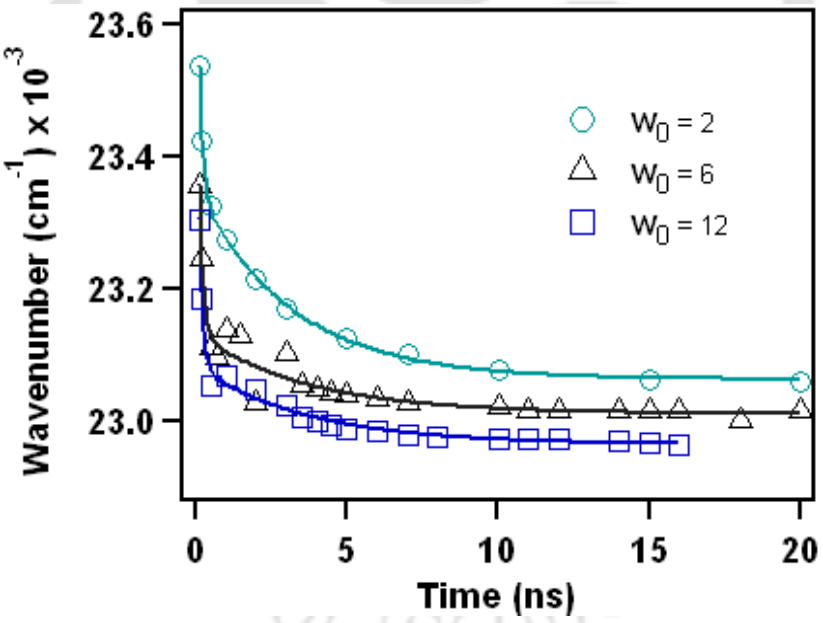

Figure 6.7. Solvation dynamics of HPTS inside DDAB/water/cyclohexane reverse micelle at w_0 = 2, 6 and 12, respectively. Solid lines denote fit to a double exponential function.

The parameters of the fit are listed in **Table 6.3**. The fitted parameter shows that the emission frequency of the protonated form undergoes a fast (~0.12 ns) solvent relaxation followed by a slower relaxation (3.2-3.7 ns). As the slow component of the hydration is in the same order of magnitude of ESPT (2.1ns), we propose that the corresponding solvation process may be more critical to induce ESPT. The 0.12 ns component which is much faster than the ESPT dynamics, may be ascribed to the stabilization of the excited state dipole of the protonated form by ionic

Table 6.3. Solvation dynamics fit parameters of the protonated form of HPTS in water/DDAB/cyclohexane reverse micelle system at different w_0 values.

w_0	$\nu(0)^a$	$\nu(\infty)^a$	a_1	τ_1 (ns)^b	τ_2 (ns)^b
2	23750	23050	0.58	0.13	3.2
6	23600	23000	0.79	0.13	3.6
12	23600	22950	0.81	0.12	3.7

[a]±100 cm^{-1} [b]0.1 ns

species and water in its immediate vicinity. Whereas, the slower component may arise due to the accumulation of distant water molecules by translational diffusion and rearrangement of water molecules near the hydroxyl group. It is often suggested that a critical size of water cluster is necessary for the ESPT event to occur.[271] Inside the relatively less hydrated rigid interfacial region, availability of the optimal size of water cluster may be achieved only after transportation of significant number of remote water molecules to the proton donating site (hydroxyl group in this case) and the process may occurs in several ns. Very recently, Pal and co-workers reported that solvation dynamics precede ESPT for 1-napthol in the binary di-oxane-water cluster.[272]

6.2.3. Fluorescence Anisotropy.

Fluorescence anisotropy of a fluorophore is intimately related to its location inside reverse micelle.[208] If the probe HPTS stays in the core (as in anionic reverse micelle), the rotational anisotropy would be relatively faster compared to an interface localized case (as in cationic reverse micelle). Moreover, if the probe is strongly bound to the interface, part of the anisotropy decay may arise from the overall rotation of the assembly and hence, may be sensitive to the structural transitions. We indeed observed a strong break in the measured steady-state anisotropy against w_0 plot at w_0 = 9 (**Figure 6.8a**). The anisotropy values suddenly drops after the w_0 = 9. The change in the anisotropy can be ascribed to the very different rotational dynamics of cylinder and sphere. The time transient fluorescence anisotropy decays (**Figure 6.8b**) can be fitted with a bi-exponential function retaining a constant residual anisotropy(r_∞) described in **eq. 2.17** ***Chapter 2*****.** The anisotropy decay parameters were analysed in terms of "wobbling-in-cone (WIC)" model, where the fluorophore may undergo a wobbling motion tracing a cone with a semi-cone angle of

θ along with lateral diffusion of the probe along the interface, described in details in *chapter 2*.[219-221] The time scale is expected to be very long compared to the life time of HPTS. Thus, we do not explicitly includes the overall rotation here and rather assume that the effect of the very slow overall motion may be reflected in the observed residual anisotropy. The wobbling time constants

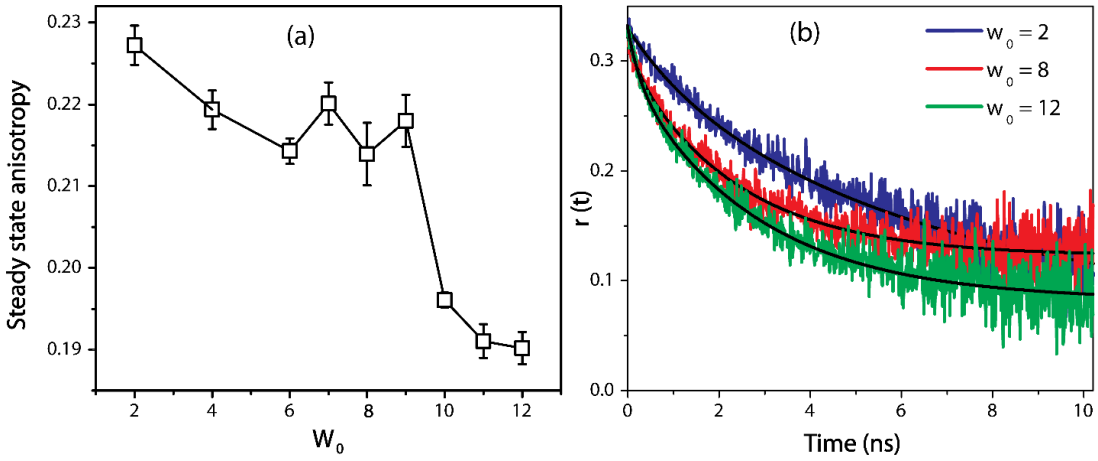

Figure 6.8. (a) Steady state fluorescence anisotropy decays of HPTS in DDAB RM at various w_0 values measured at λ_{ex} = 390 nm and λ_{em} = 440 nm. A strong break appears around w_0 = 9. The error bars represent spread of data obtained from three independent measurements. (b) Time transients fluorescence anisotropy decays of HPTS in DDAB RM at w_0 values of 2 (blue), 8 (red), and 12 (green) measured at λ_{ex} = 375 nm and λ_{em} = 440 nm. The black lines indicate bi-exponential fit according to **eq. 2.17, *chapter 2***.

Table 6.4. Anisotropy decay parameters of HPTS in water/DDAB/cyclohexane reverse micellar system at different w_0 values. Error bars on each parameter are also provided.

W_0	r(0)[a]	r(α) [a]	a(s) [a]	τ_s (ns)[b]	τ_f (ns)[b]	τ_W(ns)[b]	θ(deg)[a]	D_w(nS^{-1})[c]
2	0.34	0.07	0.86	6.1	1.04	1.25	18.4	0.024
6	0.34	0.12	0.88	3.2	0.25	0.27	16.6	0.089
8	0.34	0.13	0.86	2.4	0.23	0.25	18.1	0.11
10	0.33	0.06	0.78	3.6	0.42	0.47	22.8	0.09
12	0.36	0.08	0.77	2.8	0.27	0.3	23.7	0.16

[a]±0.01 [b]0.1 ns [c]0.01 ns^{-1}

(τ_w) and the semi-cone angle (θ) and the wobbling diffusion coefficient (D_w) are supplied in **Table 6.4**. The contribution of the faster anisotropy decay component is significantly higher at w_0 = 10 and 12 compared to lower w_0 (≤8). Also the wobbling angle increases with increase in the w_0 values (**Figure 6.9**). The plot of different anisotropy parameters points toward significant modification after w_0 = 8 (**Figure 6.9**). This is consistent with the break observed in the steady state anisotropy around w_0 ~ 8. Note that the rotational time constant of HPTS in bulk water is 0.14 ns which corresponds to a rotational diffusion coefficient of 1.2 ns^{-1}. The wobbling diffusion coefficient found for HPTS in the RM is much smaller compared to this bulk rotational value. Thus, the rotational relaxation is reduced by 14 time at w_0 = 2 and 2−5 times at other w_0 values.

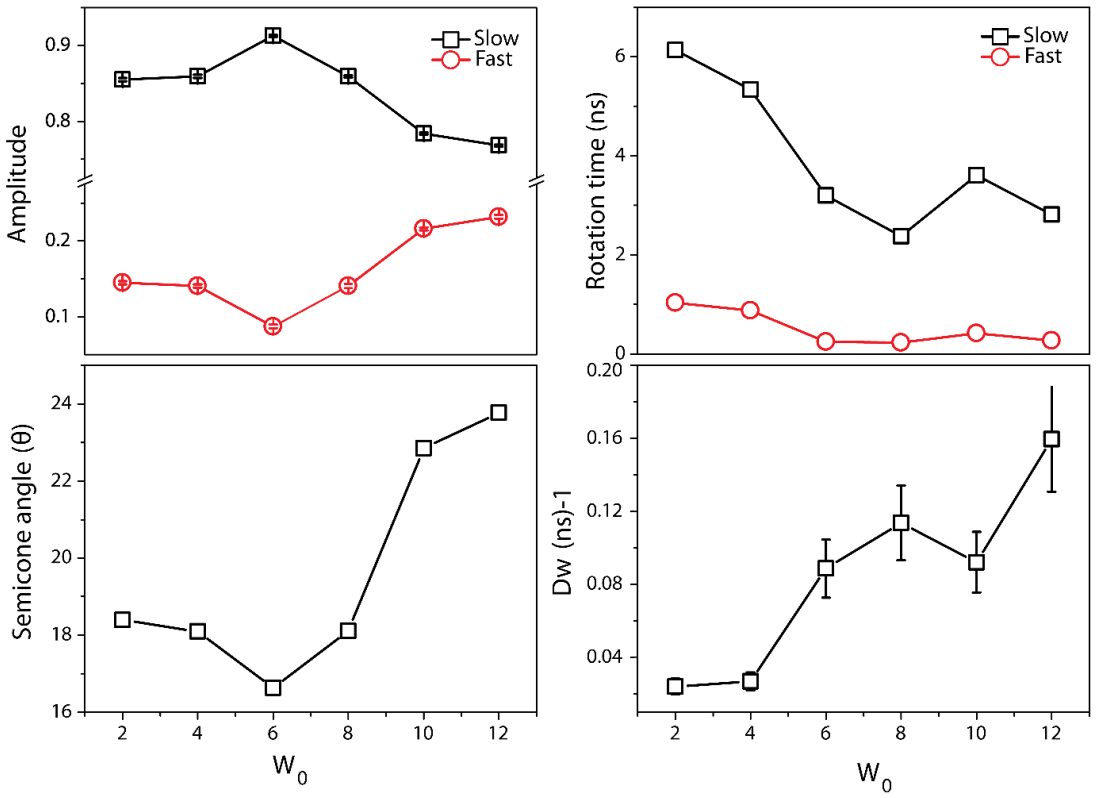

Figure 6.9. The plots of the variation of the anisotropy parameters (amplitude, time constants of anisotropy decay, semi-cone angles, and diffusion coefficients) with w_0, inside DDAB RM.

6.3. SUMMARY AND CONCLUSIONS:

In this chapter, we have discussed ESPT dynamics of a localized photoacid HPTS within DDAB/water/cyclohexane RM interface and found that the observed dynamics is well-correlated to shape change of the reverse micelle. We have analysed the ESPT results by assuming presence of two very different interfacial regions: hydrated and dehydrated. Our results showed that with increase of w_0, the dehydrated population decreases, followed by enhancement of the hydrated region. The relative ratio of these population varies differentially at low w_0 and high w_0 regimes. Thus, the structural change does have important impact on the interfacial hydration or on surfactant headgroup water interaction. Our results lead us to summarize the ESPT process through a very simple model without considering ion-pair formation and recombination. Additionally, the steady state fluorescence anisotropy of the same probe shows a clear break at the transition point. This may be due to coupling of the overall rotation of the assembly with the local (wobbling) motion of probe inside the interface layer.

Chapter-7

How do the Interfacial Properties of Zwitterionic Sulfobetaine Micelles differ from those of Cationic Alkyl Quaternary Ammonium Micelles?

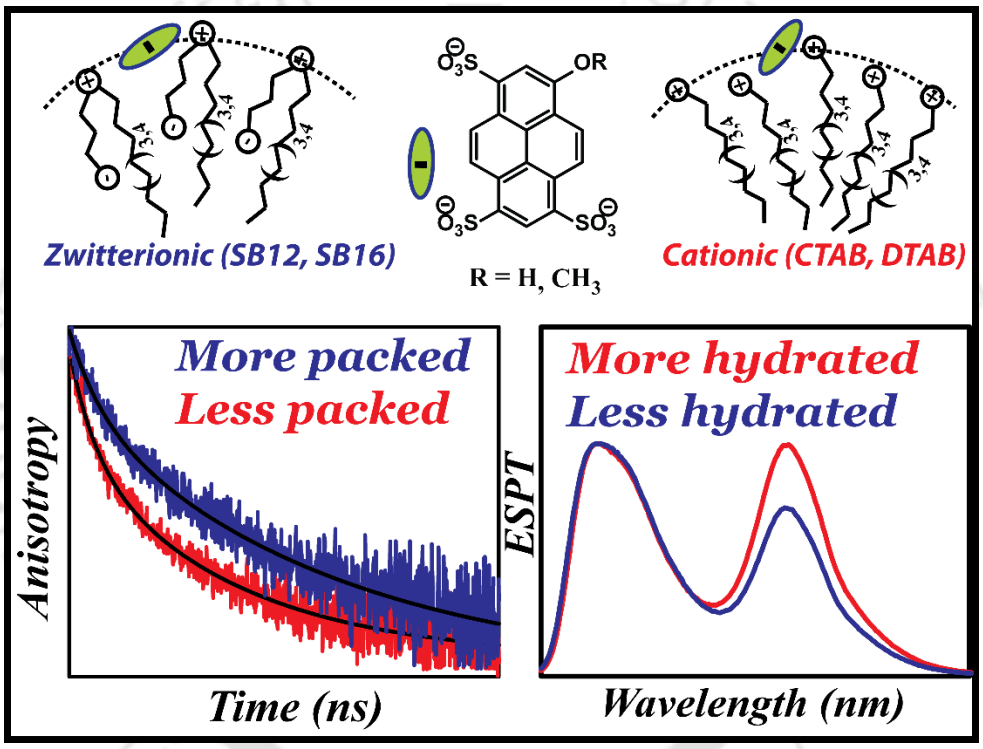

#This work has been published in *Phys. Chem. Chem. Phys.* **2017**, *19*, 31461-1468.

भारतीय प्रौद्योगिकी संस्थान गुवाहाटी
Indian Institute of Technology Guwahati

CHAPTER 7:
HOW DO THE INTERFACIAL PROPERTIES OF ZWITTERIONIC SULFOBETAINE MICELLES DIFFER FROM THOSE OF CATIONIC ALKYL QUATERNARY AMMONIUM MICELLES?[273]

7.1 INTRODUCTION:

Zwitterionic surfactant molecules possess two distinct opposite charges separated by a spacer in their hydrophilic headgroup. They can be divided into several subgroups on the basis of the length and nature of spacer separating the quaternary ammonium center from the sulfonate group.[274] Due to these structural characteristics they exhibit many intriguing features compared with common ionic or neutral surfactants. For example, they show excellent biocompatibility and biodegradability, good water solubility, and can withstand higher temperature compared with common surfactants.[213-215] Consequently, zwitterionic surfactants are favoured in cosmetic, biomedical and pharmaceutical applications and in chemical reactions.[275-278] The interface of zwitterionic micelle possesses cationic nature despite of the presence of both cationic and anionic hydrophilic headgroup. A recent molecular dynamics simulation study referred this cationic interfacial properties to orientation of surfactant molecule. The surfactant molecules are arranged in such a manner that the ammonium headgroups are relatively more exposed to water compared to the sulfonate groups. Because of this special arrangement, the interface has more tendency to preferentially adsorb external anion.[214] Excited state proton transfer (ESPT) can offer beneficial information about the nature and dynamics of water inside this interface. Nome and co-workers used this ESPT process to investigate the hydrogen ion concentration inside a zwitterionic sulfobetaine micelle using 2-naphthol as ESPT probe.[279]

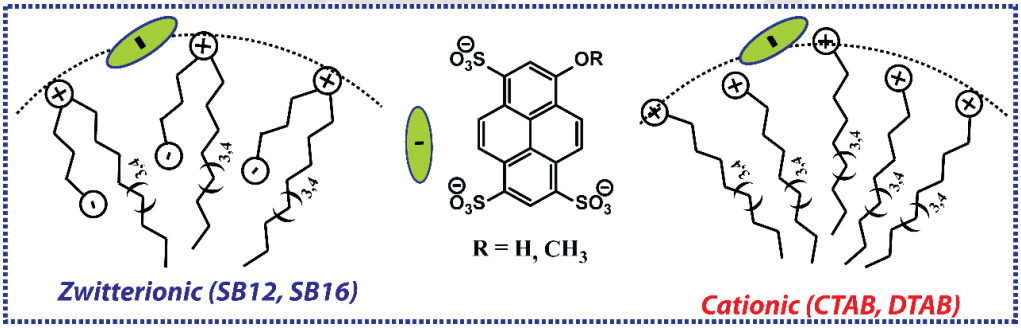

Scheme 7.1: Schematic representation of micellar interface. The zwitterionic sulfo-betaine surfactant molecules possess two oppositely charge headgroups linked by alkyl chain (C_3 in this case) are arranged in L shaped pattern, exposing the cationic headgroup towards the interface similar to cationic alkyl-ammonium surfactant assembly.

In this chapter we have discussed our study on nature of zwitterionic 3-(dodecyldimethylammonio)-propane sulfonate (SB12) and 3-(hexadecyldimethylammonio)-

propane sulfonate (SB16) micellar interface and variation of their properties from the interface of cationic alkyl-ammonium (e.g. DTAB, CTAB) micelle with matching alkyl tails (**Scheme 7.1**). To study these medium we have employed ESPT behaviour of a site selective anionic probe 8-hydroxypyrene-1, 3, 6-trisulphonate (HPTS). The emission nature of HPTS is sensitive to local hydration inside micelles[158,280,281] and reverse micelles[205,226,240,250,254] and may be a better alternative of Nome ESPT probe[279] because of its stronger photoacidity than 2-naphthol.[14,282,283] Moreover HPTS with three and four negative charges in the protonated and deprotonated forms respectively, serves as a prototype of large anion which can be accommodated at the interface.

7.2. RESULTS:

7.2.1. Steady-state Absorbance and Emission Spectroscopy:

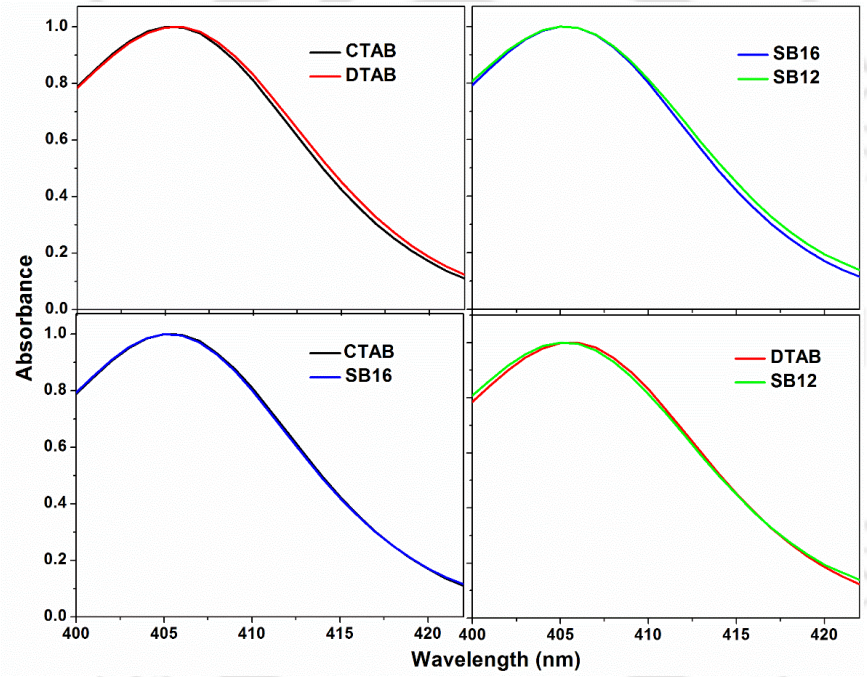

Figure 7.1: Normalize absorption spectra of HPTS (~ 8 µM) in different micelles at pH 5.6. All the absorptions spectra are very similar to each other.

The absorption spectra of HPTS inside all the micelles are very similar with a common absorption maximum at ~405 nm and the absence of any absorbance at higher wavelengths (>430 nm) eliminates the possibility of any ground-state deprotonation of HPTS at a bulk pH of 5.6 (**Figure 7.1**).

The emission features alter greatly within the micelles; both the protonated and deprotonated bands have comparable intensities (**Figure 7.2**). The ratio (r) of the emission intensities of the two forms (protonated/deprotonated) is a qualitative estimate of the retardation of the ESPT process.[226] The r increases from 0.84 in the DTAB micelles to 1.01 in the CTAB

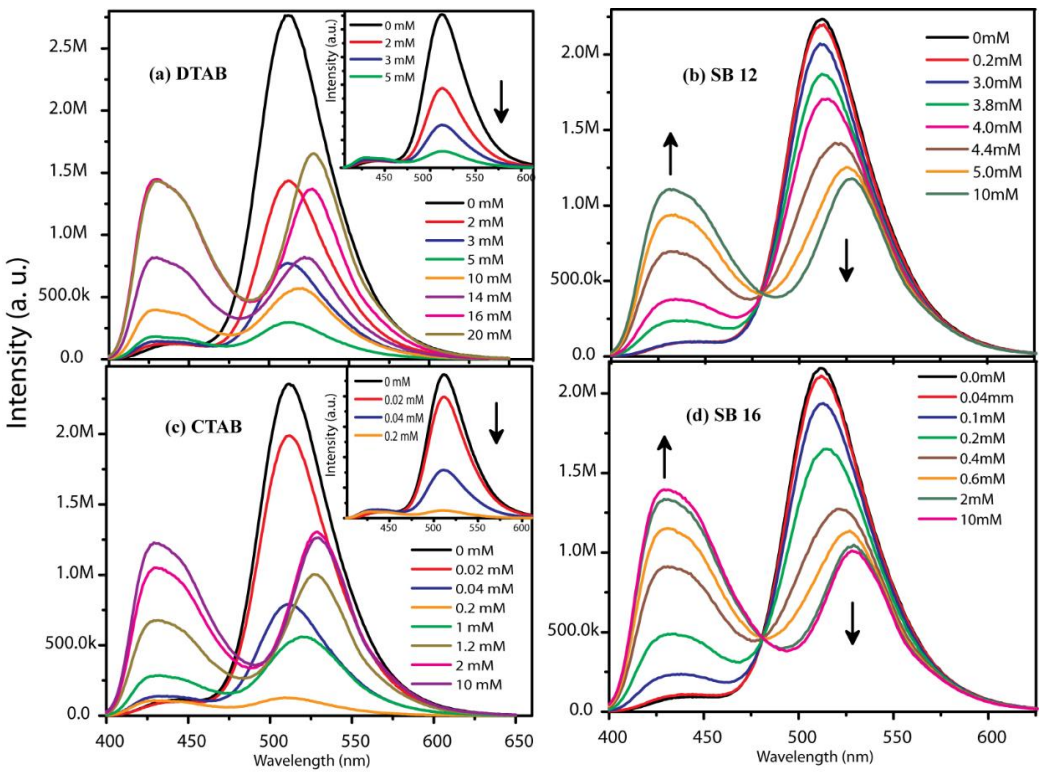

Figure 7.2. Emission spectra of HPTS (8 µM) in the presence of different surfactants (a) DTAB, (b) SB-12, (c) CTAB and (d) SB-16 (λ_{ex}= 390 nm). For cationic surfactants (CTAB and DTAB) strong quenching of fluorescence was observed (inset of a, c).

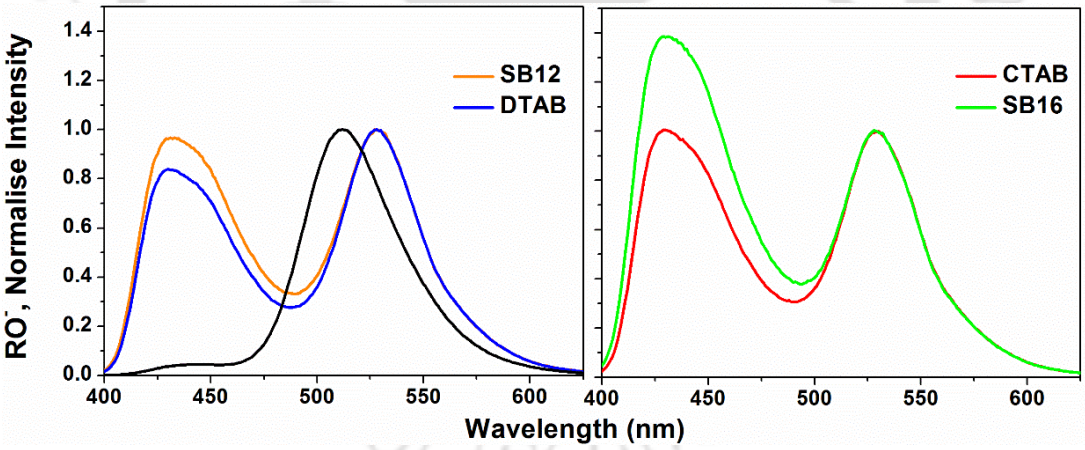

Figure 7.3: Emission spectra (normalized at the deprotonated emission band) of HPTS inside cationic and sulfobetaine micelles (left panel: DTAB vs. SB12; right panel: CTAB vs. SB16). Emission spectrum of water is added for comparison.

micelles. Similarly, the r increases from 0.97 in the SB12 micelles to 1.4 in the SB16 micelles (**Figure 7.3**). Thus, ESPT may be more suppressed inside the zwitterionic micelles compared to the cationic micelles. The ESPT is also suppressed significantly with the increase in the tail length of the surfactant (**Figure 7.4**). Thus, the steady-state emission measurements imply that the ESPT

inside a micelle is modulated significantly by changing either the headgroup or the tail length of the surfactant.

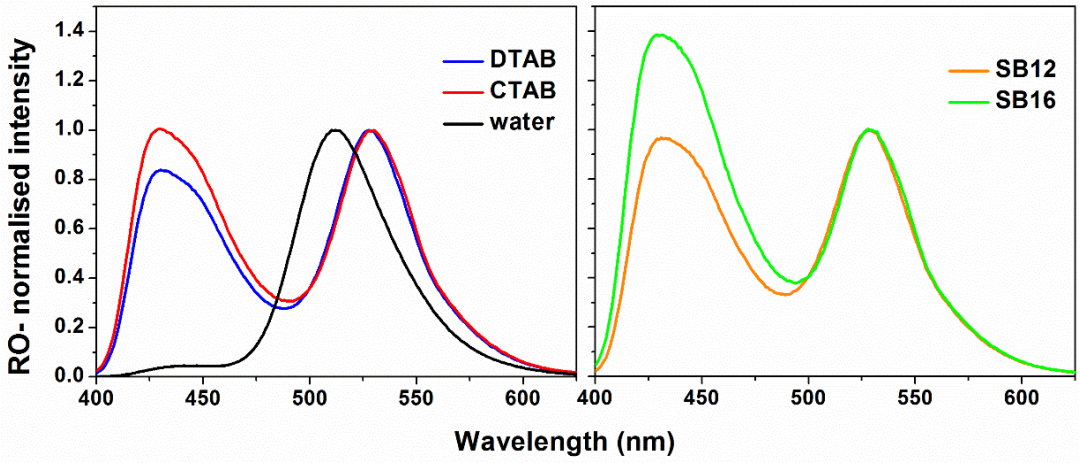

Figure 7.4: Comparison of the emission spectra (normalized at the deprotonated emission band) of HPTS inside micelles with variation of the tail length of the surfactant. Emission spectrum of water is added for comparison.

7.2.2. Time-resolved fluorescence:

To monitor the ESPT dynamics, fluorescence transients of HPTS were recorded at two selective emission wavelengths, 425 nm and 570 nm, representing the protonated and deprotonated emissions, respectively (**Figure 7.5**) as discussed in earlier chapters. In water, the fluorescence decay of HPTS occurs in multiple timescales, but the ESPT mainly occurs with a time constant of ~100ps.[25, 224, 284] The fluorescence decays of the protonated form are much slower inside both the micelles compared to that in bulk water. The slow decays imply that the ESPT dynamics are severely retarded inside the micelles compared with that in bulk water. Note that minor but systematic variations are present among the fluorescence decays recorded for different micelles. The fluorescence decays inside the SB micelles are relatively slower compared to those of the cationic micelles having identical chain length (**Figure 7.5**). Moreover, the decays also become slower with the increase in the alkyl length chain (**Figure 7.6**).

A clear ultraslow rise component is observed in the deprotonated emission transients indicative of the ESPT phenomena. The rise times of the deprotonated form are of similar magnitude to that of the decay times of the corresponding protonated emission (**Table 7.1)**. The rise times also become longer for the sulfo-betaine micelles than those of the cationic micelles for the same tail length of the surfactants. Thus, the ESPT dynamics in the SB micelles are more retarded than those of the corresponding cationic micelles.

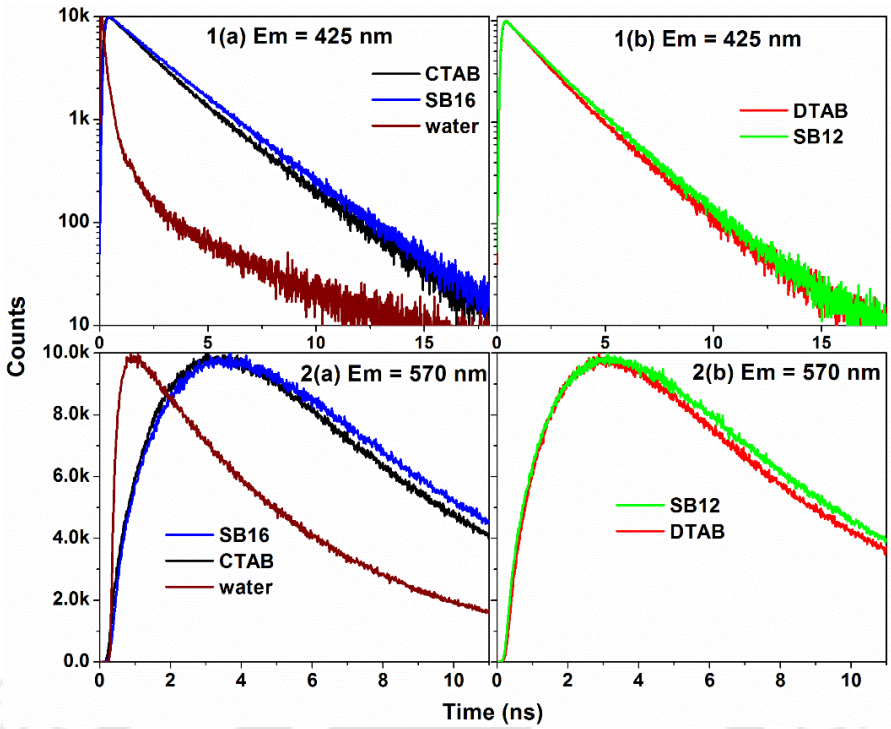

Figure 7.5: Fluorescence transients of the protonated (λ_{em} = 425 nm) and de-protonated (λ_{em} = 570) forms of HPTS inside cationic and SB micelles. The fluorescence tranisent of HPTS in water is also added for comparison.

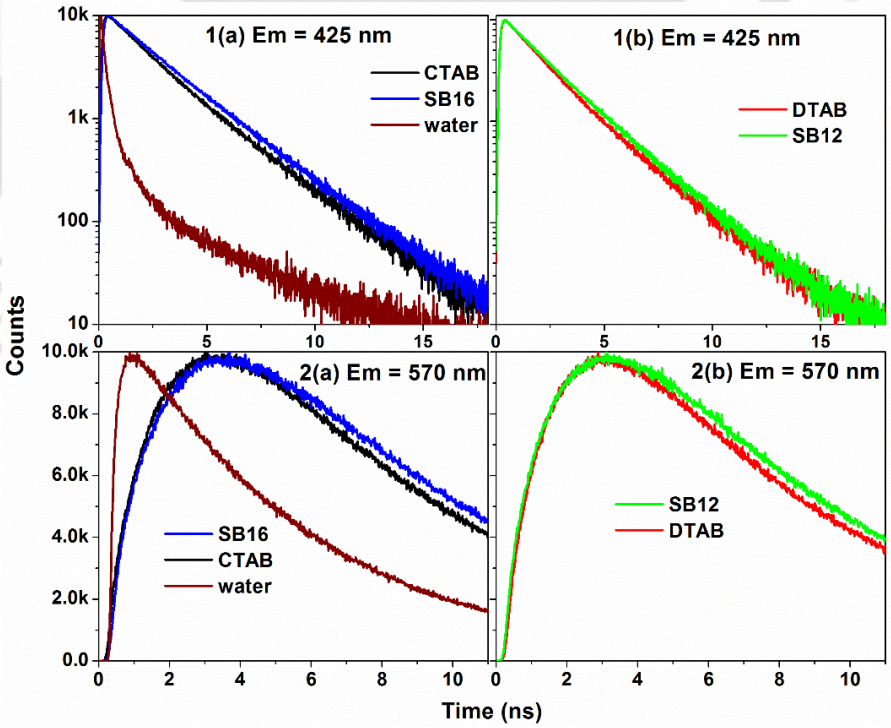

Figure 7.6: Comparison of the fluorescence transients of the protonated and deprotonated form of HPTS inside micelles with variation of the tail length of the surfactant (λ_{em}= 425 nm and 570 nm).

Table 7.1: Fitting parameters of the protonated (ROH^*, λ_{em} = 425 nm) and deprotonated (ROH^{-*}, λ_{em} = 570 nm) emission transients of HPTS inside different micelles.

Micelle	ROH^*				RO^{-*}			
	τ_1(ps)	τ_2 (ps)	τ_3 (ps)	χ^2	τ_1(ps)	τ_2 (ps)	τ_2 (ps)	χ^2
CTAB	655 (0.17)	2215 (0.77)	4970 (0.05)	1.08	655 (-2.05)	2215 (-10.9)	6230 (13.96)	1.03
SB16	460 (0.18)	2590 (0.76)	4550 (0.06)	1.05	460 (-0.73)	2590 (-9.36)	6255 (11.09)	1.18
DTAB	840 (0.21)	1990 (0.74)	4240 (0.05)	1.09	840 (-2.70)	1990 (-8.78)	6230 (12.49)	1.13
SB12	360 (0.14)	2060 (0.82)	4000 (0.04)	1.15	360 (-0.25)	2060 (-6.79)	6310 (8.04)	1.05

However to get more insight of water dynamics we monitored fluorescence transient emission decays at interval of 5nm across the emission spectra, followed by the construction of time-resolved emission spectra (TRES) or time-resolved area-normalized emission spectra (TRANES).[217,218] At an early time (t = 0.1 ns), the TRANES contributed solely by the protonated form and are identical for all the micelles irrespective of the headgroup or chain length (**Figure 7.7**). This virtually rules out the possibility of occurrence of any ultrafast component of ESPT in these micellar systems.

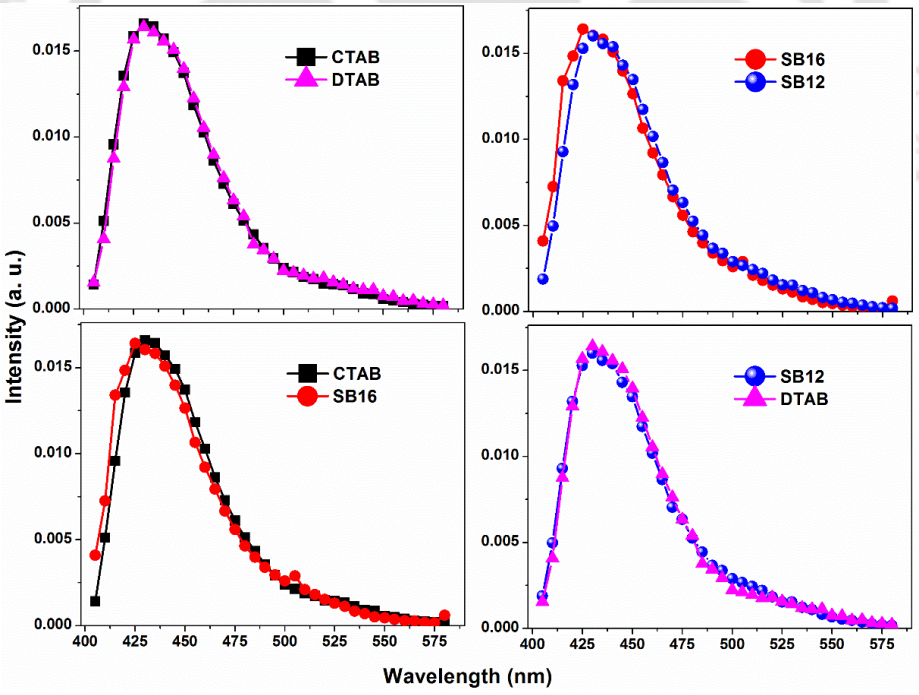

Figure 7.7: Comparison of TRANES emission spectra in different micelles at early time (t = 0.1ns).

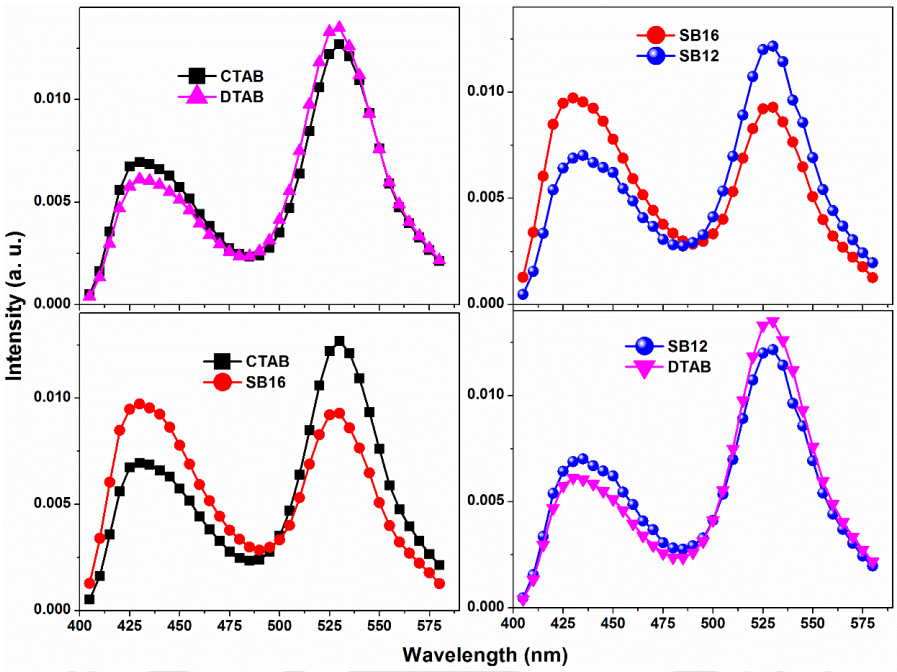

Figure 7.8: Comparison of time-resolved area-normalized emission spectra (TRANES) of HPTS inside cationic and sulfo-betaine micelles (CTAB vs. SB16; DTAB vs. SB12) and with variation of chain length at t = 5 ns.

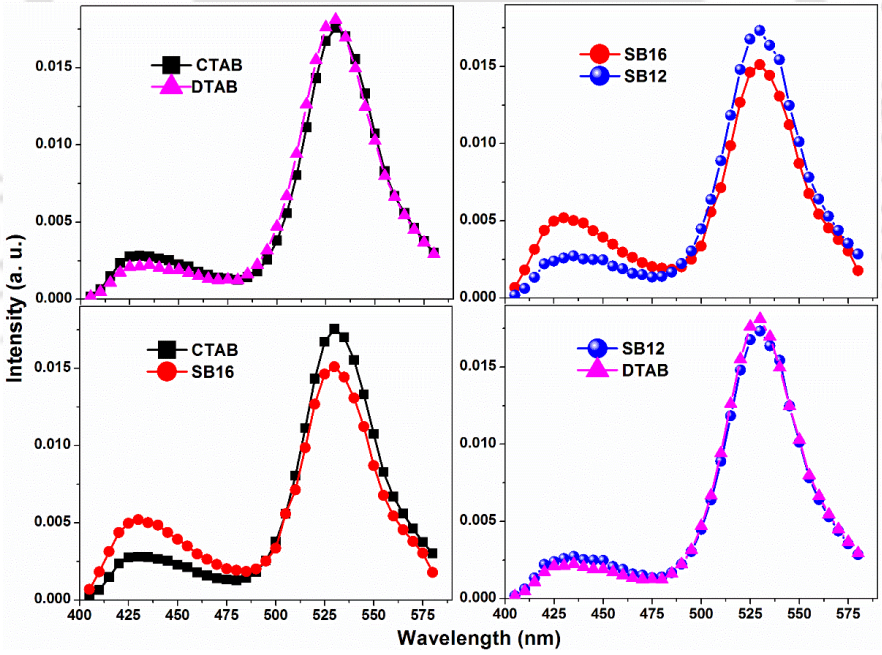

Figure 7.9: Comparison of TRANES emission spectra in different micelles at long time (t =10ns).

However, at a longer delay time, the TRANES have distinct contributions from both the protonated and deprotonated forms. Notably, the relative contributions of the protonated and de-protonated emission bands differ for different micelles. For example, for the TRANES at t = 5 ns, a higher fraction of the protonated form has been converted to the deprotonated form inside the CTAB micelles compared with that of the SB-16 micelles (**Figure 7.8**). Long after excitation (e.g.,

t = 10 ns), the protonated emission band further decays along with the concomitant increase of the deprotonated emission band, for all the micelles but the relative population of the protonated emission is higher for the SB micelles than that of the cationic micelle with identical chain length. This further confirms the slower ESPT inside the SB micelles than that in the cationic micelles (**Figure 7.9**). Moreover, at a particular time, more of the protonated form is present for the higher alkyl chain surfactant within the same series of surfactants. Thus, ESPT is indeed slower for the surfactant micelles with a longer tail.

We performed detailed analysis of the TRES and TRANES to get more quantitative description of the ESPT process.[216,217] The emission intensity (or equivalently, excited state population) of the protonated form decays as a result of proton transfer (i.e., conversion to the deprotonated form) as well as relaxation to the ground state. On the other hand, the intensity of the deprotonated form can develop from the deprotonation of the protonated form, and the intensity may decay to the ground state. Since the area of TRES is proportional to the total population of both the protonated and deprotonated forms, the decay of the TRES area with time may represent the average lifetime of HPTS.[208] We found that the decay of the TRES area can be fitted by two exponentials (**Table 7.2**). Thus, two different subpopulation of HPTS may exist at the interface. One of the sub-populations has a lifetime close to that in water (~5.4 ns). However, there also exists a quite shorter lifetime (1.24–2.25 ns) fraction. We do not know the exact origin of this shorter lifetime. This may be due to a fraction of HPTS that strongly interacts with the headgroup by ion-pairing or H-bonding.

In TRANES, the total area (i.e., total excited state population) is fixed (unity) and thus, the inter-conversion of the two forms can be best represented by the time evolution of TRANES. We further extracted the ESPT time constant by fitting the decay of the TRANES intensity of the protonated emission and the rise of the deprotonated emission (**Figure 7.10**). The ESPT time constants are summarized in **Table 7.2**.

Table 7.2: The parameters obtained from TRANES analysis of HPTS inside different micelles.

Micelles	ESPT time constant		Lifetime (ns)	
	ROH* (430 nm)	RO^{-}* (530 nm)	τ_{f1} (ns)	τ_{f2} (ns)
SB16	10.35±0.26	9.74±0.20	1.24 (0.18)	2.80 (0.72)
SB12	5.65±0.05	5.8±0.09	1.40 (0.43)	5.12 (0.56)
CTAB	5.62±0.02	5.45±0.04	1.24 (0.38)	4.8 (0.62)
DTAB	4.99±0.05	4.97±0.04	2.25 (0.51)	5.6 (0.49)
CTAC	4.86±0.05	4.78±0.06	1.68 (0.56)	5.7 (0.44)

Interestingly, the ESPT dynamics is found to be exponential and the time constant agrees well between the two data sets (protonated vs. deprotonated forms). We found that the ESPT is slowest for the SB16 micelle and occurs with a time constant of ~10 ns (**Table 7.2**). The ESPT time constant decreases with the shortening of the chain length. For similar chain length surfactants, the deprotonation time is faster for the cationic micelle compared to the sulfo-betaine surfactant (**Table 7.2**). For the cationic micelles, the ESPT time depends on both the chain length and the counter ion. The ESPT rate is slower for the CTAB micelle compared to the CTAC micelle.

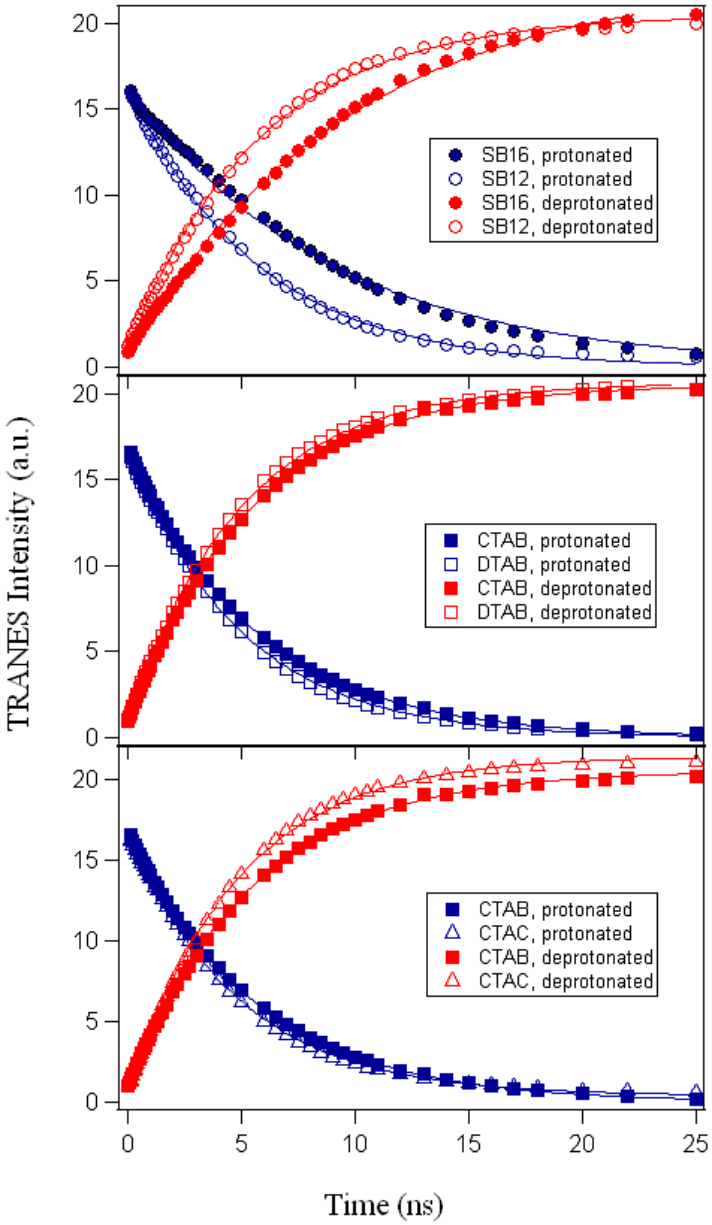

Figure 7.10. The time evolution of the TRANES intensity of protonated (blue) and deprotonated (red) forms representing the true deprotonation kinetics inside different micelles.

7.2.3. Fluorescence Anisotropy:

In bulk water, the fluorescence anisotropy of MPTS decays with a time constant of 170 ps. However, when the MPTS is hosted inside a micellar medium, its movement becomes restricted as was observed by the appearance of very slow anisotropy decays. The extent of retardation of the rotational dynamics is more dramatic for the SB surfactant micelles compared to that of the cationic micelles with an equal chain length. The result implies a better packing of the SB surfactant headgroups at the interfacial region of the micelles compared to that of the cationic micelles. With the increase in the surfactant chain length, the rotational dynamics was found to be faster within a specific surfactant series (**Figure 7.11**). Thus, we may infer that the SB surfactant micelles confer consistently more confinement to the MPTS host. This is in agreement with the results of Chakrabarty et al.[285] They also found that the rotational dynamics of coumarin 102 inside alkyltrimethylammonium bromide micelles become slower with an increase in the alkyl chain lengths of the surfactant. They concluded that the increase in the length of the alkyl chain leads to a more compact interface.[285] Thus, the increase in the chain length may indirectly affect the headgroup packing which resulted in a more confined environment for the fluorophore (HPTS or MPTS) to exert slower ESPT or rotational dynamics. The anisotropy decays can be fitted by a bi-exponential function

$$r(t) = r_0\left[\beta\, e^{-t/\tau_s} + (1-\beta)\, e^{-t/\tau_f}\right] \qquad (7.1)$$

Where r_0 denotes initial anisotropy; τ_S and τ_f are slow and fast time rotational constants, respectively and β is the contribution of the slow component. The anisotropy decay fitting parameters are further analysed by *wobbling in cone model* discussed in details in ***chapter 2***. All the analysed parameters are given in **Table 7.3**.

Table 7.3: Fitting parameters of the anisotropy decays of MPTS (λ_{em}= 440 nm) inside different micelles.

System	r_0	a_s	τ_s /ns	τ_f/ns	τ_w/ns	τ_M/ns	τ_D/ns	Θ°	D_W/ ns^{-1}
CTAB	0.27	0.69	4.00	0.64	0.71	13.0	5.78	38.7	0.28
SB16	0.29	0.79	6.58	0.87	0.96	20.0	9.81	31.5	0.15
DTAB	0.29	0.73	2.47	0.55	0.63	5.3	4.63	36.1	0.28
SB12	0.32	0.69	3.81	0.9	1.08	12.5	5.48	38.7	0.18

The semi-cone angles are very similar for all the micelles indicating a close similarity of the local environments. However, the wobbling and the translational time constants differ significantly among different micelles. In the zwitterionic micelles, the wobbling time constants and the translational time constants are longer than the corresponding cationic micelles. The

wobbling diffusion constants are higher for the cationic micelles than the zwitterionic micelles of the same chain length. The results indicate that the interface of the sulfobetaine micelles is more compact compared to the cationic micelles having identical tail length.

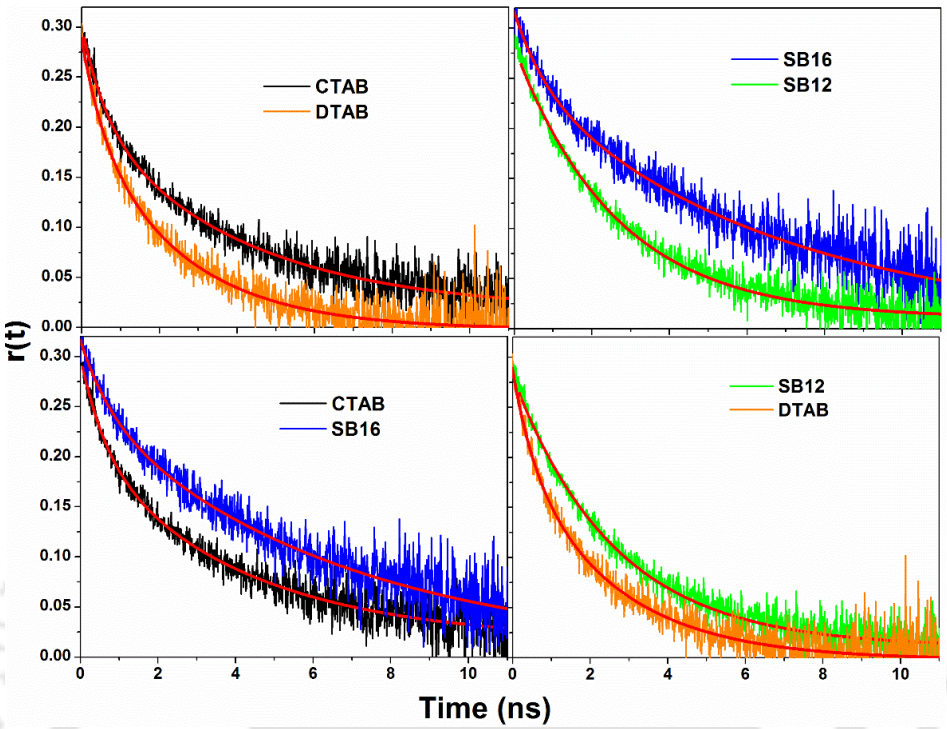

Figure 7.11: Fluorescence anisotropy decay of **MPTS** inside cationic and sulfo-betaine micelles (λ_{em} = 440 nm).

7.3. EFFECT OF COUNTER IONS:

The alkyl quaternary ammonium surfactant may have other counter ions rather than the bromide anion and thus, the results may depend on the nature of the counter ion used. To look at the effect of the counter ions (Br^- vs.Cl^-), we compared the ESPT dynamics of HPTS between the CTAB and CTAC micelles and found that the ESPT dynamics of CTAC is considerably faster than the CTAB micelles (**Figure 7.10**). Chloride ions are more hydrated than the Br^- and hence, Br^- ions like to reside more at the interface. Thus, for CTAB, the headgroup charges are more neutralized and may require less water at the interface for further stabilization of the headgroups. For the same chain length surfactants, the ESPT rate follows the order: CTAC > CTAB > SB16. The counter ion binding is higher in CTAB than in CTAC.[286] The sulfobetaine SB16 surfactant may be generalized as an alkylammonium surfactant with a propyl sulfonate counter-anion. This counter ion is expected to be more hydrophobic than bromide and cannot leave the interface. From these considerations, hydration at the interface of the sulfobetaine should be lower. Thus, the behaviour of the zwitterionic surfactant has similarity to the cationic surfactant with a very hydrophobic counter ion.

7.4. SUMMARY AND CONCLUSIONS:

In summary, we compared the interfacial properties, in particular, the nature of the interfacial hydration and rigidity, of cationic and zwitterionic sulfobetaine micelles using the ESPT behavior of HPTS and rotational anisotropy of MPTS. The slower ESPT and rotational dynamics found inside the zwitterionic micelles compared with that of the cationic micelles with the identical alkyl tail length; imply that the interface of zwitterionic sulfobetaine micelles is more packed and less hydrated. The slower ESPT is mainly arise because of reduction in the mobility of water molecules due to their strong hydrogen bond formation with the surfactant headgroups. Moreover, we also show that both the interfacial ESPT dynamics and fluorescence anisotropy decay depend on the nature of the counter anion of the cationic micelles; the hydrophobic bromide makes the dynamics slower than that of the Cl^- counter ion. Thus, the slower dynamics inside the sulfobetaine surfactant in comparison with the corresponding alkylammoium surfactant may be ascribed to the counter ion effect. The interfacial properties of a zwitterionic sulfobetaine micelle may be modelled as a cationic alkyl-ammonium surfactant micelle with a similar tail but with a hydrophobic counter ion.

REFERENCES:

(1) Shi, Z.; Peng, P.; Strohecker, D.; Liao, Y.: Long-Lived Photoacid Based upon a Photochromic Reaction. *J. Am. Chem. Soc.* **2011**, *133*, 14699-14703.

(2) Presiado, I.; Erez, Y.; Huppert, D.: Excited-State Intermolecular Proton Transfer of Firefly Luciferin III. Proton Transfer to a Mild Base. *J. Phys. Chem. A* **2010**, *114*, 13337-13346.

(3) Baranov, M. S.; Lukyanov, K. A.; Borissova, A. O.; Shamir, J.; Kosenkov, D.; Slipchenko, L. V.; Tolbert, L. M.; Yampolsky, I. V.; Solntsev, K. M.: Conformationally Locked Chromophores as Models of Excited-State Proton Transfer in Fluorescent Proteins. *J. Am. Chem. Soc.* **2012**, *134*, 6025-6032.

(4) Scheiner, S.: Theoretical Studies of Excited State Proton Transfer in Small Model Systems. *J. Phys. Chem. A* **2000**, *104*, 5898-5909.

(5) Pradhan, R.; Harshan, A. K.; Krishnavilasam Chandrika, G. S.; Srinivasan, A.; Lourderaj, U.: Time-Dependent Density Functional Theoretical Investigation of Photoinduced Excited-State Intramolecular Dual Proton Transfer in Diformyl Dipyrromethanes. *J. Phys. Chem. A* **2016**, *120*, 9894-9906.

(6) Coe, J. D.; Levine, B. G.; Martínez, T. J.: Ab Initio Molecular Dynamics of Excited-State Intramolecular Proton Transfer Using Multireference Perturbation Theory. *J. Phys. Chem. A* **2007**, *111*, 11302-11310.

(7) Clark, J. H.; Shapiro, S. L.; Campillo, A. J.; Winn, K. R.: Picosecond studies of excited-state protonation and deprotonation kinetics. The laser pH jump. *J. Am. Chem. Soc.* **1979**, *101*, 746-748.

(8) Politi, M. J.; Fendler, J. H.: Laser pH-jump initiated proton transfer on charged micellar surfaces. *J. Am. Chem. Soc.* **1984**, *106*, 265-273.

(9) Simkovitch, R.; Shomer, S.; Gepshtein, R.; Huppert, D.: How Fast Can a Proton-Transfer Reaction Be beyond the Solvent-Control Limit? *J. Phys. Chem. B* **2015**, *119*, 2253-2262.

(10) Agmon, N.; Huppert, D.; Masad, A.; Pines, E.: Excited-state proton transfer to methanol-water mixtures. *J. Phys. Chem.* **1991**, *95*, 10407-10413.

(11) Karton-Lifshin, N.; Albertazzi, L.; Bendikov, M.; Baran, P. S.; Shabat, D.: "Donor–Two-Acceptor" Dye Design: A Distinct Gateway to NIR Fluorescence. *J. Am. Chem. Soc.* **2012**, *134*, 20412-20420.

(12) Agmon, N.; Pines, E.; Huppert, D.: Geminate recombination in proton-transfer reactions. II. Comparison of diffusional and kinetic schemes. *J. Chem. Phys.* **1988**, *88*, 5631-5638.

(13) Simkovitch, R.; Pines, D.; Agmon, N.; Pines, E.; Huppert, D.: Reversible Excited-State Proton Geminate Recombination: Revisited. *J. Phys. Chem. B* **2016**, *120*, 12615-12632.

(14) Bardez, E.; Goguillon, B. T.; Keh, E.; Valeur, B.: Dynamics of excited-state reactions in reversed micelles. 1. Proton transfer involving a hydrophilic fluorescent probe. *J. Phys. Chem.* **1984**, *88*, 1909-1913.

(15) Ohno, Y.; Iguchi, A.; Shinzato, C.; Inoue, M.; Suzuki, A.; Sakai, K.; Nakamura, T.: An aposymbiotic primary coral polyp counteracts acidification by active pH regulation. *Sci Rep* **2017**, *7*, 40324.

(16) Holcomb, M.; Venn, A. A.; Tambutté, E.; Tambutté, S.; Allemand, D.; Trotter, J.; McCulloch, M.: Coral calcifying fluid pH dictates response to ocean acidification. *Sci Rep* **2014**, *4*, 5207.

(17) Giuliano, K. A.; Gillies, R. J.: Determination of intracellular pH of BALBc-3T3 cells using the fluorescence of pyranine. *Anal. Biochem.* **1987**, *167*, 362-371.

(18) Overly, C. C.; Lee, K. D.; Berthiaume, E.; Hollenbeck, P. J.: Quantitative measurement of intraorganelle pH in the endosomal-lysosomal pathway in neurons by using ratiometric imaging with pyranine. *Proc. Natl. Acad. Sci.* **1995**, *92*, 3156-3160.

(19) Hulth, S.; Aller, R. C.; Engström, P.; Selander, E.: A pH plate fluorosensor (optode) for early diagenetic studies of marine sediments. *Limnol Oceanogr* **2002**, *47*, 212-220.

(20) Li, H.; Su, X.; Bai, C.; Xu, Y.; Pei, Z.; Sun, S.: Detection of carbon dioxide with a novel HPTS/NiFe-LDH nanocomposite. *Sens. Actuators, B* **2016**, *225*, 109-114.

(21) Bhosale, R. S.; Shitre, G. V.; Kumar, R.; Biradar, D. O.; Bhosale, S. V.; Narayan, R.; Bhosale, S. V.: A 8-hydroxypyrene-1,3,6-trisulfonic acid trisodium salt (HPTS) based colorimetric and green turn-on fluorescent sensor for the detection of arginine and lysine in aqueous solution. *Sens. Actuators, B* **2017**, *241*, 1270-1275.

(22) Ando, K.; Hynes, J. T.: Molecular Mechanism of HCl Acid Ionization in Water: Ab Initio Potential Energy Surfaces and Monte Carlo Simulations. *J. Phys. Chem. B* **1997**, *101*, 10464-10478.

(23) Ando, K.; Hynes, J. T.: Molecular Mechanism of HF Acid Ionization in Water: An Electronic Structure−Monte Carlo Study. *J. Phys. Chem. A* **1999**, *103*, 10398-10408.

(24) Geissler, P. L.; Dellago, C.; Chandler, D.; Hutter, J.; Parrinello, M.: Autoionization in Liquid Water. *Science* **2001**, *291*, 2121-2124.

(25) Simkovitch, R.; Rozenman, G. G.; Huppert, D.: A fresh look into the time-resolved fluorescence of 8-hydroxy-1,3,6-pyrenetrisulfonate with the use of the fluorescence up-conversion technique. *J. Photochem. Photobiol.* **2017**, *344*, 15-27.

(26) Pines, E.; Huppert, D.: Geminate recombination proton-transfer reactions. *Chem. Phys. Lett.* **1986**, *126*, 88-91.

(27) Leiderman, P.; Genosar, L.; Huppert, D.: Excited-State Proton Transfer: Indication of Three Steps in the Dissociation and Recombination Process. *J. Phys. Chem. A* **2005**, *109*, 5965-5977.

(28) Tran-Thi, T. H.; Gustavsson, T.; Prayer, C.; Pommeret, S.; Hynes, J. T.: Primary ultrafast events preceding the photoinduced proton transfer from pyranine to water. *Chem. Phys. Lett.* **2000**, *329*, 421-430.

(29) Mohammed, O. F.; Dreyer, J.; Magnes, B.-Z.; Pines, E.; Nibbering, E. T. J.: Solvent-Dependent Photoacidity State of Pyranine Monitored by Transient Mid-Infrared Spectroscopy. *ChemPhysChem* **2005**, *6*, 625-636.

(30) Eigen, M.: Proton Transfer, Acid-Base Catalysis, and Enzymatic Hydrolysis. Part I: ELEMENTARY PROCESSES. *Angewandte Chemie International Edition in English* **1964**, *3*, 1-19.

(31) Ando, K.; Hynes, J. T.: Ionization of Acids in Water. In *Structure and Reactivity in Aqueous Solution*; American Chemical Society, 1994; Vol. 568; pp 143-153.

(32) Zundel, G.: Hydrogen Bonds with Large Proton Polarizability and Proton Transfer Processes in Electrochemistry and Biology. In *Adv. Chem. Phys.*; John Wiley & Sons, Inc., 2007; pp 1-217.

(33) Siwick, B. J.; Bakker, H. J.: On the Role of Water in Intermolecular Proton-Transfer Reactions. *J. Am. Chem. Soc.* **2007**, *129*, 13412-13420.

(34) Marx, D.; Tuckerman, M. E.; Hutter, J.; Parrinello, M.: The nature of the hydrated excess proton in water. *Nature* **1999**, *397*, 601.

(35) Markovitch, O.; Chen, H.; Izvekov, S.; Paesani, F.; Voth, G. A.; Agmon, N.: Special Pair Dance and Partner Selection: Elementary Steps in Proton Transport in Liquid Water. *J. Phys. Chem. B* **2008**, *112*, 9456-9466.

(36) Woutersen, S.; Bakker, H. J.: Ultrafast Vibrational and Structural Dynamics of the Proton in Liquid Water. *Phys. Rev. Lett* **2006**, *96*, 138305.

(37) Mohammed, O. F.; Pines, D.; Dreyer, J.; Pines, E.; Nibbering, E. T. J.: Sequential Proton Transfer Through Water Bridges in Acid-Base Reactions. *Science* **2005**, *310*, 83-86.

(38) Noyes, A. A.; Kato, Y.: THE EQUIVALENT CONDUCTANCE OF HYDROGEN-ION DERIVED FROM TRANSFERENCE EXPERIMENTS WITH NITRIC ACID. *J. Am. Chem. Soc.* **1908**, *30*, 318-334.

(39) Johnston, J.: THE CHANGE OF THE EQUIVALENT CONDUCTANCE OF IONS WITH THE TEMPERATURE. *J. Am. Chem. Soc.* **1909**, *31*, 1010-1020.

(40) Noyes, A. A.; Melcher, A. C.; Cooper, H. C.; Eastman, G. W.; Kato, Y.: THE CONDUCTIVITY AND IONIZATION OF SALTS, ACIDS, AND BASES IN AQUEOUS SOLUTIONS AT HIGH TEMPERATURES. *J. Am. Chem. Soc.* **1908**, *30*, 335-353.

(41) Stryer, L.: Excited-State Proton-Transfer Reactions. A Deuterium Isotope Effect on Fluorescence. *J. Am. Chem. Soc.* **1966**, *88*, 5708-5712.

(42) Gajst, O.; Simkovitch, R.; Huppert, D.: Anomalous H+ and D+ Excited-State Proton-Transfer Rate in H2O/D2O Mixtures. *J. Phys. Chem. A* **2017**, *121*, 6917-6924.

(43) Awasthi, A. A.; Singh, P. K.: Proton Transfer Reaction Dynamics of Pyranine in DMSO/Water Mixtures. *ChemPhysChem* **2018**, *19*, 198-207.

(44) Suwaiyan, A.; Al-Adel, F.; Hamdan, A.; Klein, U. K. A.: Dynamics of proton transfer from photon-initiated acids in alcohol/water mixtures. *J. Phys. Chem.* **1990**, *94*, 7423-7429.

(45) Spies, C.; Shomer, S.; Finkler, B.; Pines, D.; Pines, E.; Jung, G.; Huppert, D.: Solvent dependence of excited-state proton transfer from pyranine-derived photoacids. *Phys. Chem. Chem. Phys.* **2014**, *16*, 9104-9114.

(46) Douhal, A.: Ultrafast Guest Dynamics in Cyclodextrin Nanocavities. *Chem. Rev.* **2004**, *104*, 1955-1976.

(47) Nandi, N.; Bhattacharyya, K.; Bagchi, B.: Dielectric Relaxation and Solvation Dynamics of Water in Complex Chemical and Biological Systems. *Chem. Rev.* **2000**, *100*, 2013-2046.

(48) Lee, J. W.; Samal, S.; Selvapalam, N.; Kim, H.-J.; Kim, K.: Cucurbituril Homologues and Derivatives: New Opportunities in Supramolecular Chemistry. *Acc. Chem. Res.* **2003**, *36*, 621-630.

(49) Lagona, J.; Mukhopadhyay, P.; Chakrabarti, S.; Isaacs, L.: The Cucurbit[n]uril Family. *Angew. Chem. Int. Ed.* **2005**, *44*, 4844-4870.

(50) Halterman, R. L.; Moore, J. L.; Yip, W. T.: Cucurbit[7]uril Disrupts Aggregate Formation Between Rhodamine B Dyes Covalently Attached to Glass Substrates. *J Fluoresc* **2011**, *21*, 1467-1478.

(51) Halterman, R. L.; Moore, J. L.; Mannel, L. M.: Disrupting Aggregation of Tethered Rhodamine B Dyads through Inclusion in Cucurbit[7]uril. *J. Org. Chem.* **2008**, *73*, 3266-3269.

(52) Choudhury, S. D.; Mohanty, J.; Pal, H.; Bhasikuttan, A. C.: Cooperative Metal Ion Binding to a Cucurbit[7]uril−Thioflavin T Complex: Demonstration of a Stimulus-Responsive Fluorescent Supramolecular Capsule. *J. Am. Chem. Soc.* **2010**, *132*, 1395-1401.

(53) Mondal, S. K.; Sahu, K.; Ghosh, S.; Sen, P.; Bhattacharyya, K.: Excited-State Proton Transfer from Pyranine to Acetate in γ-Cyclodextrin and Hydroxypropyl γ-Cyclodextrin. *J. Phys. Chem. A* **2006**, *110*, 13646-13652.

(54) Basílio, N.; Laia, C. A. T.; Pina, F.: Excited-State Proton Transfer in Confined Medium. 4-Methyl-7-hydroxyflavylium and β-Naphthol Incorporated in Cucurbit[7]uril. *J. Phys. Chem. B* **2015**, *119*, 2749-2757.

(55) Szejtli, J.: Past, present and futute of cyclodextrin research. In *Pure Appl. Chem.*, 2004; Vol. 76; pp 1825.

(56) Sayed, M.; Pal, H.: Supramolecularly assisted modulations in chromophoric properties and their possible applications: an overview. *J. Mater. Chem.C* **2016**, *4*, 2685-2706.

(57) He, J.; Li, Y.; Wang, C.; Zhang, K.; Lin, D.; Kong, L.; Liu, J.: Rapid adsorption of Pb, Cu and Cd from aqueous solutions by β-cyclodextrin polymers. *Appl. Surf. Sci.* **2017**, *426*, 29-39.

(58) Sousa, F. B. D.; Denadai, Â. M. L.; Lula, I. S.; Nascimento Jr, C. S.; Neto, N. S. G. F.; Lima, A. C.; Almeida, W. B. D.; Sinisterra, R. D.: Supramolecular Self-Assembly of Cyclodextrin and Higher Water Soluble Guest: Thermodynamics and Topological Studies. *J. Am. Chem. Soc.* **2008**, *130*, 8426-8436.

(59) Shaikh, M.; Mohanty, J.; Sundararajan, M.; Bhasikuttan, A. C.; Pal, H.: Supramolecular Host–Guest Interactions of Oxazine-1 Dye with β- and γ-Cyclodextrins: A Photophysical and Quantum Chemical Study. *J. Phys. Chem. B* **2012**, *116*, 12450-12459.

(60) Inoue, Y.; Hakushi, T.; Liu, Y.; Tong, L.; Shen, B.; Jin, D.: Thermodynamics of molecular recognition by cyclodextrins. 1. Calorimetric titration of inclusion complexation of

naphthalenesulfonates with .alpha.-, .beta.-, and .gamma.-cyclodextrins: enthalpy-entropy compensation. *J. Am. Chem. Soc.* **1993**, *115*, 475-481.

(61) Alsbaiee, A.; Smith, B. J.; Xiao, L.; Ling, Y.; Helbling, D. E.; Dichtel, W. R.: Rapid removal of organic micropollutants from water by a porous β-cyclodextrin polymer. *Nature* **2016**, *529*, 190-194.

(62) Jana, B.; Mohapatra, S.; Mondal, P.; Barman, S.; Pradhan, K.; Saha, A.; Ghosh, S.: α-Cyclodextrin Interacts Close to Vinblastine Site of Tubulin and Delivers Curcumin Preferentially to the Tubulin Surface of Cancer Cell. *ACS Appl. Mater. Interfaces* **2016**, *8*, 13793-13803.

(63) Uekama, K.; Hirayama, F.; Irie, T.: Cyclodextrin Drug Carrier Systems. *Chem. Rev.* **1998**, *98*, 2045-2076.

(64) Szejtli, J.: Dimethyl-β-cyclodextrin as parenteral drug carrier. *J Incl Phenom Macrocycl Chem* **1983**, *1*, 135-150.

(65) Challa, R.; Ahuja, A.; Ali, J.; Khar, R. K.: Cyclodextrins in drug delivery: An updated review. *AAPS PharmSciTech* **2005**, *6*, E329-E357.

(66) Loftsson, T.; Jarho, P.; Másson, M.; Järvinen, T.: Cyclodextrins in drug delivery. *Expert Opin. Drug Deliv* **2005**, *2*, 335-351.

(67) Karnes, J. J.; Benjamin, I.: SN2 Reaction Rate Enhancement by β-Cyclodextrin at the Liquid/Liquid Interface. *J. Phys. Chem. C* **2017**, *121*, 19209-19217.

(68) Gepshtein, R.; Leiderman, P.; Huppert, D.; Project, E.; Nachliel, E.; Gutman, M.: Proton Antenna Effect of the γ-Cyclodextrin Outer Surface, Measured by Excited State Proton Transfer. *J. Phys. Chem. B* **2006**, *110*, 26354-26364.

(69) Mondal, S. K.; Sahu, K.; Sen, P.; Roy, D.; Ghosh, S.; Bhattacharyya, K.: Excited state proton transfer of pyranine in a γ-cyclodextrin cavity. *Chem. Phys. Lett.* **2005**, *412*, 228-234.

(70) Agricultural and Biological ChemistryBiochemical JournalPeters Jr, T.: 2 - The Albumin Molecule: Its Structure and Chemical Properties. In *All About Albumin*; Academic Press: San Diego, 1995; pp 9-II.

(71) Sahu, K.; Mondal, S. K.; Roy, D.; Karmakar, R.; Bhattacharyya, K.: Study of interaction of a cationic protein with a cationic surfactant using solvation dynamics: Lysozyme: CTAB. *Chem. Phys. Lett.* **2005**, *413*, 484-489.

(72) Cohen, B.; Martin Álvarez, C.; Alarcos Carmona, N.; Organero, J. A.; Douhal, A.: Proton-Transfer Reaction Dynamics within the Human Serum Albumin Protein. *J. Phys. Chem. B* **2011**, *115*, 7637-7647.

(73) Awasthi, A. A.; Singh, P. K.: Excited-State Proton Transfer on the Surface of a Therapeutic Protein, Protamine. *J. Phys. Chem. B* **2017**, *121*, 10306-10317.

(74) Johnson, W. C.: Protein secondary structure and circular dichroism: A practical guide. *Proteins: Struct., Funct., Bioinf.* **1990**, *7*, 205-214.

(75) Kelly, S. M.; Jess, T. J.; Price, N. C.: How to study proteins by circular dichroism. *Biochim. Biophys. Acta, Proteins Proteomics* **2005**, *1751*, 119-139.

(76) Whitmore, L.; Wallace, B. A.: Protein secondary structure analyses from circular dichroism spectroscopy: Methods and reference databases. *Biopolymers* **2008**, *89*, 392-400.

(77) Jackson, M.; Mantsch, H. H.: The Use and Misuse of FTIR Spectroscopy in the Determination of Protein Structure. *Crit. Rev. Biochem. Mol. Biol.* **1995**, *30*, 95-120.

(78) Byler, D. M.; Susi, H.: Examination of the secondary structure of proteins by deconvolved FTIR spectra. *Biopolymers* **1986**, *25*, 469-487.

(79) Sattler, M.; Schleucher, J.; Griesinger, C.: Heteronuclear multidimensional NMR experiments for the structure determination of proteins in solution employing pulsed field gradients. *Prog Nucl Magn Reson Spectrosc* **1999**, *34*, 93-158.

(80) Mertens, H. D. T.; Svergun, D. I.: Structural characterization of proteins and complexes using small-angle X-ray solution scattering. *J. Struct. Biol.* **2010**, *172*, 128-141.

(81) Alexander, N.; Al-Mestarihi, A.; Bortolus, M.; McHaourab, H.; Meiler, J.: De Novo High-Resolution Protein Structure Determination from Sparse Spin-Labeling EPR Data. *Structure* **2008**, *16*, 181-195.

(82) Eftink, M. R.: The use of fluorescence methods to monitor unfolding transitions in proteins. *Biophys. J* . **1994**, *66*, 482-501.

(83) Vivian, J. T.; Callis, P. R.: Mechanisms of Tryptophan Fluorescence Shifts in Proteins. *Biophys. J* . **2001**, *80*, 2093-2109.

(84) J M Beechem, a.; Brand, L.: Time-Resolved Fluorescence of Proteins. *Annu. Rev. Biochem* **1985**, *54*, 43-71.

(85) Amdursky, N.: Photoacids as a new fluorescence tool for tracking structural transitions of proteins: following the concentration-induced transition of bovine serum albumin. *Phys. Chem. Chem. Phys.* **2015**, *17*, 32023-32032.

(86) Carter, D. C.; Ho, J. X.: Structure of Serum Albumin. In *Advances in Protein Chemistry*; Anfinsen, C. B., Edsall, J. T., Richards, F. M., Eisenberg, D. S., Eds.; Academic Press, 1994; Vol. 45; pp 153-203.

(87) Dockal, M.; Carter, D. C.; Rüker, F.: The Three Recombinant Domains of Human Serum Albumin: STRUCTURAL CHARACTERIZATION AND LIGAND BINDING PROPERTIES. *J. Biol. Chem.* **1999**, *274*, 29303-29310.

(88) Sadler, P. J.; Tucker, A.: pH-induced structural transitions of bovine serum albumin. *Eur. J. Biochem.* **1993**, *212*, 811-817.

(89) El Kadi, N.; Taulier, N.; Le Huérou, J. Y.; Gindre, M.; Urbach, W.; Nwigwe, I.; Kahn, P. C.; Waks, M.: Unfolding and Refolding of Bovine Serum Albumin at Acid pH: Ultrasound and Structural Studies. *Biophys. J* . **2006**, *91*, 3397-3404.

(90) Barbosa, L. R. S.; Ortore, M. G.; Spinozzi, F.; Mariani, P.; Bernstorff, S.; Itri, R.: The Importance of Protein-Protein Interactions on the pH-Induced Conformational Changes of Bovine Serum Albumin: A Small-Angle X-Ray Scattering Study. *Biophys. J* . **2010**, *98*, 147-157.

(91) Buck, M.; Schwalbe, H.; Dobson, C. M.: Characterization of Conformational Preferences in a Partly Folded Protein by Heteronuclear NMR Spectroscopy: Assignment and

Secondary Structure Analysis of Hen Egg-White Lysozyme in Trifluoroethanol. *Biochemistry* **1995**, *34*, 13219-13232.

(92) Ghosh, A.; Brinda, K. V.; Vishveshwara, S.: Dynamics of Lysozyme Structure Network: Probing the Process of Unfolding. *Biophys. J* . **2007**, *92*, 2523-2535.

(93) Jollès, P.; Jollès, J.: What's new in lysozyme research? *Mol Cell Biochem* **1984**, *63*, 165-189.

(94) Blake, C. C. F.; Koenig, D. F.; Mair, G. A.; North, A. C. T.; Phillips, D. C.; Sarma, V. R.: Structure of Hen Egg-White Lysozyme: A Three-dimensional Fourier Synthesis at 2 Å Resolution. *Nature* **1965**, *206*, 757.

(95) Das, I.; Panja, S.; Halder, M.: Modulation and Salt-Induced Reverse Modulation of the Excited-State Proton-Transfer Process of Lysozymized Pyranine: The Contrasting Scenario of the Ground-State Acid–Base Equilibrium of the Photoacid. *J. Phys. Chem. B* **2016**, *120*, 7076-7087.

(96) Huppert, D.; Kolodney, E.; Gutman, M.; Nachliel, E.: Effect of water activity on the rate of proton dissociation. *J. Am. Chem. Soc.* **1982**, *104*, 6949-6953.

(97) Smith, P. E.; Brunne, R. M.; Mark, A. E.; Van Gunsteren, W. F.: Dielectric properties of trypsin inhibitor and lysozyme calculated from molecular dynamics simulations. *J. Phys. Chem.* **1993**, *97*, 2009-2014.

(98) Jordanides, X. J.; Lang, M. J.; Song, X.; Fleming, G. R.: Solvation Dynamics in Protein Environments Studied by Photon Echo Spectroscopy. *J. Phys. Chem. B* **1999**, *103*, 7995-8005.

(99) Rozema, D.; Gellman, S. H.: Artificial Chaperone-Assisted Refolding of Denatured-Reduced Lysozyme: Modulation of the Competition between Renaturation and Aggregation. *Biochemistry* **1996**, *35*, 15760-15771.

(100) CELEJ, M. S.; D'ANDREA, M. G.; CAMPANA, P. T.; FIDELIO, G. D.; BIANCONI, M. L.: Superactivity and conformational changes on alpha-chymotrypsin upon interfacial binding to cationic micelles. *Biochem. J* **2004**, *378*, 1059-1066.

(101) Sahu, K.; Roy, D.; Mondal, S. K.; Karmakar, R.; Bhattacharyya, K.: Study of protein–surfactant interaction using excited state proton transfer. *Chem. Phys. Lett.* **2005**, *404*, 341-345.

(102) Stenstam, A.; Khan, A.; Wennerström, H.: The Lysozyme−Dodecyl Sulfate System. An Example of Protein−Surfactant Aggregation. *Langmuir* **2001**, *17*, 7513-7520.

(103) Chatterjee, A.; Moulik, S. P.; Majhi, P. R.; Sanyal, S. K.: Studies on surfactant-biopolymer interaction. I. Microcalorimetric investigation on the interaction of cetyltrimethylammonium bromide (CTAB) and sodium dodecylsulfate (SDS) with gelatin (Gn), lysozyme (Lz) and deoxyribonucleic acid (DNA). *Biophys. Chem.* **2002**, *98*, 313-327.

(104) Jaracz, S.; Chen, J.; Kuznetsova, L. V.; Ojima, I.: Recent advances in tumor-targeting anticancer drug conjugates. *Bioorganic Med. Chem.* **2005**, *13*, 5043-5054.

(105) Chiosis, G.; Neckers, L.: Tumor Selectivity of Hsp90 Inhibitors: The Explanation Remains Elusive. *ACS Chem. Biol.* **2006**, *1*, 279-284.

(106) Goldman, S. D.; Funk, R. S.; Rajewski, R. A.; Krise, J. P.: Mechanisms of amine accumulation in, and egress from, lysosomes. *Bioanalysis* **2009**, *1*, 1445-1459.

(107) Duvvuri, M.; Konkar, S.; Hong, K. H.; Blagg, B. S. J.; Krise, J. P.: A New Approach for Enhancing Differential Selectivity of Drugs to Cancer Cells. *ACS Chem. Biol.* **2006**, *1*, 309-315.

(108) Chowdhury, R.; Saha, A.; Mandal, A. K.; Jana, B.; Ghosh, S.; Bhattacharyya, K.: Excited State Proton Transfer in the Lysosome of Live Lung Cells: Normal and Cancer Cells. *J. Phys. Chem. B* **2015**, *119*, 2149-2156.

(109) Amdursky, N.; Simkovitch, R.; Huppert, D.: Excited-State Proton Transfer of Photoacids Adsorbed on Biomaterials. *J. Phys. Chem. B* **2014**, *118*, 13859-13869.

(110) Simkovitch, R.; Huppert, D.: Excited-State Proton Transfer of Weak Photoacids Adsorbed on Biomaterials: Proton Transfer to Glucosamine of Chitosan. *J. Phys. Chem. A* **2015**, *119*, 641-651.

(111) Fielden, K. E.; Newton, J. M.; O'Brien, P.; Rowe, R. C.: Thermal Studies on the Interaction of Water and Microcrystalline Cellulose. *J. Pharm. Pharmacol.* **1988**, *40*, 674-678.

(112) Di Renzo, F.; Cambon, H.; Dutartre, R.: A 28-year-old synthesis of micelle-templated mesoporous silica. *Microporous Mater.* **1997**, *10*, 283-286.

(113) Taguchi, A.; Schüth, F.: Ordered mesoporous materials in catalysis. *Microporous Mesoporous Mater.* **2005**, *77*, 1-45.

(114) Perego, C.; Millini, R.: Porous materials in catalysis: challenges for mesoporous materials. *Chem. Soc. Rev.* **2013**, *42*, 3956-3976.

(115) Martín-Aranda, R. M.; Čejka, J.: Recent Advances in Catalysis Over Mesoporous Molecular Sieves. *Top. Catal.* **2010**, *53*, 141-153.

(116) Huo, Q.; Zhao, D.; Feng, J.; Weston, K.; Buratto, S. K.; Stucky, G. D.; Schacht, S.; Schüth, F.: Room temperature growth of mesoporous silica fibers: A new high-surface-area optical waveguide. *Adv. Mater.* **1997**, *9*, 974-978.

(117) Hayward, R. C.; Alberius-Henning, P.; Chmelka, B. F.; Stucky, G. D.: The current role of mesostructures in composite materials and device fabrication. *Microporous Mesoporous Mater.* **2001**, *44-45*, 619-624.

(118) Aznar, E.; Casasús, R.; García-Acosta, B.; Marcos, M. D.; Martínez-Máñez, R.; Sancenón, F.; Soto, J.; Amorós, P.: Photochemical and Chemical Two-Channel Control of Functional Nanogated Hybrid Architectures. *Adv. Mater.* **2007**, *19*, 2228-2231.

(119) Zhang, J.; Zou, Q.; Tian, H.: Photochromic Materials: More Than Meets The Eye. *Adv. Mater.* **2013**, *25*, 378-399.

(120) Alarcos, N.; Cohen, B.; Douhal, A.: A slowing down of proton motion from HPTS to water adsorbed on the MCM-41 surface. *Phys. Chem. Chem. Phys.* **2016**, *18*, 2658-2671.

(121) Lu, J.; Lu, S.; Jiang, S. P.: Highly ordered mesoporous Nafion membranes for fuel cells. *Chem. Commun.* **2011**, *47*, 3216-3218.

(122) Spry, D. B.; Goun, A.; Glusac, K.; Moilanen, D. E.; Fayer, M. D.: Proton Transport and the Water Environment in Nafion Fuel Cell Membranes and AOT Reverse Micelles. *J. Am. Chem. Soc.* **2007**, *129*, 8122-8130.

(123) Thomaz, J. E.; Lawler, C. M.; Fayer, M. D.: Proton Transfer in Perfluorosulfonic Acid Fuel Cell Membranes with Differing Pendant Chains and Equivalent Weights. *J. Phys. Chem. B* **2017**, *121*, 4544-4553.

(124) Moilanen, D. E.; Spry, D. B.; Fayer, M. D.: Water Dynamics and Proton Transfer in Nafion Fuel Cell Membranes. *Langmuir* **2008**, *24*, 3690-3698.

(125) Moilanen, D. E.; Piletic, I. R.; Fayer, M. D.: Tracking Water's Response to Structural Changes in Nafion Membranes. *J. Phys. Chem. A* **2006**, *110*, 9084-9088.

(126) Moilanen, D. E.; Piletic, I. R.; Fayer, M. D.: Water Dynamics in Nafion Fuel Cell Membranes: The Effects of Confinement and Structural Changes on the Hydrogen Bond Network. *J. Phys. Chem. C* **2007**, *111*, 8884-8891.

(127) Burai, T. N.; Datta, A.: Slow Solvation Dynamics in the Microheterogeneous Water Channels of Nafion Membranes. *J. Phys. Chem. B* **2009**, *113*, 15901-15906.

(128) Attard, G. S.; Bartlett, P. N.; Coleman, N. R. B.; Elliott, J. M.; Owen, J. R.; Wang, J. H.: Mesoporous Platinum Films from Lyotropic Liquid Crystalline Phases. *Science* **1997**, *278*, 838-840.

(129) Vallooran, J. J.; Handschin, S.; Pillai, S. M.; Vetter, B. N.; Rusch, S.; Beck, H.-P.; Mezzenga, R.: Lipidic Cubic Phases as a Versatile Platform for the Rapid Detection of Biomarkers, Viruses, Bacteria, and Parasites. *Adv. Funct. Mater.* **2016**, *26*, 181-190.

(130) Angelova, A.; Angelov, B.; Mutafchieva, R.; Lesieur, S.; Couvreur, P.: Self-Assembled Multicompartment Liquid Crystalline Lipid Carriers for Protein, Peptide, and Nucleic Acid Drug Delivery. *Acc. Chem. Res.* **2011**, *44*, 147-156.

(131) Pebay-Peyroula, E.; Rummel, G.; Rosenbusch, J. P.; Landau, E. M.: X-ray Structure of Bacteriorhodopsin at 2.5 Angstroms from Microcrystals Grown in Lipidic Cubic Phases. *Science* **1997**, *277*, 1676-1681.

(132) Garti, N.; Libster, D.; Aserin, A.: Lipid polymorphism in lyotropic liquid crystals for triggered release of bioactives. *Food Funct.* **2012**, *3*, 700-713.

(133) Mezzenga, R.; Schurtenberger, P.; Burbidge, A.; Michel, M.: Understanding foods as soft materials. *Nat. Mater.* **2005**, *4*, 729.

(134) Fong, C.; Le, T.; Drummond, C. J.: Lyotropic liquid crystal engineering-ordered nanostructured small molecule amphiphile self-assembly materials by design. *Chem. Soc. Rev.* **2012**, *41*, 1297-1322.

(135) Kulkarni, C. V.; Wachter, W.; Iglesias-Salto, G.; Engelskirchen, S.; Ahualli, S.: Monoolein: a magic lipid? *Phys. Chem. Chem. Phys.* **2011**, *13*, 3004-3021.

(136) Larsson, K.; Fontell, K.; Krog, N.: Structural relationships between lamellar, cubic and hexagonal phases in monoglyceride-water systems. possibility of cubic structures in biological systems. *Chem. Phys. Lipids* **1980**, *27*, 321-328.

(137) Deng, Y.; Marko, M.; Buttle, K. F.; Leith, A.; Mieczkowski, M.; Mannella, C. A.: Cubic Membrane Structure in Amoeba (Chaos carolinensis) Mitochondria Determined by Electron Microscopic Tomography. *J. Struct. Biol.* **1999**, *127*, 231-239.

(138) Kulkarni, C. V.: Lipid crystallization: from self-assembly to hierarchical and biological ordering. *Nanoscale* **2012**, *4*, 5779-5791.

(139) Rivas, E.; Luzzati, V.: Polymorphisme des lipides polaires et des galacto-lipides de chloroplastes de maïs, en présence d'eau. *J. Mol. Biol.* **1969**, *41*, 261-275.

(140) Negrini, R.; Mezzenga, R.: pH-Responsive Lyotropic Liquid Crystals for Controlled Drug Delivery. *Langmuir* **2011**, *27*, 5296-5303.

(141) Sun, W.; Vallooran, J. J.; Mezzenga, R.: Enzyme Kinetics in Liquid Crystalline Mesophases: Size Matters, But Also Topology. *Langmuir* **2015**, *31*, 4558-4565.

(142) Kijima, T.; Yoshimura, T.; Uota, M.; Ikeda, T.; Fujikawa, D.; Mouri, S.; Uoyama, S.: Noble-Metal Nanotubes (Pt, Pd, Ag) from Lyotropic Mixed-Surfactant Liquid-Crystal Templates. *Angew. Chem. Int. Ed.* **2004**, *43*, 228-232.

(143) Oka, T.; Hojo, H.: Single Crystallization of an Inverse Bicontinuous Cubic Phase of a Lipid. *Langmuir* **2014**, *30*, 8253-8257.

(144) Mishraki-Berkowitz, T.; Ben Ishai, P.; Aserin, A.; Feldman, Y.; Garti, N.: The dielectric study of insulin-loaded reverse hexagonal (HII) liquid crystals. *Phys. Chem. Chem. Phys.* **2015**, *17*, 9499-9508.

(145) Mackay, A. L.: Periodic minimal surfaces. *Nature* **1985**, *314*, 604.

(146) Mojumdar, S. S.; Chowdhury, R.; Mandal, A. K.; Bhattacharyya, K.: In what time scale proton transfer takes place in a live CHO cell? *J. Chem. Phys.* **2013**, *138*, 215102.

(147) Roy, B.; Satpathi, S.; Hazra, P.: Topological Influence of Lyotropic Liquid Crystalline Systems on Excited-State Proton Transfer Dynamics. *Langmuir* **2016**, *32*, 3057-3065.

(148) Levinger, N. E.: Water in Confinement. *Science* **2002**, *298*, 1722-1723.

(149) Moilanen, D. E.; Fenn, E. E.; Wong, D.; Fayer, M. D.: Water dynamics in large and small reverse micelles: From two ensembles to collective behavior. *J. Chem. Phys.* **2009**, *131*, 014704.

(150) Peterson, M. D.; Mooseker, M. S.: Characterization of the enterocyte-like brush border cytoskeleton of the C2BBe clones of the human intestinal cell line, Caco-2. *J. Cell Sci.* **1992**, *102*, 581-600.

(151) Kramer, W.; Girbig, F.; Corsiero, D.; Pfenninger, A.; Frick, W.; Jähne, G.; Rhein, M.; Wendler, W.; Lottspeich, F.; Hochleitner, E. O.; Orsó, E.; Schmitz, G.: Aminopeptidase N (CD13) Is a Molecular Target of the Cholesterol Absorption Inhibitor Ezetimibe in the Enterocyte Brush Border Membrane. *J. Biol. Chem.* **2005**, *280*, 1306-1320.

(152) Tso, P.; Nauli, A.; Lo, C.-M.: Enterocyte fatty acid uptake and intestinal fatty acid-binding protein. *Biochem. Soc. Trans.* **2004**, *32*, 75-78.

(153) Vrignaud, S.; Hureaux, J.; Wack, S.; Benoit, J.-P.; Saulnier, P.: Design, optimization and in vitro evaluation of reverse micelle-loaded lipid nanocarriers containing erlotinib hydrochloride. *Int. J. Pharm.* **2012**, *436*, 194-200.

(154) Cai, L.; Gochin, M.; Liu, K.: A facile surfactant critical micelle concentration determination. *Chem. Commun.* **2011**, *47*, 5527-5529.

(155) Mukherjee, T. K.; Lahiri, P.; Datta, A.: 2-(2′-Pyridyl)benzimidazole as a fluorescent probe for monitoring protein–surfactant interaction. *Chem. Phys. Lett.* **2007**, *438*, 218-223.

(156) Dutta, P.; Halder, A.; Mukherjee, S.; Sen, P.; Sen, S.; Bhattacharyya, K.: Excited State Proton Transfer of 1-Naphthol in a Hydroxypropylcellulose/Sodium Dodecyl Sulfate System. *Langmuir* **2002**, *18*, 7867-7871.

(157) Mandal, D.; Pal, S. K.; Bhattacharyya, K.: Excited-State Proton Transfer of 1-Naphthol in Micelles. *J. Phys. Chem. A* **1998**, *102*, 9710-9714.

(158) Mondal, T.; Das, A. K.; Sasmal, D. K.; Bhattacharyya, K.: Excited State Proton Transfer in Ionic Liquid Mixed Micelles. *J. Phys. Chem. B* **2010**, *114*, 13136-13142.

(159) Giestas, L.; Yihwa, C.; Lima, J. C.; Vautier-Giongo, C.; Lopes, A.; Maçanita, A. L.; Quina, F. H.: The Dynamics of Ultrafast Excited State Proton Transfer in Anionic Micelles. *J. Phys. Chem. A* **2003**, *107*, 3263-3269.

(160) Mukherjee, T. K.; Ahuja, P.; Koner, A. L.; Datta, A.: ESPT of 2-(2‘-Pyridyl)benzimidazole at the Micelle−Water Interface: Selective Enhancement and Slow Dynamics with Sodium Dodecyl Sulfate. *J. Phys. Chem. B* **2005**, *109*, 12567-12573.

(161) Barnadas-Rodríguez, R.; Estelrich, J.: Photophysical Changes of Pyranine Induced by Surfactants: Evidence of Premicellar Aggregates. *J. Phys. Chem. B* **2009**, *113*, 1972-1982.

(162) Barnadas-Rodríguez, R.; Cladera, J.: Steroidal Surfactants: Detection of Premicellar Aggregation, Secondary Aggregation Changes in Micelles, and Hosting of a Highly Charged Negative Substance. *Langmuir* **2015**, *31*, 8980-8988.

(163) Chakrabarty, A.; Das, P.; Mallick, A.; Chattopadhyay, N.: Effect of Surfactant Chain Length on the Binding Interaction of a Biological Photosensitizer with Cationic Micelles. *J. Phys. Chem. B* **2008**, *112*, 3684-3692.

(164) Pramanik, S.; Banerjee, P.; Bhattacharya, S. C.: Interaction of 8-hydroxypyrene-1,3,6-trisulphonate in alkyltrimethylammonium bromide (CnTAB) micellar medium. *J. Photochem. Photobiol.* **2007**, *187*, 384-388.

(165) Nikas, Y. J.; Blankschtein, D.: Complexation of Nonionic Polymers and Surfactants in Dilute Aqueous Solutions. *Langmuir* **1994**, *10*, 3512-3528.

(166) Maltesh, C.; Somasundaran, P.: Size of the Sodium Dodecylsulfate Aggregate Bound to Polyethylene Glycol: Effect of Different Cations. *J. Colloid Interface Sci.* **1993**, *157*, 14-18.

(167) MacKnight, W. J.; Ponomarenko, E. A.; Tirrell, D. A.: Self-Assembled Polyelectrolyte−Surfactant Complexes in Nonaqueous Solvents and in the Solid State. *Acc. Chem. Res.* **1998**, *31*, 781-788.

(168) Lum, K.; Chandler, D.; Weeks, J. D.: Hydrophobicity at Small and Large Length Scales. *J. Phys. Chem. B* **1999**, *103*, 4570-4577.

(169) Gilányi, T.: Small Systems Thermodynamics of Polymer−Surfactant Complex Formation. *J. Phys. Chem. B* **1999**, *103*, 2085-2090.

(170) Jansson, J.; Schillén, K.; Nilsson, M.; Söderman, O.; Fritz, G.; Bergmann, A.; Glatter, O.: Small-Angle X-ray Scattering, Light Scattering, and NMR Study of PEO−PPO−PEO Triblock Copolymer/Cationic Surfactant Complexes in Aqueous Solution. *J. Phys. Chem. B* **2005**, *109*, 7073-7083.

(171) Vinogradov, A. M.; Tatikolov, A. S.; Costa, S. M. B.: The effect of anionic, cationic and neutral surfactants on the photophysics and isomerization of 3,3[prime or minute]-diethylthiacarbocyanine. *Phys. Chem. Chem. Phys.* **2001**, *3*, 4325-4332.

(172) Sukul, D.; Pal, S. K.; Mandal, D.; Sen, S.; Bhattacharyya, K.: Excited State Proton Transfer as a Probe for Polymer−Surfactant Interaction. *J. Phys. Chem. B* **2000**, *104*, 6128-6132.

(173) Ghosh, S.; Dey, S.; Mandal, U.; Adhikari, A.; Mondal, S. K.; Bhattacharyya, K.: Ultrafast Proton Transfer of Pyranine in a Supramolecular Assembly: PEO−PPO−PEO Triblock Copolymer and CTAC. *J. Phys. Chem. B* **2007**, *111*, 13504-13510.

(174) Faeder, J.; Ladanyi, B. M.: Molecular Dynamics Simulations of the Interior of Aqueous Reverse Micelles. *J. Phys. Chem. B* **2000**, *104*, 1033-1046.

(175) Maitra, A.: Determination of size parameters of water-Aerosol OT-oil reverse micelles from their nuclear magnetic resonance data. *J. Phys. Chem.* **1984**, *88*, 5122-5125.

(176) Eskici, G.; Axelsen, P. H.: The Size of AOT Reverse Micelles. *J. Phys. Chem. B* **2016**, *120*, 11337-11347.

(177) Vasquez, V. R.; Williams, B. C.; Graeve, O. A.: Stability and Comparative Analysis of AOT/Water/Isooctane Reverse Micelle System Using Dynamic Light Scattering and Molecular Dynamics. *J. Phys. Chem. B* **2011**, *115*, 2979-2987.

(178) Kinugasa, T.; Kondo, A.; Nishimura, S.; Miyauchi, Y.; Nishii, Y.; Watanabe, K.; Takeuchi, H.: Estimation for size of reverse micelles formed by AOT and SDEHP based on viscosity measurement. *Colloids Surf., A* **2002**, *204*, 193-199.

(179) Crans, D. C.; Levinger, N. E.: The Conundrum of pH in Water Nanodroplets: Sensing pH in Reverse Micelle Water Pools. *Acc. Chem. Res.* **2012**, *45*, 1637-1645.

(180) Sedgwick, M.; Cole, R. L.; Rithner, C. D.; Crans, D. C.; Levinger, N. E.: Correlating Proton Transfer Dynamics To Probe Location in Confined Environments. *J. Am. Chem. Soc.* **2012**, *134*, 11904-11907.

(181) Moilanen, D. E.; Levinger, N. E.; Spry, D. B.; Fayer, M. D.: Confinement or the Nature of the Interface? Dynamics of Nanoscopic Water. *J. Am. Chem. Soc.* **2007**, *129*, 14311-14318.

(182) Zhang, J.; Bright, F. V.: Nanosecond reorganization of water within the interior of reversed micelles revealed by frequency-domain fluorescence spectroscopy. *J. Phys. Chem.* **1991**, *95*, 7900-7907.

(183) Wong, M.; Thomas, J. K.; Graetzel, M.: Fluorescence probing of inverted micelles. The state of solubilized water clusters in alkane/diisooctyl sulfosuccinate (aerosol OT) solution. *J. Am. Chem. Soc.* **1976**, *98*, 2391-2397.

(184) Wong, M.; Thomas, J. K.; Nowak, T.: Structure and state of water in reversed micelles. 3. *J. Am. Chem. Soc.* **1977**, *99*, 4730-4736.

(185) Correa, N. M.; Biasutti, M. A.; Silber, J. J.: Micropolarity of Reverse Micelles of Aerosol-OT in n-Hexane. *J. Colloid Interface Sci.* **1995**, *172*, 71-76.

(186) Harpham, M. R.; Ladanyi, B. M.; Levinger, N. E.: The Effect of the Counterion on Water Mobility in Reverse Micelles Studied by Molecular Dynamics Simulations. *J. Phys. Chem. B* **2005**, *109*, 16891-16900.

(187) Belletete, M.; Lachapelle, M.; Durocher, G.: Dynamics of interfacial interactions between the molecular probe 2-(p-(dimethylamino)phenyl)-3,3-dimethyl-3H-indole and the Aerosol OT inverted micelles. *J. Phys. Chem.* **1990**, *94*, 7642-7648.

(188) Riter, R. E.; Willard, D. M.; Levinger, N. E.: Water Immobilization at Surfactant Interfaces in Reverse Micelles. *J. Phys. Chem. B* **1998**, *102*, 2705-2714.

(189) Yuan, R.; Yan, C.; Nishida, J.; Fayer, M. D.: Dynamics in a Water Interfacial Boundary Layer Investigated with IR Polarization-Selective Pump–Probe Experiments. *J. Phys. Chem. B* **2017**, *121*, 4530-4537.

(190) Correa, N. M.; Zorzan, D. H.; D'Anteo, L.; Lasta, E.; Chiarini, M.; Cerichelli, G.: Reverse Micellar Aggregates: Effect on Ketone Reduction. 2. Surfactant Role. *J. Org. Chem.* **2004**, *69*, 8231-8238.

(191) Usui, D.; Sueishi, Y.; Yamamoto, S.: Kinetic Study of the Reaction of Leuco Methylene Blue with 2,6-Dimethyl-p-benzoquinone in a Reverse Micellar System. *J. Solution Chem.* **2008**, *37*, 1005-1014.

(192) Correa, N. M.; Zorzan, D. H.; Chiarini, M.; Cerichelli, G.: Reverse Micellar Aggregates: Effect on Ketone Reduction. 1. Substrate Role. *J. Org. Chem.* **2004**, *69*, 8224-8230.

(193) Kuchler, A.; Yoshimoto, M.; Luginbuhl, S.; Mavelli, F.; Walde, P.: Enzymatic reactions in confined environments. *Nat Nano* **2016**, *11*, 409-420.

(194) Pileni, M. P.: Reverse micelles as microreactors. *J. Phys. Chem.* **1993**, *97*, 6961-6973.

(195) Debye, P.: Reaction Rates in Ionic Solutions. *Trans. Elec. Chem. Soc.* **1942**, *82*, 265-272.

(196) Sen, S.; Dutta, P.; Sukul, D.; Bhattacharyya, K.: Solvation Dynamics in the Water Pool of Aerosol Sodium Dioctylsulfosuccinate Microemulsion: Effect of Polymer. *J. Phys. Chem. A* **2002**, *106*, 6017-6023.

(197) Rini, M.; Magnes, B.-Z.; Pines, E.; Nibbering, E. T. J.: Real-Time Observation of Bimodal Proton Transfer in Acid-Base Pairs in Water. *Science* **2003**, *301*, 349-352.

(198) Spies, C.; Finkler, B.; Acar, N.; Jung, G.: Solvatochromism of pyranine-derived photoacids. *Phys. Chem. Chem. Phys.* **2013**, *15*, 19893-19905.

(199) Mojumdar, S. S.; Mondal, T.; Das, A. K.; Dey, S.; Bhattacharyya, K.: Ultrafast and ultraslow proton transfer of pyranine in an ionic liquid microemulsion. *J. Chem. Phys.* **2010**, *132*, 194505.

(200) Politi, M. J.; Brandt, O.; Fendler, J. H.: Ground- and excited-state proton transfers in reversed micelles. Polarity restrictions and isotope effects. *J. Phys. Chem.* **1985**, *89*, 2345-2354.

(201) Politi, M. J.; Chaimovich, H.: Water activity in reversed sodium bis(2-ethylhexyl) sulfosuccinate micelles. *J. Phys. Chem.* **1986**, *90*, 282-287.

(202) Bardez, E.; Monnier, E.; Valeur, B.: Dynamics of excited-state reactions in reversed micelles. 2. Proton transfer involving various fluorescent probes according to their sites of solubilization. *J. Phys. Chem.* **1985**, *89*, 5031-5036.

(203) Cohen, B.; Huppert, D.; Solntsev, K. M.; Tsfadia, Y.; Nachliel, E.; Gutman, M.: Excited State Proton Transfer in Reverse Micelles. *J. Am. Chem. Soc.* **2002**, *124*, 7539-7547.

(204) Kwon, O.-H.; Jang, D.-J.: Excited-State Double Proton Transfer of 7-Azaindole in Water Nanopools. *J. Phys. Chem. B* **2005**, *109*, 20479-20484.

(205) Tielrooij, K. J.; Cox, M. J.; Bakker, H. J.: Effect of Confinement on Proton-Transfer Reactions in Water Nanopools. *ChemPhysChem* **2009**, *10*, 245-251.

(206) Patra, A.; Luong, T. Q.; Mitra, R. K.; Havenith, M.: The influence of charge on the structure and dynamics of water encapsulated in reverse micelles. *Phys. Chem. Chem. Phys.* **2014**, *16*, 12875-12883.

(207) Fuglestad, B.; Gupta, K.; Wand, A. J.; Sharp, K. A.: Characterization of Cetyltrimethylammonium Bromide/Hexanol Reverse Micelles by Experimentally Benchmarked Molecular Dynamics Simulations. *Langmuir* **2016**, *32*, 1674-1684.

(208) Lawler, C.; Fayer, M. D.: Proton Transfer in Ionic and Neutral Reverse Micelles. *J. Phys. Chem. B* **2015**, *119*, 6024-6034.

(209) Lang, J.; Mascolo, G.; Zana, R.; Luisi, P. L.: Structure and dynamics of cetyltrimethylammonium bromide water-in-oil microemulsions. *J. Phys. Chem.* **1990**, *94*, 3069-3074.

(210) Mills, A. J.; Wilkie, J.; Britton, M. M.: NMR and Molecular Dynamics Study of the Size, Shape, and Composition of Reverse Micelles in a Cetyltrimethylammonium Bromide (CTAB)/n-Hexane/Pentanol/Water Microemulsion. *J. Phys. Chem. B* **2014**, *118*, 10767-10775.

(211) Khan, M. F.; Singh, M. K.; Sen, S.: Measuring Size, Size Distribution, and Polydispersity of Water-in-Oil Microemulsion Droplets using Fluorescence Correlation Spectroscopy: Comparison to Dynamic Light Scattering. *J. Phys. Chem. B* **2016**, *120*, 1008-1020.

(212) Wieczorek, D.; Gwiazdowska, D.; Staszak, K.; Chen, Y.-L.; Shen, T.-L.: Surface and Antimicrobial Activity of Sulfobetaines. *J Surfactants Deterg* **2016**, *19*, 813-822.

(213) Drinkel, E.; Souza, F. D.; Fiedler, H. D.; Nome, F.: The chameleon effect in zwitterionic micelles: Binding of anions and cations and use as nanoparticle stabilizing agents. *Curr. Opin. Colloid Interface Sci.* **2013**, *18*, 26-34.

(214) Mafi, A.; Hu, D.; Chou, K. C.: Interactions of Sulfobetaine Zwitterionic Surfactants with Water on Water Surface. *Langmuir* **2016**, *32*, 10905-10911.

(215) Tiecco, M.; Roscini, L.; Corte, L.; Colabella, C.; Germani, R.; Cardinali, G.: Ionic Conductivity as a Tool To Study Biocidal Activity of Sulfobetaine Micelles against Saccharomyces cerevisiae Model Cells. *Langmuir* **2016**, *32*, 1101-1110.

(216) Maroncelli, M.; Fleming, G. R.: Picosecond solvation dynamics of coumarin 153: The importance of molecular aspects of solvation. *J. Chem. Phys.* **1987**, *86*, 6221-6239.

(217) Koti, A. S. R.; Periasamy, N.: Application of time resolved area normalized emission spectroscopy to multicomponent systems. *J. Chem. Phys.* **2001**, *115*, 7094-7099.

(218) Koti, A. S. R.; Krishna, M. M. G.; Periasamy, N.: Time-Resolved Area-Normalized Emission Spectroscopy (TRANES): A Novel Method for Confirming Emission from Two Excited States. *J. Phys. Chem. A* **2001**, *105*, 1767-1771.

(219) Sahu, K.; Mondal, S. K.; Ghosh, S.; Roy, D.; Bhattacharyya, K.: Temperature dependence of solvation dynamics and anisotropy decay in a protein: ANS in bovine serum albumin. *J. Chem. Phys.* **2006**, *124*, 124909.

(220) Douhal, A.; Angulo, G.; Gil, M.; Organero, J. Á.; Sanz, M.; Tormo, L.: Observation of Three Behaviors in Confined Liquid Water within a Nanopool Hosting Proton-Transfer Reactions. *J. Phys. Chem. B* **2007**, *111*, 5487-5493.

(221) Lipari, G.; Szabo, A.: Effect of librational motion on fluorescence depolarization and nuclear magnetic resonance relaxation in macromolecules and membranes. *Biophys. J* . **1980**, *30*, 489-506.

(222) Levitus, M.; Bourdelande, J. L.; Marqués, G.; Aramendía, P. F.: Fluorescence anisotropy of dyes included in crosslinked polystyrene. *J. Photochem. Photobiol.* **1999**, *126*, 77-82.

(223) Jung, G.; Gerharz, S.; Schmitt, A.: Solvent-dependent steady-state fluorescence spectroscopy for searching ESPT-dyes: solvatochromism of HPTS revisited. *Phys. Chem. Chem. Phys.* **2009**, *11*, 1416-1426.

(224) Spry, D. B.; Goun, A.; Fayer, M. D.: Deprotonation Dynamics and Stokes Shift of Pyranine (HPTS). *J. Phys. Chem. A* **2007**, *111*, 230-237.

(225) Iftimie, R.; Tremblay, M.-H.; Thomas, V.; Hétu, S.; de Lasalle, F.; Rivard, U.: Moderately Strong Phenols Dissociate by Forming an Ion-Pair Kinetic Intermediate. *J. Phys. Chem. A* **2013**, *117*, 13976-13987.

(226) Phukon, A.; Sahu, K.: The strikingly different miscibility of n-octanol in highly-confined and quasi-confined water. *Chem. Commun.* **2015**, *51*, 14103-14106.

(227) Thompson, W. H.: Solvation Dynamics and Proton Transfer in Nanoconfined Liquids. *Annu. Rev. Phys. Chem.* **2011**, *62*, 599-619.

(228) Piletic, I. R.; Moilanen, D. E.; Spry, D. B.; Levinger, N. E.; Fayer, M. D.: Testing the Core/Shell Model of Nanoconfined Water in Reverse Micelles Using Linear and Nonlinear IR Spectroscopy. *J. Phys. Chem. A* **2006**, *110*, 4985-4999.

(229) Martinez, A. V.; Dominguez, L.; Małolepsza, E.; Moser, A.; Ziegler, Z.; Straub, J. E.: Probing the Structure and Dynamics of Confined Water in AOT Reverse Micelles. *J. Phys. Chem. B* **2013**, *117*, 7345-7351.

(230) Luisi, P. L.; Giomini, M.; Pileni, M. P.; Robinson, B. H.: Reverse micelles as hosts for proteins and small molecules. *Biochim. Biophys. Acta, Rev. Biomembr.* **1988**, *947*, 209-246.

(231) Singha, D.; Barman, N.; Sahu, K.: A facile synthesis of high optical quality silver nanoparticles by ascorbic acid reduction in reverse micelles at room temperature. *J. Colloid Interface Sci.* **2014**, *413*, 37-42.

(232) Corbeil, E. M.; Riter, R. E.; Levinger, N. E.: Cosurfactant Impact on Probe Molecule in Reverse Micelles. *J. Phys. Chem. B* **2004**, *108*, 10777-10784.

(233) Mathew, D. S.; Juang, R.-S.: Role of alcohols in the formation of inverse microemulsions and back extraction of proteins/enzymes in a reverse micellar system. *Sep. Purif. Technol.* **2007**, *53*, 199-215.

(234) Lissi, E. A.; Engel, D.: Incorporation of n-alkanols in reverse micelles in the AOT/n-heptane/water system. *Langmuir* **1992**, *8*, 452-455.

(235) Perez-Casas, S.; Castillo, R.; Costas, M.: Effect of Alcohols in AOT Reverse Micelles. A Heat Capacity and Light Scattering Study. *J. Phys. Chem. B* **1997**, *101*, 7043-7054.

(236) Sedgwick, M. A.; Trujillo, A. M.; Hendricks, N.; Levinger, N. E.; Crans, D. C.: Coexisting Aggregates in Mixed Aerosol OT and Cholesterol Microemulsions. *Langmuir* **2011**, *27*, 948-954.

(237) Mazzacco, C. J.: The effect of solvent and micelles on the rate of excited-state deprotonation. *J. Chem. Educ.* **1996**, *73*, 254.

(238) Sangster, J.: Octanol-Water Partition Coefficients of Simple Organic Compounds. *J. Phys. Chem. Ref. Data* **1989**, *18*, 1111-1229.

(239) Roy, D.; Karmakar, R.; Mondal, S. K.; Sahu, K.; Bhattacharyya, K.: Excited state proton transfer from pyranine to acetate in a CTAB micelle. *Chem. Phys. Lett.* **2004**, *399*, 147-151.

(240) Phukon, A.; Barman, N.; Sahu, K.: Wet Interface of Benzylhexadecyldimethylammonium Chloride Reverse Micelle Revealed by Excited State Proton Transfer of a Localized Probe. *Langmuir* **2015**, *31*, 12587-12596.

(241) Roy, V. P.; Kubarych, K. J.: Interfacial Hydration Dynamics in Cationic Micelles Using 2D-IR and NMR. *J. Phys. Chem. B* **2017**, *121*, 9621-9630.

(242) Quintana, S. S.; Falcone, R. D.; Silber, J. J.; Correa, N. M.: Comparison between Two Anionic Reverse Micelle Interfaces: The Role of Water–Surfactant Interactions in Interfacial Properties. *ChemPhysChem* **2012**, *13*, 115-123.

(243) Soroka, H. P.; Simkovitch, R.; Kosloff, A.; Shomer, S.; Pevzner, A.; Tzang, O.; Tirosh, R.; Patolsky, F.; Huppert, D.: Excited-State Proton Transfer and Proton Diffusion near Hydrophilic Surfaces. *J. Phys. Chem. C* **2013**, *117*, 25786-25797.

(244) Choudhury, S. D.; Nath, S.; Pal, H.: Excited-State Proton Transfer Behavior of 7-Hydroxy-4-methylcoumarin in AOT Reverse Micelles. *J. Phys. Chem. B* **2008**, *112*, 7748-7753.

(245) Htun, T.: Excited-State Proton Transfer in Nonaqueous Solvent. *J. Fluoresc.* **2003**, *13*, 323-329.

(246) Agmon, N.: Elementary Steps in Excited-State Proton Transfer. *J. Phys. Chem. A* **2005**, *109*, 13-35.

(247) Agazzi, F. M.; Falcone, R. D.; Silber, J. J.; Correa, N. M.: Solvent Blends Can Control Cationic Reversed Micellar Interdroplet Interactions. The Effect of n-Heptane:Benzene Mixture on BHDC Reversed Micellar Interfacial Properties: Droplet Sizes and Micropolarity. *J. Phys. Chem. B* **2011**, *115*, 12076-12084.

(248) Vogeli, B.: The nuclear Overhauser effect from a quantitative perspective. *Prog Nucl Magn Reson Spectrosc* **2014**, *78*, 1-46.

(249) Agazzi, F. M.; Correa, N. M.; Rodriguez, J.: Molecular Dynamics Simulation of Water/BHDC Cationic Reverse Micelles. Structural Characterization, Dynamical Properties, and Influence of Solvent on Intermicellar Interactions. *Langmuir* **2014**, *30*, 9643-9653.

(250) Phukon, A.; Ray, S.; Sahu, K.: Effect of Cosurfactants on the Interfacial Hydration of CTAB Quaternary Reverse Micelle Probed Using Excited State Proton Transfer. *Langmuir* **2016**, *32*, 10659-10667.

(251) Nave, S.; Eastoe, J.; Heenan, R. K.; Steytler, D.; Grillo, I.: What Is So Special about Aerosol-OT? 2. Microemulsion Systems. *Langmuir* **2000**, *16*, 8741-8748.

(252) Nucci, N. V.; Valentine, K. G.; Wand, A. J.: High-resolution NMR spectroscopy of encapsulated proteins dissolved in low-viscosity fluids. *J. Magn. Reson.* **2014**, *241*, 137-147.

(253) Lefebvre, B. G.; Liu, W.; Peterson, R. W.; Valentine, K. G.; Wand, A. J.: NMR spectroscopy of proteins encapsulated in a positively charged surfactant. *J. Magn. Reson.* **2005**, *175*, 158-162.

(254) Phukon, A.; Ray, S.; Sahu, K.: How Does Interfacial Hydration Alter during Rod to Sphere Transition in DDAB/Water/Cyclohexane Reverse Micelles? Insights from Excited State Proton Transfer and Fluorescence Anisotropy. *Langmuir* **2016**, *32*, 6656-6665.

(255) Ruckenstein, E.; Nagarajan, R.: Aggregation of amphiphiles in nonaqueous media. *J. Phys. Chem.* **1980**, *84*, 1349-1358.

(256) Yu, Z.-J.; Neuman, R. D.: Giant Rodlike Reversed Micelles Formed by Sodium Bis(2-ethylhexyl) Phosphate in n-Heptane. *Langmuir* **1994**, *10*, 2553-2558.

(257) Yu, Z.-J.; Neuman, R. D.: Reversed Micellar Solution-to-Bicontinuous Microemulsion Transition in Sodium Bis(2-Ethylhexyl) Phosphate/n-Heptane/Water System. *Langmuir* **1995**, *11*, 1081-1086.

(258) Abel, S.; Sterpone, F.; Bandyopadhyay, S.; Marchi, M.: Molecular Modeling and Simulations of AOT−Water Reverse Micelles in Isooctane: Structural and Dynamic Properties. *J. Phys. Chem. B* **2004**, *108*, 19458-19466.

(259) Tian, J.; García, A. E.: Simulations of the confinement of ubiquitin in self-assembled reverse micelles. *J. Chem. Phys.* **2011**, *134*, 225101.

(260) Eastoe, J.; Heenan, R. K.: Water-induced structural changes within the L2 phase of didodecyldimethylammonium bromide-cyclohexane-water systems. *J. Chem. Soc. Faraday Trans.* **1994**, *90*, 487-492.

(261) Briman, I. M.; Rébiscoul, D.; Diat, O.; Zanotti, J.-M.; Jollivet, P.; Barboux, P.; Gin, S.: Impact of Pore Size and Pore Surface Composition on the Dynamics of Confined Water in Highly Ordered Porous Silica. *J. Phys. Chem. C* **2012**, *116*, 7021-7028.

(262) Bellissent-Funel, M.-C.; Hassanali, A.; Havenith, M.; Henchman, R.; Pohl, P.; Sterpone, F.; van der Spoel, D.; Xu, Y.; Garcia, A. E.: Water Determines the Structure and Dynamics of Proteins. *Chem. Rev.* **2016**, *116*, 7673-7697.

(263) Martinez, A. V.; Małolepsza, E.; Domínguez, L.; Lu, Q.; Straub, J. E.: Role of Charge and Solvation in the Structure and Dynamics of Alanine-Rich Peptide AKA2 in AOT Reverse Micelles. *J. Phys. Chem. B* **2015**, *119*, 9084-9090.

(264) Zemb, T. N.; Hyde, S. T.; Derian, P. J.; Barnes, I. S.; Ninham, B. W.: Microstructure from x-ray scattering: the disordered open connected model of microemulsions. *J. Phys. Chem.* **1987**, *91*, 3814-3820.

(265) Eastoe, J.; Hetherington, K. J.; Dalton, J. S.; Sharpe, D.; Lu, J. R.; Heenan, R. K.: Microemulsions with Didodecyldimethylammonium Bromide Studied by Neutron Contrast Variation. *J. Colloid Interface Sci.* **1997**, *190*, 449-455.

(266) Pines, E.; Huppert, D.: Salt effect in photoacid quantum yield measurements: a demonstration of the geminate recombination role in deprotonation reactions. *J. Am. Chem. Soc.* **1989**, *111*, 4096-4097.

(267) Barnadas-Rodríguez, R.; Estelrich, J.: Effect of salts on the excited state of pyranine as determined by steady-state fluorescence. *J. Photochem. Photobiol.* **2008**, *198*, 262-267.

(268) Leiderman, P.; Gepshtein, R.; Uritski, A.; Genosar, L.; Huppert, D.: Effect of Electrolytes on the Excited-State Proton Transfer and Geminate Recombination. *J. Phys. Chem. A* **2006**, *110*, 5573-5584.

(269) Mondal, S.; Ghosh, S.; Sahu, K.; Sen, P.; Bhattacharyya, K.: Excited-state proton transfer from pyranine to acetate in methanol. *J. Chem. Sci.* **2007**, *119*, 71-76.

(270) Fee, R. S.; Maroncelli, M.: Estimating the time-zero spectrum in time-resolved emmsion measurements of solvation dynamics. *Chem. Phys.* **1994**, *183*, 235-247.

(271) Liu, Y.-H.; Chu, T.-S.: Size effect of water cluster on the excited-state proton transfer in aqueous solvent. *Chem. Phys. Lett.* **2011**, *505*, 117-121.

(272) Rakshit, S.; Saha, R.; Verma, P. K.; Pal, S. K.: Role of Solvation Dynamics in Excited State Proton Transfer of 1-Naphthol in Nanoscopic Water Clusters Formed in a Hydrophobic Solvent. *Photochemistry and Photobiology* **2012**, *88*, 851-859.

(273) Phukon, A.; Sahu, K.: How do the interfacial properties of zwitterionic sulfobetaine micelles differ from those of cationic alkyl quaternary ammonium micelles? An excited state proton transfer study. *Phys. Chem. Chem. Phys.* **2017**, *19*, 31461-31468.

(274) Ward, R. S.; Davies, J.; Hodges, G.; Roberts, D. W.: Synthesis of Quaternary Alkylammonium Sulfobetaines. *Synthesis* **2002**, *2002*, 2431-2439.

(275) Bunton, C. A.; Mhala, M. M.; Moffatt, J. R.: Nucleophilic reactions in zwitterionic micelles of amine oxide or betaine sulfonate surfactants. *J. Phys. Chem.* **1989**, *93*, 854-858.

(276) Souza, F. D.; Souza, B. S.; Tondo, D. W.; Leopoldino, E. C.; Fiedler, H. D.; Nome, F.: Imidazolium-Based Zwitterionic Surfactants: Characterization of Normal and Reverse Micelles and Stabilization of Nanoparticles. *Langmuir* **2015**, *31*, 3587-3595.

(277) Marracino, P.; Amadei, A.; Apollonio, F.; d'Inzeo, G.; Liberti, M.; Crescenzo, A. d.; Fontana, A.; Zappacosta, R.; Aschi, M.: Modeling of Chemical Reactions in Micelle: Water-Mediated Keto–Enol Interconversion As a Case Study. *J. Phys. Chem. B* **2011**, *115*, 8102-8111.

(278) Rao, V. G.; Banerjee, C.; Mandal, S.; Ghosh, S.; Sarkar, N.: Zwitterionic micelles as a soft template for the extremely rapid synthesis of small hollow gold nanocontainers. *RSC Adv.* **2013**, *3*, 14963-14969.

(279) Pedro, J. A.; Mora, J. R.; Silva, M.; Fiedler, H. D.; Bunton, C. A.; Nome, F.: Surface Charge of Zwitterionic Sulfobetaine Micelles with 2-Naphthol as a Fluorescent Probe. *Langmuir* **2012**, *28*, 17623-17631.

(280) Mandal, A. K.; Ghosh, S.; Das, A. K.; Mondal, T.; Bhattacharyya, K.: Effect of NaCl on ESPT-Mediated FRET in a CTAC Micelle: A Femtosecond and FCS Study. *ChemPhysChem* **2013**, *14*, 788-796.

(281) Chadha, G.; Zhao, Y.: Properties of surface-cross-linked micelles probed by fluorescence spectroscopy and their catalysis of phosphate ester hydrolysis. *J. Colloid Interface Sci.* **2013**, *390*, 151-157.

(282) Pines, E.; Huppert, D.: Observation of geminate recombination in excited state proton transfer. *J. Chem. Phys.* **1986**, *84*, 3576-3577.

(283) Smith, K. K.; Kaufmann, K. J.; Huppert, D.; Gutman, M.: Picosecond proton ejection: an ultrafast pH jump. *Chem. Phys. Lett.* **1979**, *64*, 522-527.

(284) Liu, W.; Tang, L.; Oscar, B. G.; Wang, Y.; Chen, C.; Fang, C.: Tracking Ultrafast Vibrational Cooling during Excited-State Proton Transfer Reaction with Anti-Stokes and Stokes Femtosecond Stimulated Raman Spectroscopy. *J. Phys. Chem. Lett.* **2017**, *8*, 997-1003.

(285) Chakrabarty, D.; Chakraborty, A.; Seth, D.; Hazra, P.; Sarkar, N.: Effect of alkyl chain length and size of the headgroups of the surfactant on solvent and rotational relaxation of Coumarin 480 in micelles and mixed micelles. *J. Chem. Phys.* **2005**, *122*, 184516.

(286) Jiang, N.; Li, P.; Wang, Y.; Wang, J.; Yan, H.; Thomas, R. K.: Aggregation behavior of hexadecyltrimethylammonium surfactants with various counterions in aqueous solution. *J. Colloid Interface Sci.* **2005**, *286*, 755-760.